KfK 3705
März 1984

INTOR Phase IIA, Magnet System Design —European Contribution —

F. Arendt, F. Becker, H. G. Dittrich, J. Erb,
R. Flükiger, M. Hilal, U. Jeske, A. Knobloch, P. Komarek,
B. Manes, A. Nyilas, G. Ries
and J. D. Elen, N. Sacchetti, G. Véscey (SULTAN Group)

Institut für Technische Physik
Projekt Kernfusion

Kernforschungszentrum Karlsruhe

KERNFORSCHUNGSZENTRUM KARLSRUHE

Institut für Technische Physik
Projekt Kernfusion

KfK 3705

INTOR Phase IIA, Magnet System Design [+]
- European Contribution -

F. Arendt, F. Becker, H.G. Dittrich, J. Erb,
R. Flükiger, M. Hilal[1], U. Jeske, A. Knobloch[2], P. Komarek,
B. Manes, A. Nyilas, G. Ries[3]

with a contribution of
the SULTAN Group
J.D. Elen[4], N. Sacchetti[5], G. Véscey[6]

+) This work has been performed in the frame of the European Fusion Technology Programme.

1) Technological University of Michigan, USA
2) IPP Garching
3) Siemens AG, Erlangen
4) ECN, Petten, NL
5) ENEA, Frascati, I
6) SIN, Villingen, CH

KERNFORSCHUNGSZENTRUM KARLSRUHE GMBH, KARLSRUHE

Kernforschungszentrum Karlsruhe GmbH
ISSN 0303-4003

INTOR IIA - Auslegung des Magnet-Systems - Europäischer Beitrag -

Zusammenfassung

Die INTOR Hauptfeldspulen (TF-Spulen) bestehen aus zwei ineinandergesetzten Wicklungen in einem gemeinsamen Spulengehäuse. Das Gehäuse hat dünne Wände im zentralen Stützbereich. Die zentrierenden Kräfte jeder Teilspule werden im Stützbereich durch in Umfangsrichtung zylindrische Segmente abgestützt. Die Zylindersegmente aller Spulen bilden je einen gemeinsamen Stützzylinder (Gewölbe) für die TF-Teilspulen. Im Feldbereich bis 7.6 T wird der NbTi-LCT-Euratom Leiter verwendet. Für den Hochfeldteil der Spule bis 11 T wird eine hochskalierte Version des LCT-Leiters unter Verwendung von Nb_3Sn vorgesehen. Der Leiter ist für 20 kA ausgelegt. Forcierte Kühlung mit überkritischem Helium wird für beide Leiter vorgesehen.

Zum Vergleich mit dieser KfK-Studie wurden die TF-Leiterauslegungen der SULTAN-Gruppe (ECN, ENEA, SIN) und die alternative TF-Spulenstruktur des SIN in den Bericht mit aufgenommen.

Die Auslegung der Ringspulen (PF-Spulen) basiert auf einem badgekühlten 50 kA Leiter, der von JAERI vorgeschlagen wurde (im ITP wurde erst kürzlich mit der Auslegung und Entwicklung von PF Leitern begonnen). Alle PF Spulen liegen außerhalb der TF Spulen. Die Spulenquerschnitte wurden unter Berücksichtigung der maximal zulässigen Reifenspannung von 200 MPa ermittelt. Mindestens die außenliegende PF Spule mit 24 m Durchmesser muß aus Gewichts- und Hochspannungsgründen unterteilt werden. Für alle PF Spulen erscheint die NbTi Leitertechnik anwendbar, da die Induktion am Leiter 8.4 T nicht überschreitet.

Summary

The INTOR TF magnet has been designed as a two zone winding in a casing with thin side walls at the central region. Two integrated wedging cylinders are formed by the circumferential ribs at the inner leg. In the low field zone up to 7.6 T the LCP NbTi-Euratom conductor has been taken. For the high field part of the winding up to 11 T a Nb_3Sn up-grade version of the Euratom-LCP conductor has been designed with 20 kA conductor current. Supercritical forced flow cooling has been forseen for both conductors.

For comparison with this KfK study the TF-conductor designs of the SULTAN-group (ECN, ENEA, SIN) and the alternative TF coil structure of SIN are included in this report.

The PF magnet design was based on a 50 kA bath cooled conductor proposed by JAERI (which reflects the situation, that ITP has just started a PF conductor development). All PF coils are located outside the TF coils. The coil cross sections were evaluated and at least the outer 24 m diameter EF-coil needs a subdivision. For all PF coils the NbTi-technology appeared to be applicable as the induction at the conductors did not exceed 8.4 T.

Acknowledgement

We thank Dr. A. Knobloch from ITP Garching, Dr. Peter Reynolds from Rutherford Lab, Culham and the members of the ISPRA team especially Dr. G. Casini and Dr. F. Farfaletti-Casali for many helpful discussions.

The study was supported by EURATOM contracts.

Note: The notation of the different chapters is following the notation of the European INTOR report and does therefore not contain consecutent numbers.

The European INTOR Report has been printed as a report of the European Communities and is not yet available to the public.

Contents:

1) Technological University of Michigan, USA
2) IPP Garching
3) Siemens AG, Erlangen

* These chapters have been taken from the SULTAN group contribution to the INTOR workshop

Summary of the INTOR Phase IIA Study

- The main change in the overall magnet system design was the TF magnet size reduction with an important reduction in cost.

- Divertor and limiter PF coil distributions were evaluated consistent with design constraints and approximately with plasma boundary conditions. An attempt aiming at a more general PF distribution optimization was started.

- TF magnet design concepts were developed basically in two directions:

  a) a two zone winding in a casing with thin side walls and two integrated wedging cylinders formed at the central region by the circumferential ribs. (KfK)

  b) a nongraded winding without casing being supported by the out-of-plane and bucking support structure. (SULTAN group)

  a) leads to a particularly low maximum field level, but requires some sophistication for coil assembly; it also is designed especially to the needs of a conductor upgrade from EURATOM LCP; it is suitable for 24 torus segments.

  b) enables a narrower winding cross section and hence can be applied also if the torus segmentation is only in 12 segments. It requires only one conductor type. Experience from the Swiss LCP work has influenced this option.

The design calculation so far are of a simplified and approximative nature, however, they indicate the feasibility of INTOR TF coils for more than one concept.

The same holds for the conductors studied. Three different conductor concepts were developed for option a) and one for option b). For all of them supercritical He cooling was adopted corresponding to the type of cooling that was chosen for both European LCP coils.

In due course quite a number of open details questions call for further design work and design related R+D (evaluation and reduction of AC losses in the cold structure, conductor development and fabrication, insulation to be incorporated in the magnet system, complete assessment of fault situations and their design implications, manufacturing procedures a.s.o.) in order to assure feasibility.

- PF magnet design was based on a bath cooled conductor proposed by another delegation which reflects the situation that EURATOM is just about starting a PF conductor development. The realistic coil cross sections were evaluated again in a simplifying and approximative manner, and found so large for the lower outboard EF coil that a subdivision appears necessary. From the fabrication and transport point of view the larger PF coils are more demanding than the TF coils. All superconducting PF coils are outside the TF magnets, that arrangement being the only one that promises a reasonable assembly and maintenance approach for a reactor like INTOR. Whereas the nominal PF coil loads appear manageable the assessment of the possible failure modes is still in a screening stage. Active safety precautions will help to solve possible problems. Pending further detailed design work and related R+D also the PF part of the magnet system appears feasible. This result is also due to a relaxation of the start-up scenario as compared to Phase I.

Whereas the MAT outlay of the divertor and limiter case is not too different, the energy and hence power in the divertor case is much larger. As could be shown in the course of the PF configuration studies this is mainly due

to the larger vertical shift of the plasma column in the divertor case with reference to the TF coil envelope determining the possible PF coil locations.

- Studies of fault scenarios found that the quench case in large superconducting magnets can be mastered by design. The occurence of a short circuit across the terminals of one TF coil, although rather infrequent, should be considered in the design of the out-of-plane structure because it cannot be excluded entirely as a possibility.

- In accordance with the present EURATOM technology program planning the stepwise development of a INTOR TF coil prototype is outlined. Assuming that 1987 a decision on detailed design of INTOR could be taken including construction and test of a prototype TF coil, serial manufacturing of the TF coils could start 1992 at the earliest. PF magnet development will have to start from scratch in Europe. In order to be meaningful for INTOR that part of the program would have to be vigorously pursued. Until 1987 some test coils could have been brought into operation in an existing tokamak.

INTOR Phase IIA Magnet System Design

1. TF Coil System

1.1 TF Design Concept Evaluation

The TF coil design is carried out according to the following INTOR requirements:

- all PF coils are located outside the TF coils,
- use of a single null poloidal divertor giving a non-symmetric poloidal force distribution to the TF coil (the limiter case demands can be easier satisfied),
- no intercoil force support in the access door region - in a height of 7 m - between each TF coil,
- the centering forces have to be supported by a vault which allows a free access to the central ohmic heating (OH) coil,
- a Nb_3Sn conductor has to be used in the high field region,
- material fatigue has to be considered in the structural support layout.

1.1.1 Coil Configuration and geometry

The coil geometry has been defined from accessibility and maintenance considerations with respect to blanket and shield elements. The shape given in fig. 1 is therefore not optimized with respect to the bending moments in the winding package.

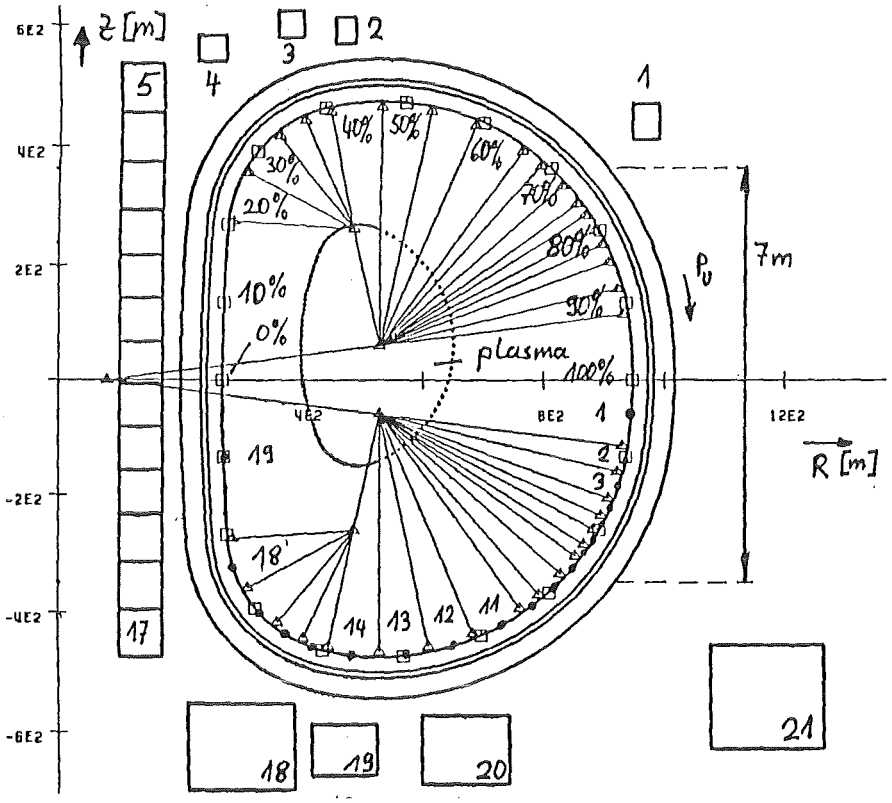

Fig. 1 INTOR TF and PF Coil Configuration

Based on the EURATOM LCT experience forced flow conductors with outer steel jackets have been selected. In order to minimize space constraints in the center and to get free access to the central OH coil a vault structure has been chosen.

The coil consists of two subcoils. In the range 0 - 7,5 T the EURATOM LCT conductor with 10.9 kA conductor current has been chosen and in the range 6.9 - 11 T a 20 kA Nb_3Sn conductor is provided.

The two subcoils are seperated by an additional steel jacket of 10 cm thickness which reduces the hoop stresses in the Nb_3Sn subcoil.

In the vault region this leads to a double vault where the centering forces of each subcoil are taken up individually in order to limit the compressive load on the NbTi conductor in that region. (fig. 2)

Due to the limited space and in order to keep the vault stresses below the design value the cross sectional shape of the winding package has to be cylindrical in the vault region.

There is a transition region to the rectangular cross section of the winding packages outside the central vault. The complete construction dimensions are given in Appendix A.

1.1.2. Winding Design

The NbTi subcoil consists of two parts. Each with an equal number of double pancakes.

The pancake connections can be done completely in the dome area after inserting the subcoil parts into the outer steel jacket. After insertion of the NbTi part the support vault of the Nb_3Sn coil is mounted and welded to the Nb_3Sn steel support jacket with the NbTi coil in place.

The Nb_3Sn subcoil consists also of two parts. Each with several double pancakes and one single pancake. The electric connections of each winding package part have to be finished before assembling the coil parts. The two winding package parts are connected at the inner side at the top of the coil after insertion into the support ring. Thus, there is one electric connection in the higher field region.

The coil is completed by an addtitional inner steel ring. This ring closes up the coil towards the inside. Side walls of 1.5 cm thickness are considered so that a defined vacuum boundary for each coil exists. Mechanically, the inner ring acts together with the out-of-plane support structure which can be seeh in Fig. 3.

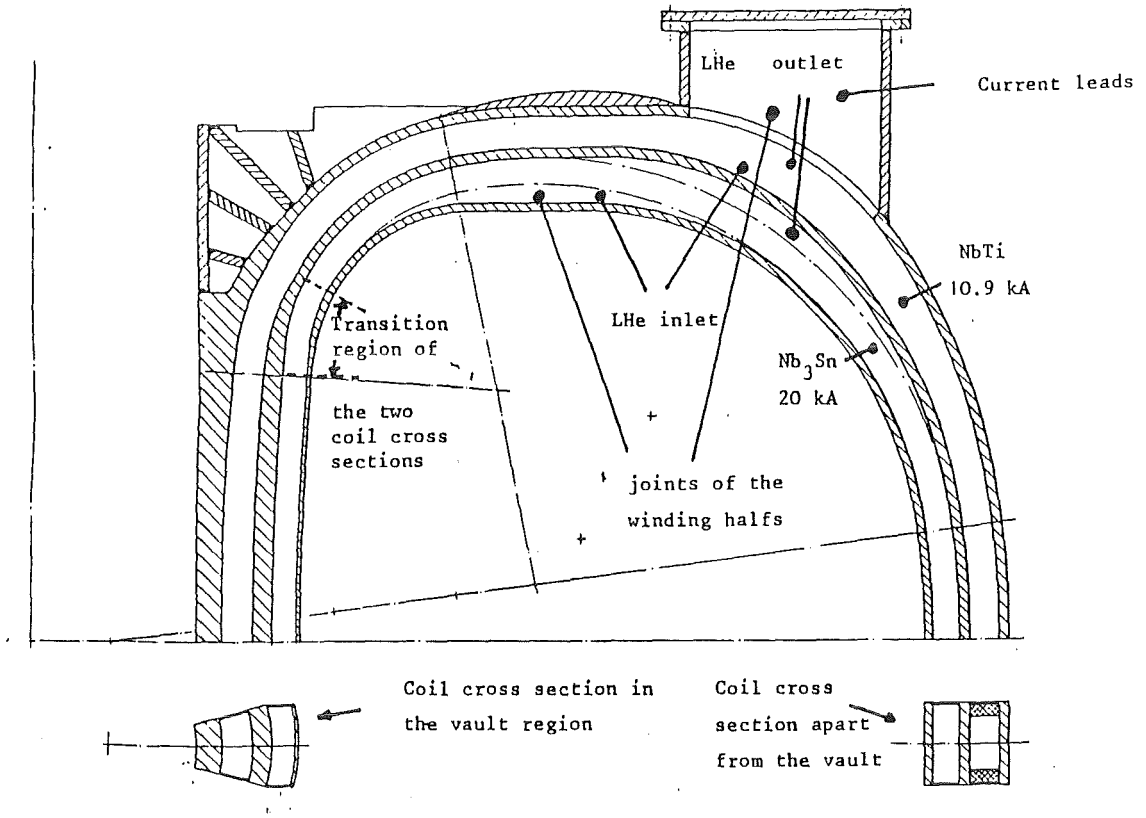

Fig. 2 INTOR TF Coil Design

There might be an advantage in connecting each subcoil to its own power supply and thus allowing for two discharge resistors.

Table I . and fig. 4 show the main data of the winding design.

The He-loss power at 4 K which is summarized in Table II, consists of the nuclear radiation load, the ac losses due to the PF-transients and the pumping power for the forced flow of supercritical He. Radiation losses are taken into account only for the inner Nb_3Sn-subcoil (negligible in the NbTi-subcoil). It is further assumed that the steel supports of the coil are cooled by own cooling channels.

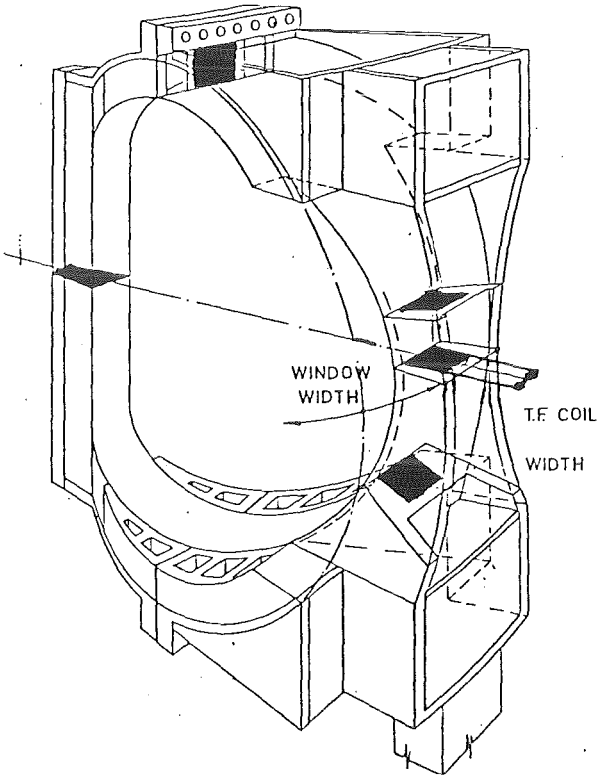

Fig. 3
Perspective view of the TF coil structure

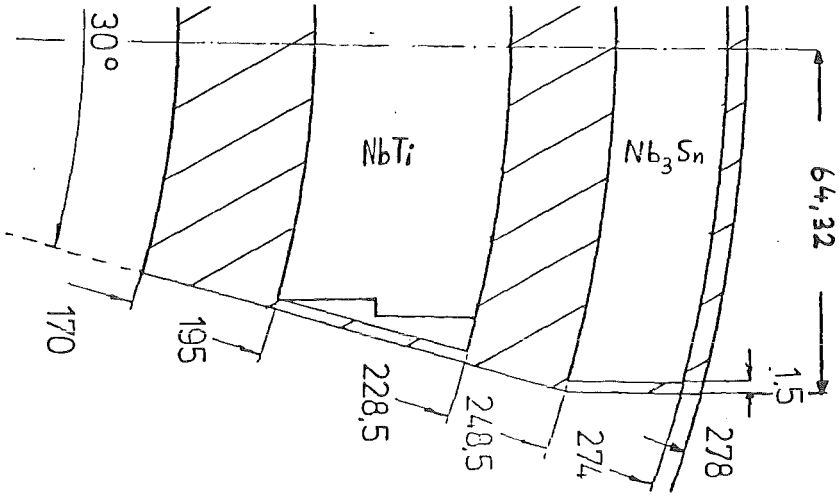

Fig. 4 TF coil cross section dimensions at the horizontal midplane of the vault

Table I . INTOR Winding Design

	Nb_3Sn	NbTi
Number of turns	234	670
Average length of a single turn /m/	28	30
Conductor current /kA/	20	10.93
Cross sectional area /cm^2/	118 x 25,5	106 x 17,2
		+ 97,2 x 16,3
Current density /kA/cm^2/	1,56	2,15
Induction range /T/	11 - 6,9	7,5 - -0,6
Number of pancakes per coil	18	25
Number of parallel He channels per pancake	1 (2)	4
Channel length /m/	368 (184)	210
Hydraulic diameter /mm/	2,38	1,6
He mass flow rate /g/s/	10 (10)	10
Pressure drop /bar/	0,5 (0,25)	2
Heat load [J/m conductor] to conductor due to		
- radiation (inner coil leg)	0,05	negligible
- ac losses during start up and shut down (26 s)	0,16	0,135
Temperature rise /K/ due to		
- pressure drop	0,1 (0,05)	0,43
- ac losses	0,03 (0,03)	0,06
- radiation	0,7 (0,35)	--
Loss power per subcoil /W/		
- pressure drop	57	1266
- ac losses	112 - 496	302
- radiation	328	--

1.1.3 Study of a 20 kA-12T-Nb_3Sn Conductor based on the LCT-EURATOM technology

1.1.3.1 PRESENTATION OF Nb_3Sn AS SUPERCONDUCTING MATERIAL FOR FIELDS ABOVE 10 T

Due to its superconducting properties, in particular the high T_c value of 18 K and the high upper critical field of ~ 21 T at 4.2 K, but also for economical reasons, the material Nb_3Sn is to date the only candidate for fusion magnets producing fields $\geq$ 11 T, as required in INTOR.
The brittleness of Nb_3Sn renders the wire production very difficult, since it excludes any plastic deformation, i.e. wire drawing. Nevertheless, long lengths of wire are industrially produced today by the so-called bronze route. The Nb_3Sn phase is formed by reacting the wire at 700° C once the deformation process is over. The critical current density, J_c, of Nb_3Sn wires is very sensitive to the stresses acting on the individual filaments, as a consequence of crystallographical changes: if an external tensile stress is applied to a Nb_3Sn wire, J_c increases up to a maximum value, J_{cm}, at strain values ε_m ranging from 0.2 to 0.5 %.
There is a strain value ε_{irr} (ranging from 0.2 to 0.5%) above which J_c shows irreversible degradation due to filament rupture. A conductor with a sufficient safety factor can thus only be obtained if the bending strains arising from the coil winding operation after reaction at 700°C do not exceed 0.2%. These bending strains can be minimized by concentrating the Nb_3Sn filaments as close as possible to the neutral axis of the conductor. The uniaxial strain arising from the Lorentz forces during operation has to be kept below 0.2% by appropriate stainless steel reinforcement of the conductor: for an INTOR type conductor, $\geq$ 35% steel would be required (Table IV).

1.1.3.2 FABRICATION PROCESSES FOR Nb_3Sn CONDUCTORS

The large size of INTOR magnets suggest the application of the so-called "react and wind" technique, where the conductor is reacted at 700° C prior to coil winding. The reinforcing stainless steel can be included either before or after the reaction heat treatment. These two cases are characterized by the denominations "global" and "selective" heat treatment, respectively.

Two different variations of the "react and wind" technique are possible: a) All components, including the reinforcing stainless stell undergo the reaction heat treatment at 700°C ("global" heat treatment) and b) the steel reinforcement is added after the reaction heat treatment of the other components ("selective" heat treatment).

Table II Different processes for fabrication of an INTOR conductor.

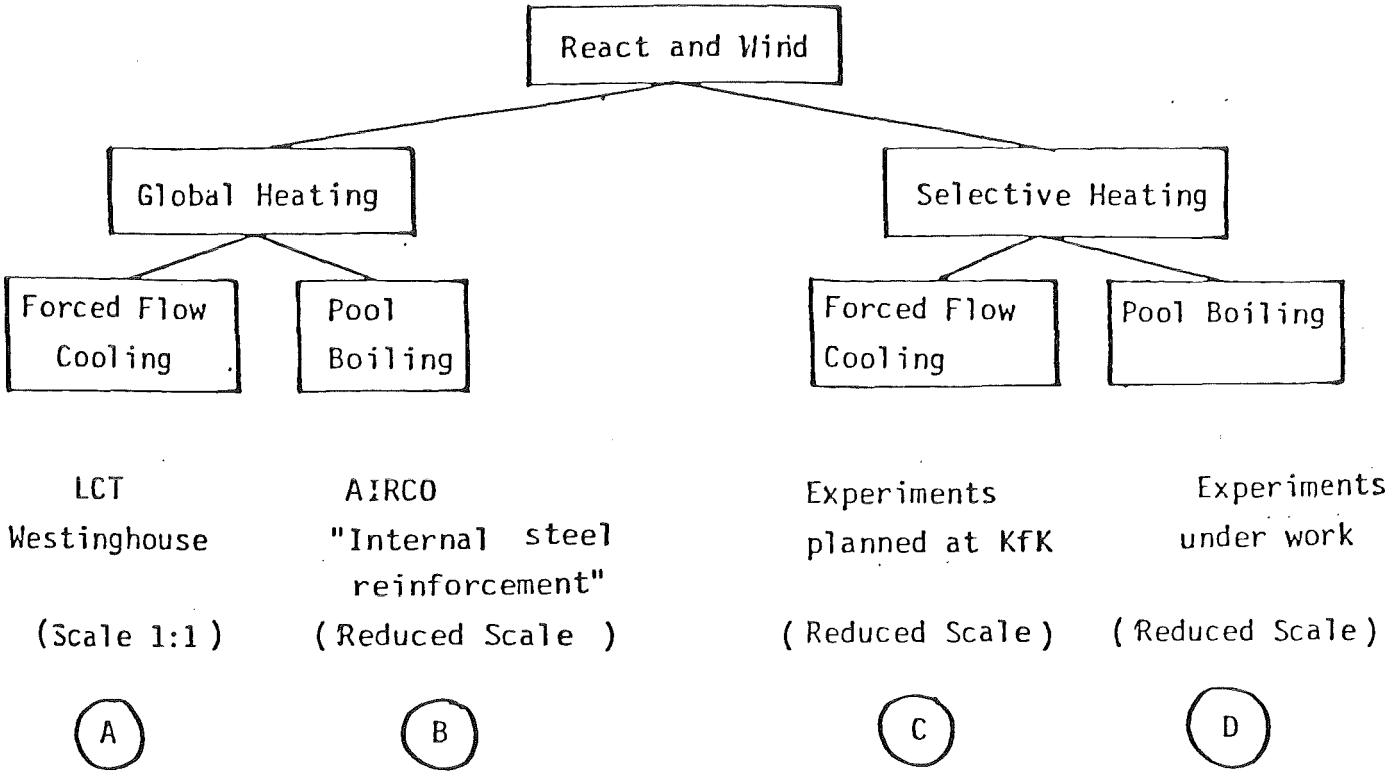

It is obvious that the global heating method would be most convenient for the fabrication of the conductor, in virtue of its simplicity. It has been chosen for the Westinghouse LCT coil. The "selective" heating method requires the use of solder after the reaction, but introduces the problem of handling unprotected reacted Nb_3Sn conductors (the Cu-stabilization cannot be considered as a mechanical reinforcement).

Before to decide about the appropriate way to produce the INTOR conductor it should be recalled that both methods listed in Table II contain several unknown steps. First of all, the very first Nb_3Sn magnets pro-

duced by "react and wind" techniques have just been completed. The first tests on magnets with diameters $\leq$ Ø 50 cm show that the technique can be applied successfully, after the correct determination of the fabrication parameters. The Westinghouse LCT coil, the first really large Nb_3Sn coil produced to date, serves as a model but the final tests which will give the expected informations will not be undertaken before mid or even end 1983.

The multitude of criteria which have to be optimized when designing a conductor design for a fusion magnet is schematically illustrated in Table III.

Thus, the most important unknown point of crucial importance is the coexistence of stainless steel and Nb_3Sn: a) How does the presence of stainless steel influence the critical current density of Nb_3Sn, and b) what are the conditions for handling the steel reinforced conductor without to degrade the current carrying properties. At KfK, we have recently untertaken a program in order to get an experimental answer to these questions. The results obtained so far are quite surprising and of great importance for the design of the INTOR conductor. They will be presented here together with several propositions for a conductor design. We estimate that a definite choice for a particular design and its complete characterization can only be made at a more advanced stage of investigation. Nevertheless, all preliminary tests confirm the feasibility of a large Nb_3Sn coil, but in order to obtain an optimum performance, these practical tests are necessary. Last but not least, these tests will also help in deciding for a lowest cost-solution.

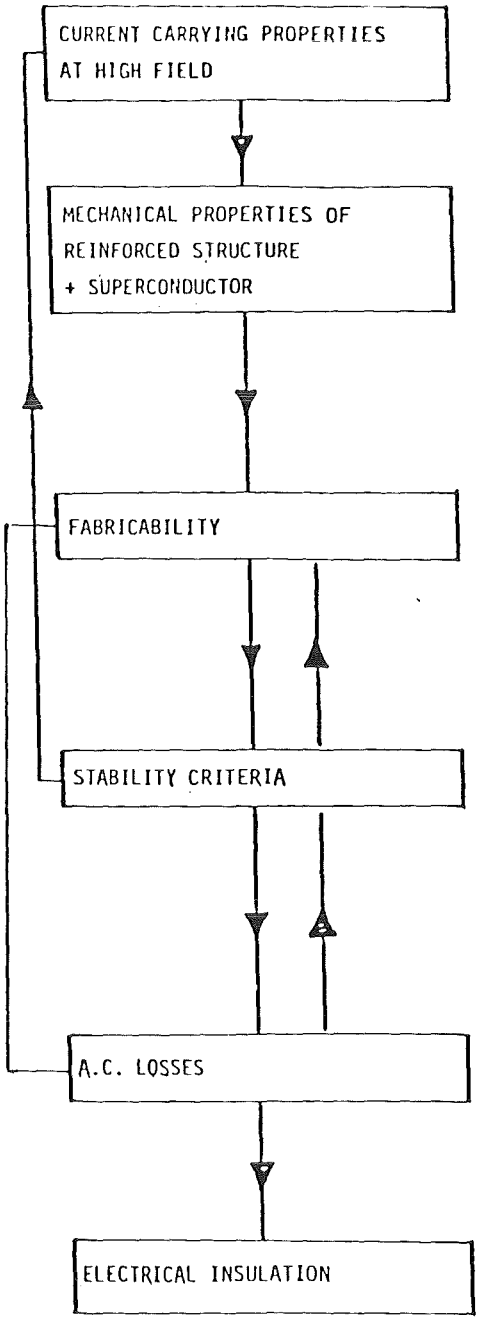

PARAMETER

- choice of Nb_3Sn as basis material
- ternary and quaternary additions to Nb_3Sn
- superconducting cross section

- forces taken by conductor and case
- choice of steel
- steel cross section
- configuration of the reinforced structure
- response of superconductor to stress field
- type of welding technique

(- eventually, steel + weldments must support reaction at 700°C without degradation)

- selective or global annealing
- low costs
- soldering problems
- reduction of fabrication steps
- high mechanical reserve (bending strains)

- choice of stabilizer (Cu, under particular conditions: Al)
- distribution and cross section of the stabilizer
- cooled perimeter (surface state of stabiliz
- if forced flow cooling: He cross section (cross section, friction coefficient)

- type and distribution of barriers (CuNi, solder, ...)
- twist pitch of wires and strands.
- electrical resistivity between strands

- insulation material
- thickness

Table III Criteria to be optimized for a fusion conductor design.

It was found in our laboratories that the variation of J_c with the applied strain is strongly enhanced for steel reinforced Nb_3Sn conductors. As shown by Fig. 5, the ratios J_{cm}/J_{co} at 10 and 14 T reach the values $\sim$ 3 and $\sim$ 8, respectively, i. e. a factor 4 higher than the ratios of unreinforced Nb_3Sn wires at these fields. This is a consequence of the dramatic decrease of H_{c2}^* from $\sim$ 20 T to 16.5 T which is in turn due to the enhanced prestress in steel reinforced wires. Fortunately, these negative effects on J_c can be almost compensated, as shown as follows.

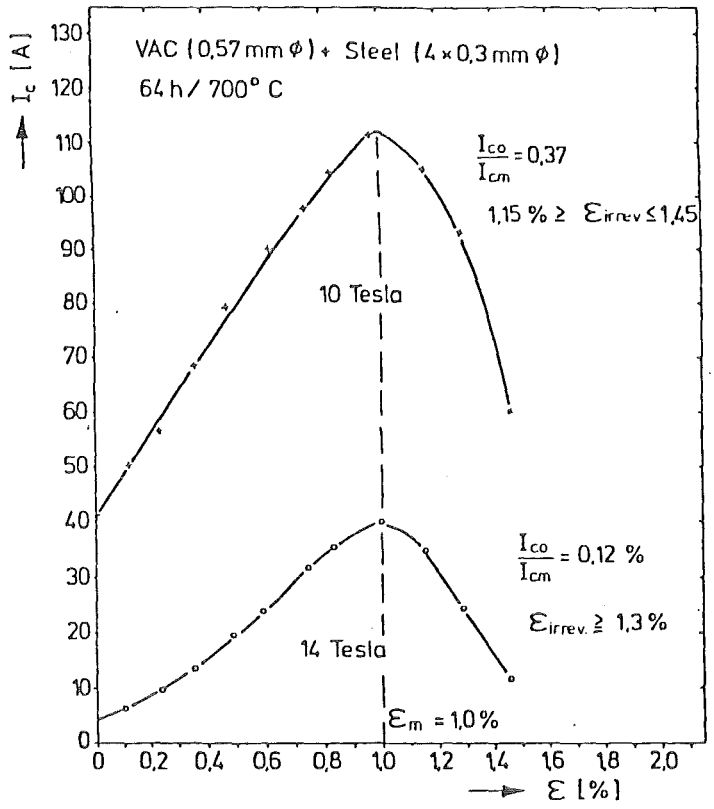

Fig. 5 J_c vs. applied strain for the steel reinforced conductor at B_o = 10 T and 12 T. ε_m is about 1 % and $\varepsilon_{irr} \simeq 1.35$ %.

Global heating yields lower J_c values than selective heating, due to enhanced precompression, which would be in favour of the latter. However, a perhaps decisive advantage in favor of global heating is the enhancement of ε_m up to ~ 1% and of ε_{irr} up to > 1%. This larger mechanical reserve (see Fig. 6) constitutes a precious safety margin. The competitivity of global heating is increased by the possibility to strongly reduce the strain sensitivity of J_c above 10 T by ternary additions to Nb_3Sn, as Ta, Ti or Ni + Zn. For the present considerations, global heating has thus been retained.

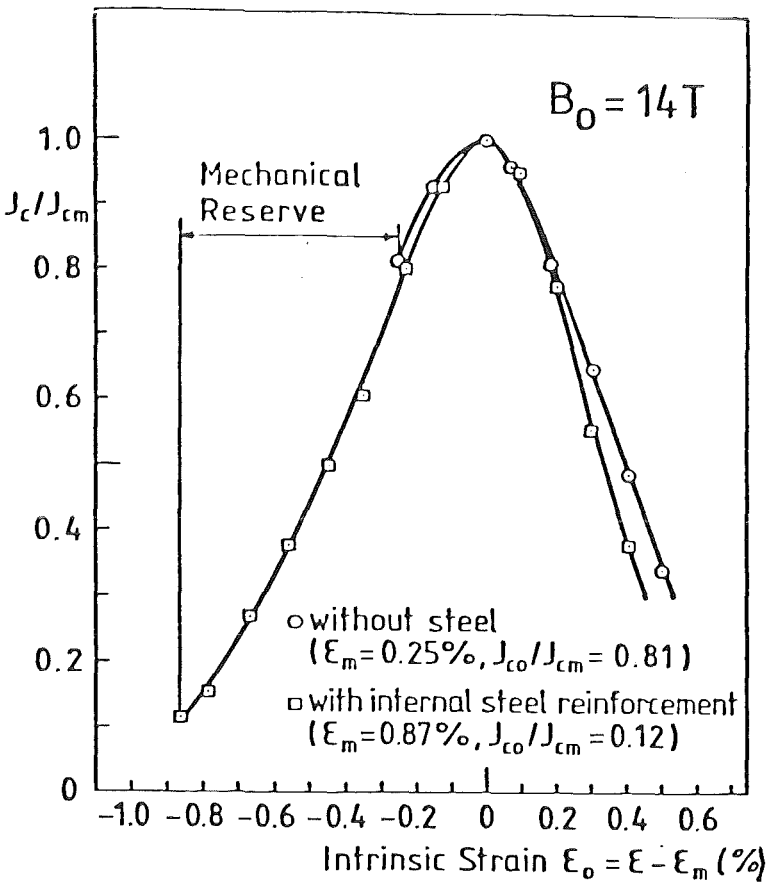

Fig. 6:

J_c vs. effective strain for the steel reinforced conductor shown in Fig. 2. At 14 T, J_c is lowered by a factor 8 as a consequence of the decrease in H^*_{c2} from 20 to 16.5 T. The prestrain is about 1 %.

A good heat exchange between the Nb_3Sn strands and the He can be realized by direct contact: only high conductivity Cu is allowed as intermediate material between the strands and liquid He. The simplest way would consist in concentrating the stainless steel at the center of the conductor. This would lead to a central steel bar of ~ 20 × 20 mm^2. Besides the high values of bending stresses obtained by such a solution, there is another objection: during the coil winding process, the conductor should be under a tension of several kN, and the Nb_3Sn strands on the periphery of the conductor would not be sufficiently protected during the transmission of this force to the forming tools. This suggests that forced flow cooling rather than bath cooling would be preferable.

Thus, a 20 kA- 12T. Nb_3Sn conductor is calculated assuming the following boundary conditions:

- Forced flow cooling
- Global annealing (no soldering)
- Ternary (or quaternary) additions to Nb_3Sn
- Stekly stability criterion.

IX. 1.1.3.3 Conductor Profile

a) Square conductor profile. The minimum bending radius for the INTOR coil is 2300 mm, which means that the distance between neutral axis and external Nb_3Sn filaments should be smaller than 10 mm in order to limit to bending strains on winding to values below 0.4 %. Assuming a Nb_3Sn strand diameter of 4 mm, a maximum space of 12 × 12 mm^2 inside the strands for both stabilizing Cu and He conduit would remain, i.e. ~ 14 % of the total conductor cross section of 1050 mm^2 (see Table I). Such a conductor does not meet the Stekly stability criterion, unless additional He channels and stabilizing Cu are added between the Nb_3Sn strands and the stainless steel conduit, thus adding in complexity.

b) Rectangular profile. In order to minimize the bending strains, the Nb_3Sn strands can be placed closer to the center of the conductor if a rectangular profile is chosen. The center would consist of a CrNi strip, similar to the EURATOM LCT conductor. Such a rectangular conductor would exhibit bending strains well below 0.2 %, which is a considerable advantage if considering safe handling and operation conditions of the conductor.

1.1.3.4 The design principles of the 11 kA-8T-NbTi EURATOM-LCT conductor

The design should rely as much as possible on existing technologies or such ones which will be proven soon (LCT). Therefore the EURATOM-LCT-coil experiences are taken as a basis for the design principles

- Cabled conductor with internal forced flow cooling with supercritical He,
- Double pancake winding with epoxy impregnation to form rigid blocks,
- Steel reinforcement of the conductor cable,
- Encapsulation of the winding in a steel case with friction type locking by epoxy filled steel cushions.

Table IV shows the main parameters of the EURATOM NbTi-LCT-conductor.

1.1.3.5 Model calculation of a 20 kA-12T-Nb_3Sn conductor

Design principles

Based on experimental investigations /1/ on the behaviour of J_c in Nb_3Sn as a function of steel reinforcement (added either before or after the reaction heat treatment), the following criteria for the KfK-INTOR conductor have been used:

- Simultaneous annealing of conductor and reinforcing steel (no soldering),
- Additions to Nb_3Sn (Ta, Ti, Ni + Zn, ...) for counterbalancing the degrading effects of reinforcing steel in J_c,
- Thermal stability similar to Stekly conditions,
- Minimum bending stresses (rectangular conductor),
- Minimum ac losses,
- Parts of the coil forces are transmitted to the support rings and to the vault.

A model calculation of the parameters for a rectangular conductor has been carried out on the base of the EURATOM-LCT technology acquired at KfK. For this calculation, NbTi has been replaced by Nb_3Sn and the mechanical requirements have been scaled up to 12 T (at the conductor). This conductor concept is not definitive: it is expected that manufacturing aspects which are still under study will lead to a different configuration. Nevertheless, the obtained parameters can be considered as representative.

Table IV. NbTi Conductor Parameters

Overall Parameters	
Critical current (guaranteed)	15 kA 4.2 K/8 T
Design current	11 kA 3.8 K/8 T
Overall dimensions[+)]	40 x 10 mm^2
Material fractions: NbTi 50	29 mm^2
Cu	138 mm^2
SS+CrNi	134 mm^2
He	95 mm^2
Hydraulic cross section	1.37 mm^2
Cooled perimeter	170 mm
Normal conducting heat flux	0.3 W/cm^2
Conduit Parameters	
Thickness of conduit	0.8 mm
Number of spacers	6
Dimension of spacers	7 x 0.6 mm^2
Cable Parameters	
Number of strands	23
Cabling length	400 mm
Distance between strands	0.9 mm
Solder	Sn58Pb39In3
Strand Parameters (Cu/NbTi	
Dimensions	2.35 x 3.1 mm^2
Measured critical current density (4.2 K, 8 T)	$\geq$ 80 kA/cm^2
Copper resistivity (8 T)	$\leq 5.5 \times 10^{-10}$ Ωm
Number of filaments	774 (each 46 µm)
Twist pitch	35 mm
Core Parameters (Cr20Ni80)	
Dimensions	33.8 x 1 mm^2
Capton foil (thickness)	50 µm

[+)] with electric insulation (glass fibre epoxy)
1 mm more in both directions.

Fig. 7 shows a schematic view of the Nb_3Sn conductor. Theoretically, one possibility to manufacture the strand is the cabling of the N = 19 wires around a copper rod, shaping it afterwards into the required cross section and filling up the spacings with copper (e. g. electrolytically). Another, more realistic possibility to manufacture the strand is a monolithic strand where the Nb_3Sn-bronze wires are embedded in a copper matrix.

Model calculation

A number of strands is assumed. In the Stekly criterion formula

$$Q = h \cdot p \cdot \Delta T \cdot (T_W/T_B)^{-0.716} = \frac{I_{Str}^2 \cdot \rho_{Cu}(12T)}{A_{Cu}}$$

we chose:

$$\rho_{Cu}(12T) = 7.16 \cdot 10^{-10} \Omega cm$$

$$h = 0.1 \ W/cm^2K$$

$$\Delta T = 10.5 \ K - 3.8 \ K = 6.5 \ K$$

$$(T_W/T_B)^{-0.716} = (10.5/3.8)^{-0.716} = 0.483$$

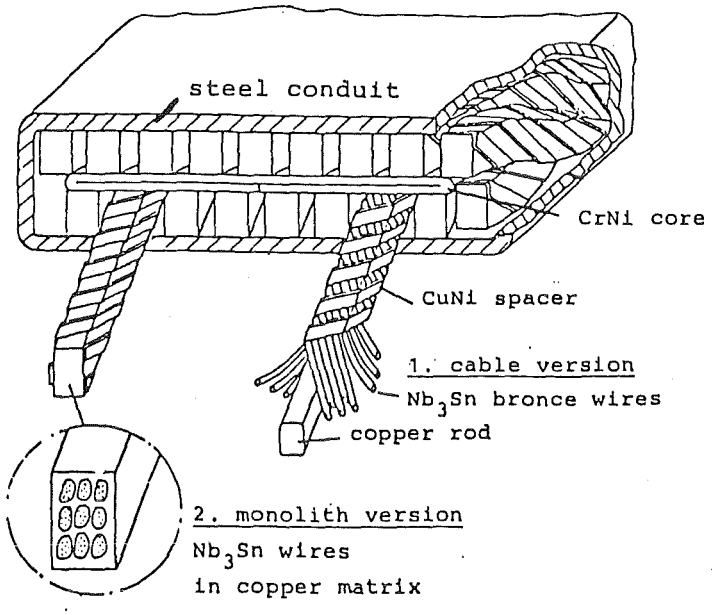

Fig. 7 Nb_3Sn - 20 kA - 12 T forced flow conductor.
Two versions for the Nb_3Sn strands are shown.

The design value for J_c is obtained by multiplying J_c (12 T) of a commercial wire with the factor $2/3 \cdot 1/2$, which takes also into account the effects of steel reinforcement. With the design value

$$J_c = \frac{2}{3} \cdot \frac{1}{2} \cdot 5 \cdot 10^4 \text{ A/cm}^2 = 1.67 \cdot 10^4 \text{ A/cm}^2$$

we obtain the number of wires per strand $N = 19$, and thus

$$A_{Cu} \cdot p = 0.178 \text{ cm}^3.$$

Assuming strands with an aspect ratio 1.5, the strand dimensions are calculated to $(0.326 \times 0.542)\,\text{cm}^2$. The conductor cross section is represented in Fig. 8.

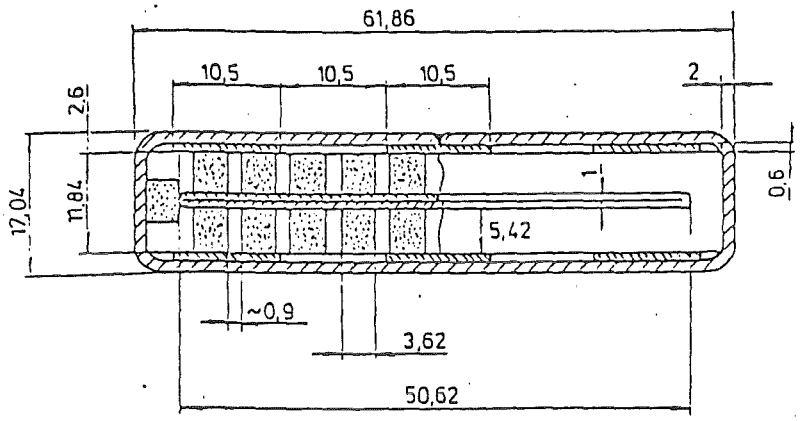

Fig. 8 Dimensions of the 20 kA - 12 T - Nb_3Sn conductor for INTOR based on LCT-EURATOM-technology

Some conductor parameters are represented in Table V.

Table V Nb_3Sn Conductor Parameters

Overall parameter	
Critical current	30 kA/3.8 K/12 T
Design current	20 kA/3.8 K/12 T
Overall dimensions	61,86 x 17,04 mm^2
Material fractions:	
Superconductor + bronze	123.6 mm^2 = 11.9%
Helium	214.8 mm^2 = 20.7%
Copper	327.7 mm^2 = 31.6%
Stainless steel	372.0 mm^2 = 35.8%
Total cross section	1038.1 mm^2 = 100%
Ratio Cu/ (s.c. + bronze)	α = 2.65
Number of strands	23 (each 19 wires)
Wire diameter	0,6 mm
Number of filaments/wire	10 000
Filament diameter	3 µm
Hydraulic parameters	
Hydraulic diameter	2,38 mm
Wetted perimeter	36,1 cm

1.1.4 FIELD AND FORCE CALCULATIONS

1.1.4.1 In-plane-loads on the TF coil

The in-plane-forces on the TF coil are calculated to

$$F_x = -222 \text{ MN} \quad \text{(NbTi part)}$$

$$\text{and} \quad F_x = -175 \text{ MN} \quad (Nb_3Sn \text{ part}).$$

These forces act on the TF coil vault.

A detailed list of the forces on the TF coil elements, see Fig. 1, is given in Table VI.

Table VII shows the in-plane pressure on the coil elements. The values of the elements 19 and 20 are the pressure values of the vault region.

TABLE VI. IN-PLANE LOADS ON THE TF COIL
(NORMAL LOAD CONDITION, FORCES IN MN)

ELEMENT	NB3SN FX	SUBCOIL FZ	NBTI FX	SUBCOIL FZ	SUM OF FORCES SFX	SFZ	
1	22.72	1.52	1.97	0.14	24.69	1.66	
2	9.23	1.76	1.05	0.20	10.28	1.96	
3	9.94	3.14	1.29	0.41	11.23	3.55	
4	6.21	2.67	0.86	0.37	7.07	3.04	
5	5.09	2.64	0.74	0.39	5.83	3.03	
6	5.44	3.32	0.83	0.51	6.27	3.83	
7	4.36	3.08	0.70	0.50	5.06	3.58	
8	6.51	5.41	1.11	0.92	7.62	6.33	
9	7.58	7.85	1.41	1.46	8.99	9.31	
10	5.33	6.88	1.09	1.40	6.42	8.28	
11	9.76	17.81	2.28	4.20	12.04	22.01	
12	5.47	17.92	1.55	5.13	7.02	23.05	
13	2.07	20.69	0.70	7.20	2.77	27.89	
14	-2.48	23.43	-1.09	9.99	-3.57	33.42	
15	-4.40	13.31	-2.37	7.15	-6.77	20.46	
16	-9.19	14.81	-5.52	8.87	-14.71	23.68	
17	-22.49	18.76	-15.21	12.61	-37.70	31.37	
18	-35.71	10.47	-26.58	7.74	-62.29	18.21	
19	-52.21	2.75	-34.79	1.83	-87.00	4.58	} Element 19 in Fig. 3
20	-60.69	1.11	-40.81	0.75	-101.50	1.86	
SUM	-87.46	179.33	-110.79	71.77	-198.25	251.10	
TOTAL COIL	-174.92	0.0	-221.58	0.0	-396.50	0.0	

TABLE VII. IN-PLANE PRESSURE ON THE COIL ELEMENTS IN MPA

ELEMENT	NB3SN	NBTI	
1	17.2	1.6	
2	17.4	2.1	
3	17.6	2.4	
4	17.8	2.6	
5	17.9	2.7	
6	18.0	2.9	
7	18.1	3.0	
8	18.2	3.2	
9	18.4	3.6	
10	18.7	4.0	
11	19.2	4.7	
12	20.2	6.0	
13	21.4	7.7	
14	23.4	10.3	
15	25.5	13.2	
16	27.5	15.9	
17	30.5	19.8	
18	34.1	24.4	
19	35.7	26.7	} Element 19 in Fig. 3
20	36.3	27.4	

1.1.4.2. Hoop stresses in the subcoil

The hoop stresses in the winding (!) packages are given in Table VIII The values are calculated at the center of each of the 19 sectors, the coil is subdivided too. These sectors can be seen in Fig. 1 .

Table VIII Hoop stress in the winding packages of the TF coil

Radius	Point	Nb_3Sn |MPa|	NbTi |MPa|
1	1	623	37
2	2	310	28
	3	312	30
	4	316	35
	5	317	37
	6	319	38
	7	321	41
	8	323	43
	9	327	47
	10	334	55
	11	339	50
	12	356	78
	13	370	102
	14	412	137
3	15	234	92
	16	252	110
	17	270	136
	18	309	168

In the vault region (point 19) the hoop stress calculation is of no interest because the radial forces are supported by the vault and not via the hoop stresses.

Including the additional support ring cross section and applying the rule of mixture to the Nb_3Sn coil, the hoop stresses in the different materials of the coil can be calculated. The cross sectional fractions are 66% steel, 25% Cu and 9% SC, with Youngs moduli $2.1 \cdot 10^5$ MPa, $1.2 \cdot 10^5$ MPa and $1.4 \cdot 10^5$ MPa respectively. The results for the Nb_3Sn coil are given in Table IX. For the NbTi coil the stresses are below 100 MPa.

Table IX Hoop stresses in the Nb_3Sn winding package taking into account the material fractions of the conductor and the additional support ring

Point	σ_{total} |MPa|	σ_{steel} |MPa|	σ_{Cu} |MPa|	σ_{SC} |MPa|
1	554	643	367	429
14	367	426	244	284
18	275	319	183	213

The hoop stresses at point 1 can not be accepted. The stresses can be reduced by either increasing the support ring thickness or increasing

the Nb_3Sn coil thickness (going further down with the NbTi coil induction) or using the NbTi coil as additional support (feasible due to the smaller strain in the NbTi coil!). This last possibility would be preferable.

1.1.4.3 Mechanical stresses in the vault

To get a first idea of the necessary wall thickness of the two vaults, different models were considered, e. g. with rectangular cross section of the winding package and thick plates as vault elements forming a polygonal vault. Too high stress values due to the bending of the plates resulted. Therefore a solution was considered where the winding package cross section in the vault region was chosen cylindrically with a transition to a rectangular cross section outside of the inner coil leg, see fig. 2.

2-D finite element calculations were carried out to determine the mechanical stresses in the vault, neglecting the influence of torsion due to the overturning forces. An attempt was made to find a solution near 300 MPa in order to have enough margin to include torsional and unsymmetric effects later. Fig. 9 shows a contour plot of the equivalent stresses in the vault.

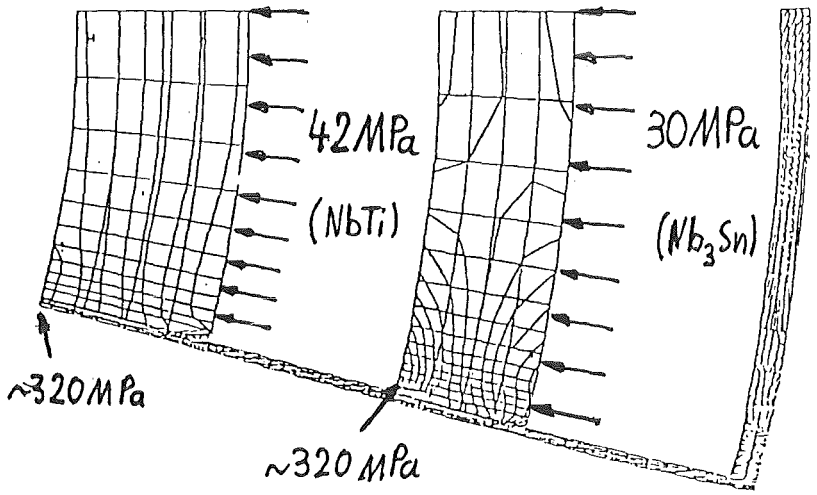

Fig. 9 Equivalent stresses in the TF coil vault due to the centering forces

The maximum stresses are about 320 MPa in both vaults. The vault thicknesses are 25 cm and 20 cm respectively. To avoid additional bending moments, the side wall thickness was chosen to be only 1.5 cm, so that the covering of the vault with conductors is nearly homogeneous.

1.1.4.4. Poloidal fields and forces on the TF coil

The poloidal induction components perpendicular and tangential to the subcoil central perimeters B_n and B_t are calculated as function of the perimeter p_u. They are represented in Fig.10 for the end of the burn time (t = 211 s) inclusive the plasma current. The induction components B_n and B_t of the plasma current are shown in Fig. 11.

The overturning moments due to the poloidal induction acting around the R-axis, see Fig. 1 , are given in Table X. The total overturning moment is 163 MNm with a plasma current contribution of -87 MNm.

Table X. Overturning moments due to the poloidal induction on the TF coil (divertor case)

Subcoil	Moment due to plasma |MNm| at t = 211 s	Moment due to poloidal fields including plasma current |MNm| at t = 211 s
NbTi	-57	95
Nb_3Sn	-30	68

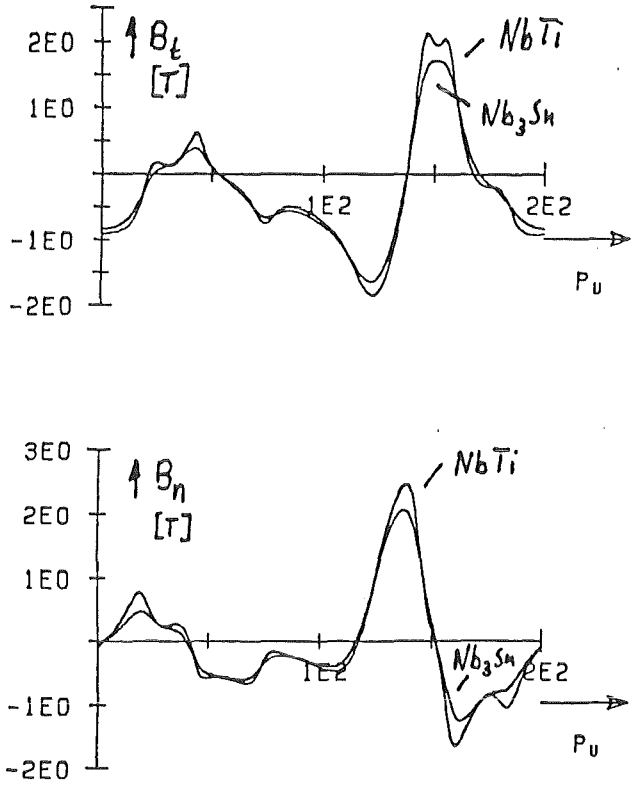

Fig. 10 Poloidal induction components on the subcoils (inclusive plasma current) (t = 211 s)

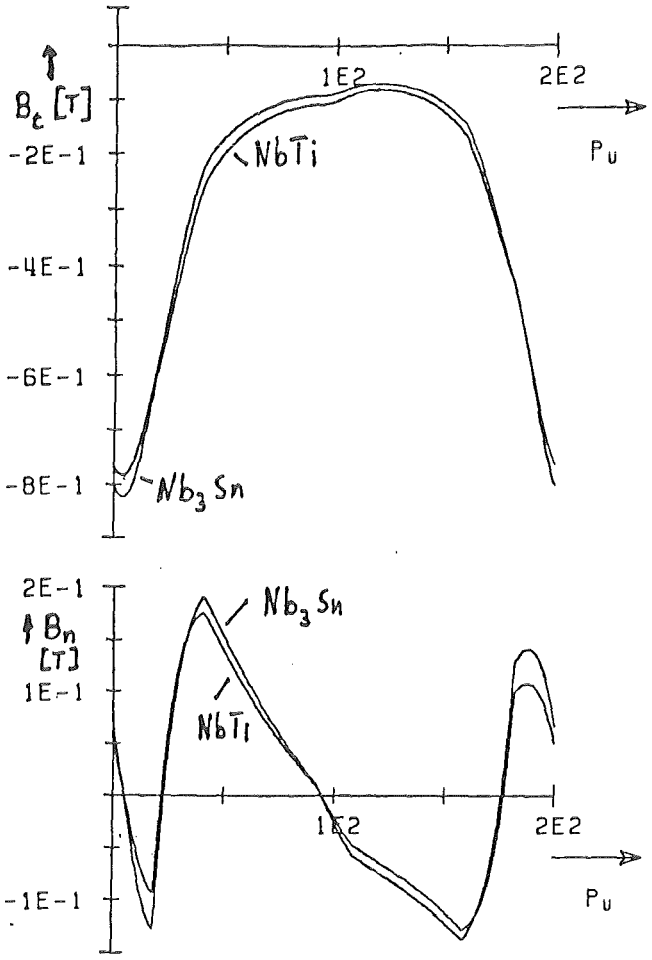

Fig. 11 Plasma induction components on the subcoils (t = 211 s)

1.1.4.5 Ac-losses in the conductors due to the poloidal induction

The ac-losses in the TF coil windings were estimated. Values are given in Table XI for the case of the recommended conductors.

Table XI. Ac-losses in the subcoil windings [J/m pulse]

Losses due to	NbTi	Nb_3Sn
- hysterisis	1.0	0.075
- eddy currents in copper	1.8	2.5
- cable coupling	0.5	1.6 - 16 (depending on the contact resistance)
- longitudinal losses	0.18	0.02
	3.5	4.2 - 18.6

1.1.4.6 Field Ripple Contour

The calculations of the field ripple contour which are of importance for the plasma physics performance, can be summarized by Fig. 12.

At the outer plasma edge the ripple is $\delta \simeq \pm$ 1%. The plasma shape in Fig. 12 is an approximate indication.

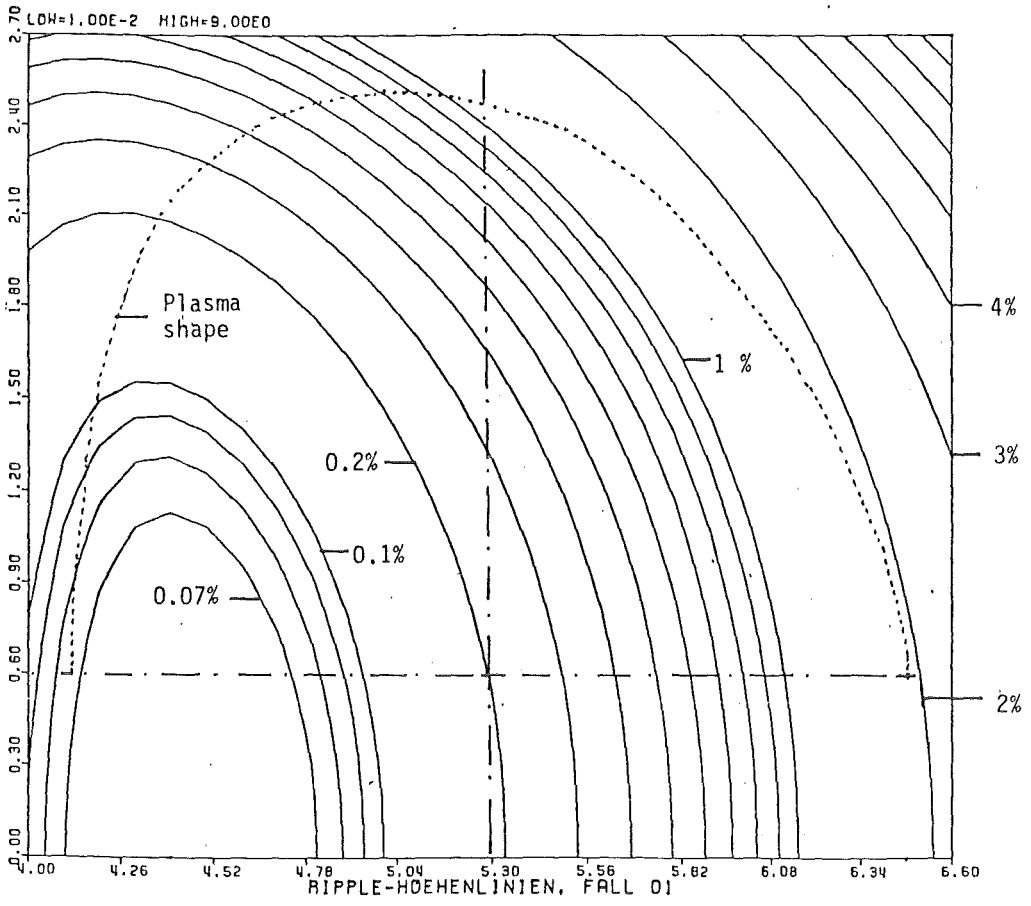

Fig. 12 Field Ripple Contour Plot

The ripple equation used for the contour plot is

$$\Gamma = 2 \cdot \frac{B_{max} - B_{min}}{B_{max} + B_{min}} ,$$

with $\Gamma \simeq 2 \cdot \delta$.

1.1.4.7. Field calculations with the code EFFI

The code EFFI (Electromagnetic Fields Forces and Inductances), originally written for a CRAY-1 machine, has been implemented for an IBM-370 machine and is now available at KfK. An input generator for a TOKAMAK coil configuration has also been developed at KfK.

It was thus possible to complete and check the calculations of fields and forces, which until now were executed with the HEDO code.

Fig. 13 shows the INTOR coil configuration generated by the EFFI plot routine.

Fig. 14 represents the induction at the horizontal midplane of the TF coil vault as function of the radius.

The coil cross section is assumed to be rectangular in the vault for reason of simplicity. The centering force support plate thickness is 10 cm instead of 20 cm in the cylindrical vault, so that the maximum induciton of the NbTi subcoil is lower compared to the cylindrical case. (see fig. 3)

Fig. 15 and 16 show the constant induction contour plots at the horizontal midplane of the TF coil assembly and at the vertical midplane of one TF coil, respectively.

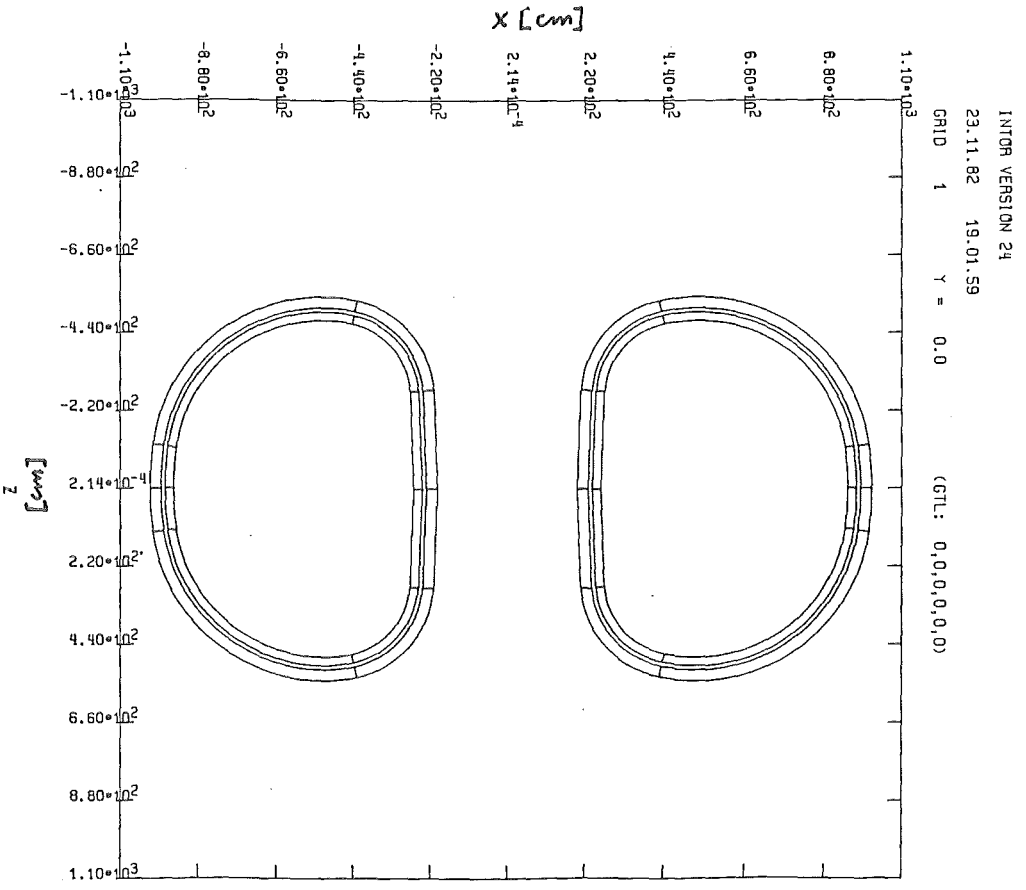

Fig. 13a INTOR coil configuration generated by the EFFI plot routine, vertical cross section

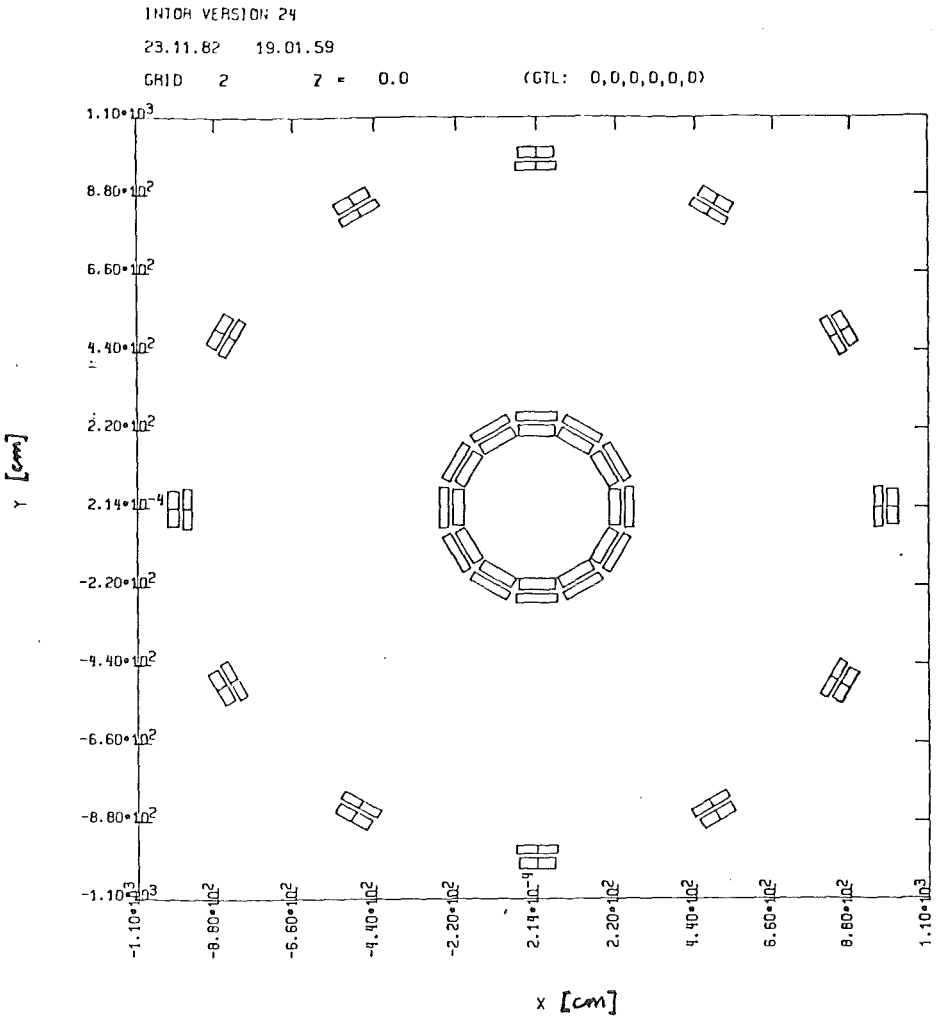

Fig.13b Horizontal cross section of the INTOR coil configuration

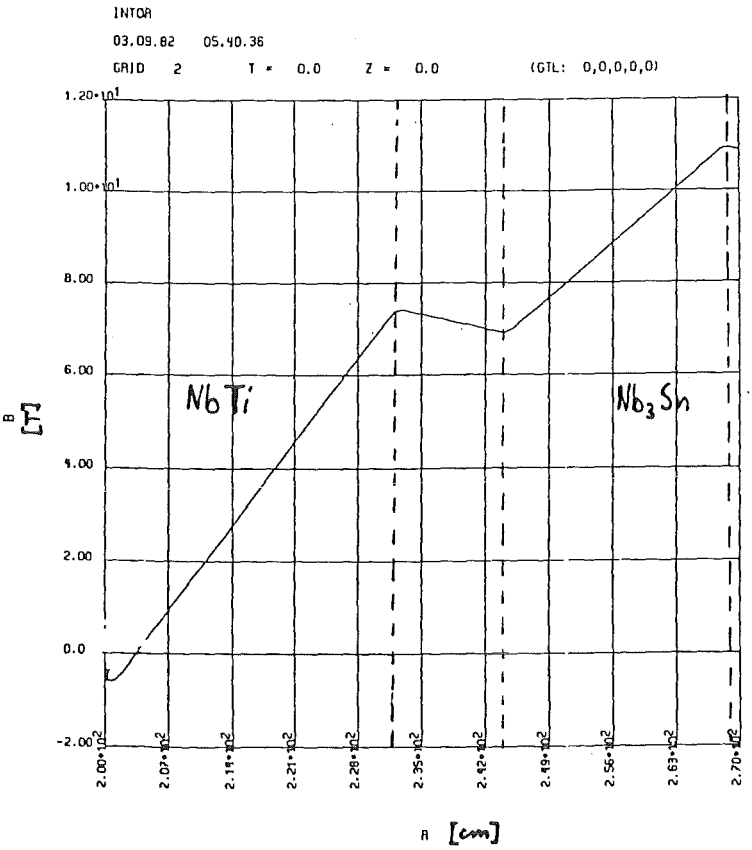

Fig.14 Induction B at the horizontal mid-plane of the inner TF coil leg as function of the radius R

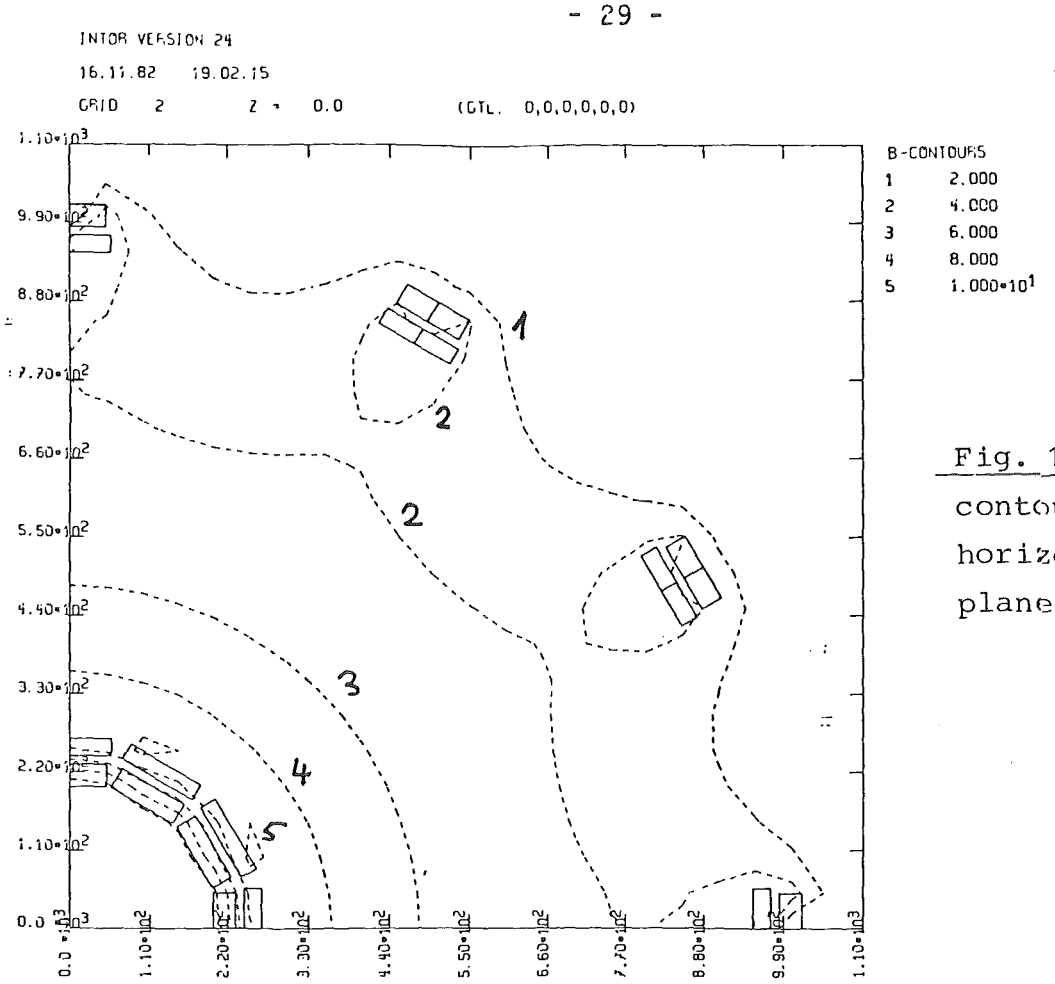

Fig. 15 Induction contour plot at the horizontal mid-plane

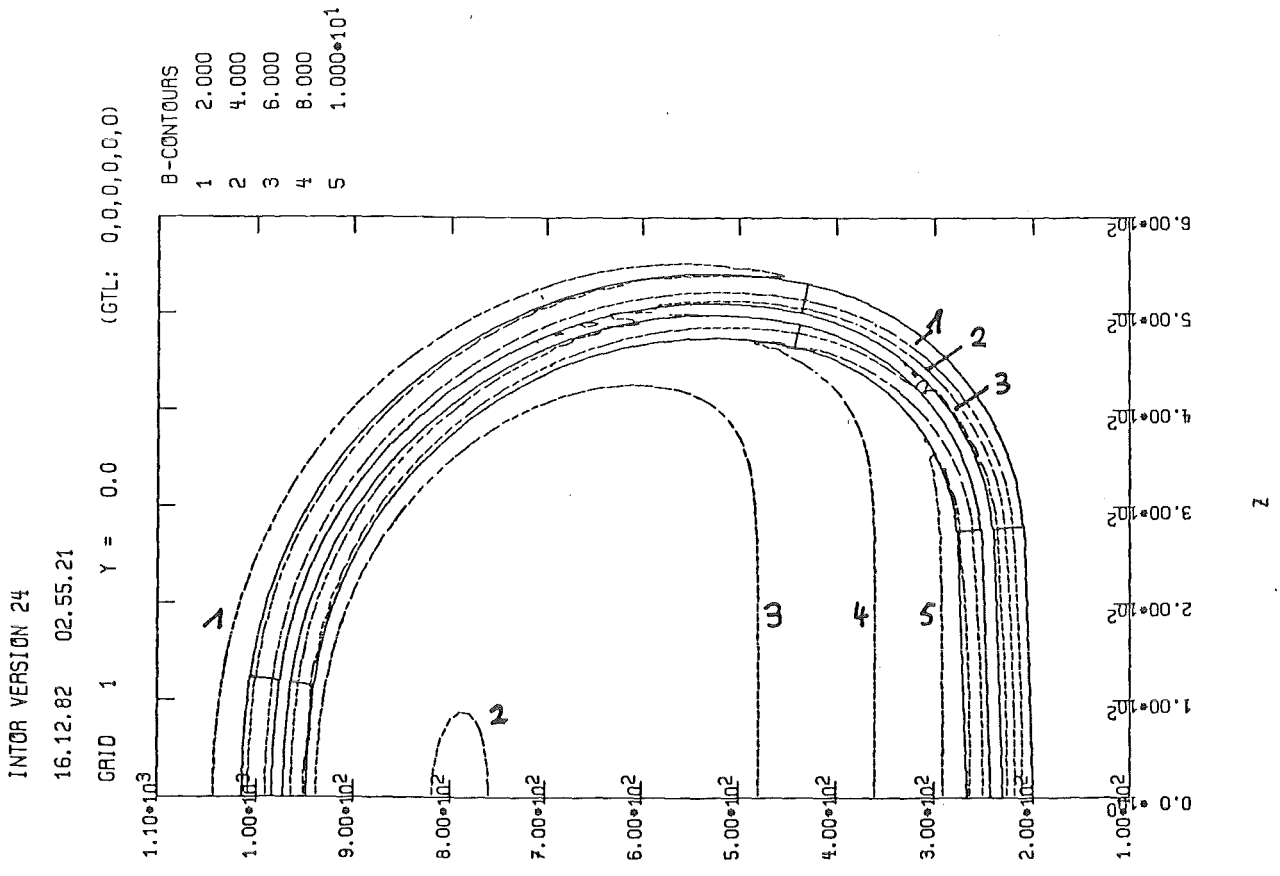

Fig.16 Induction contour plot at the vertical midplane

1.1.5 Conclusions

The basic assumptions in the coil design to have free access to the OH coil and to separate the winding package give severe complications in the winding package design in the vault region (transition from cylindrical to rectangular coil cross section). The vault itself in fact is a double vault. The main advantage of this concept is the limitation of the forces in the NbTi part of the coil (vault region and hoop stresses). There might be some troubles from the rather high hoop stress level in the outer leg of the Nb_3Sn subcoil. Further investigations including asymmetric load cases and the poloidal forces are necessary to assure the chosen concept.

1.1.6 References

/1/ R. Flükiger, W. Goldacker and W. Specking,
Presented at ICMC 9, May 1982, Kobe (Japan),
to be published in Adv. Cryo. Eng.

1.2 Toroidal Field Coil Design Concept Evaluation*

* With kind permission of the authors,

J. D. Elen, ECN Petten, NL;
N. Sacchetti, ENEA Frascati, I;
G. Véscey, SIN Villingen, CH.

The following chapters 1.2.1, 1.2.2, 1.2.3 are taken from the SULTAN-Group contribution to the INTOR Phase IIA workshop /1/ in order to have a better possibility for comparison with this KfK Study.

1.2.1 INTRODUCTION

Three different INTOR-TF-conductor designs were investigated by the SULTAN-Group.

Two conductors ENEA (1.2.3.2) and ECN (1.2.3.3) are fitted to the KfK reference coil design matching the available winding space in the corresponding coil case. The third design SIN (1.2.3.1) is based on an alternate TF coil concept described in section 1.2.2 which has been evaluated by SIN.

1.2.2. SIN TF-COIL DESIGN ALTERNATIVE

An alternate design having sufficient stainless steel reinforcement in the conductor to support the in-plane-loads is presented in the following sections. Main advantages of this design are:

- considerable reduction of AC-losses due to elimination of coil case
- high current density and corresponding reduction of coil cross section.
- minimization of mechanical stresses due to optimization of coil shape
- no electrical and hydraulic connection inside the coil.

The required magnetic field of 5.5 T at the plasma axis is obtained by energizing a copper stabilized Nb3Sn hollow conductor with a current of 24 kA. The cooling is provided by forced flow of supercritical Helium. Since hydraulic and electrical connections inside the coil are very difficult because of the limited space available, the SIN solution is to use only one grade of superconductor, with one Helium inlet and outlet in each pie. This solution has only minor economic disadvantages since the conductor costs are a small fraction of the total magnet costs.

Figure 1.2.-1

INTOR - CH

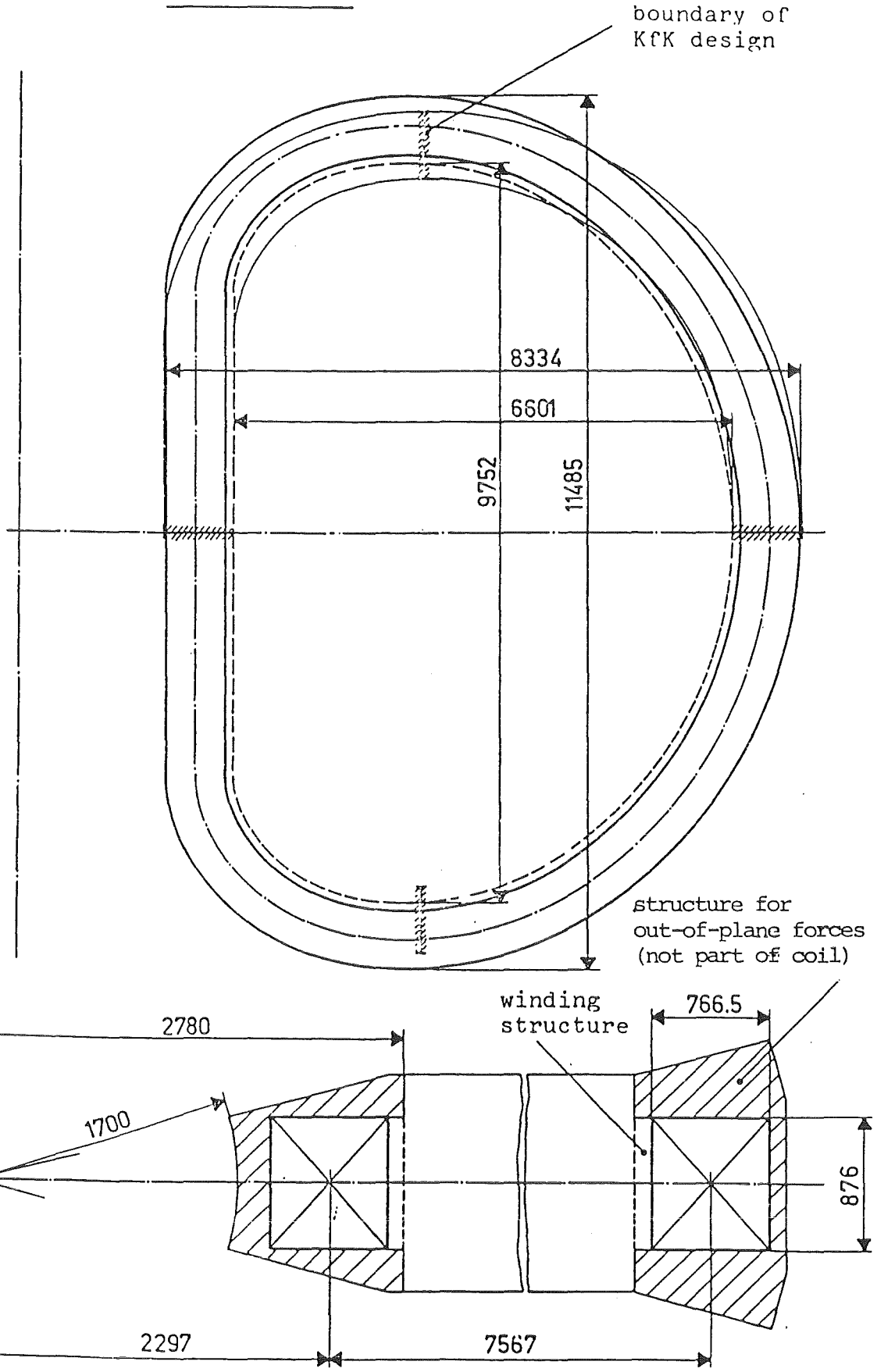

27.9.82

SIN-coil characteristics

Max. Field at Conductor [T]	~11.5
Operating Current [kA]	24
Grading Concept	1 Grade
Superconductor Material	Copper Stabilized Nb3Sn
Cooling	Forced Flow of Supercritical Helium
Conductor Cross Section [mm^2]	36.5 x 36.5
Number of Turns	504
Number of Pies	24
Number of Turns per Pie	21
Conductor Length (one Pie) [m]	632.1

In order to minimize the mechanical stresses resulting from the electromechanical loading (in-plane forces), the shape of the coil center-line was optimized as a constant tension curve, corrected to include the magnetic field deviation from the ideal torus to the 12-coil sectored array. This D-shape curve has minimum and maximum bending radii of 1.95 m and 5.87 m respectively. The coil configuration is shown in Fig. 1. In spite of one minor deviation from the dimensions set up by the INTOR Design Group - the external coil size on the y-axis is 11485 mm instead of 11080 mm, the shape of the SIN coil is deemed to be an optimal and feasible compromise between structural and geometrical constraints.

The conductor as described in section 3.1, insulated by a multilayer glass tape, will be wound 21 times into a pie. All 24 pies will then be vacuum impregnated to form a monolytic block.

According to preliminary estimations (see next Section), based on the assumption of pure tension (no bending) and taking into account the out-of-plane forces due the the poloidal field, the stresses in the conductor steel jacket and in the epoxy insulation are such that the winding package is self-supporting. This implies that no structural case is needed for the coil. A check of this result is now in progress with an accurate 3-dimensional finite element stress analysis. If needed, structural reinforcement will be added locally in the critical areas.

1.2.3. CONDUCTOR CONCEPTS

1.2.3.1 SIN-conductor

As discussed in detail in /1/, current density at nominal and quench conditions, coil geometry (bending radius), electro-thermal and mechanical stability, cryogenic loads, production considerations and costs are the requirements on which the selection of the SIN-INTOR conductor was based. It is a three-stage cable of Nb3Sn strands cabled around a central cooling tube and enclosed together with copper stabilizing strips in a stainless steel jacket (Fig. 1.2.-2). The purpose of this jacket is to withstand all the in-plane loads and the integral reaction of the out-of-plane loads due to the poloidal field. Because of the compact dimensions of the coil, it was possible to increase the steel cross section by 20%, with a corresponding stress reduction. SIN-Conductor geometry is given in the next Table:

SIN-Conductor

Overall dimensions [mm^2]	36.5 x 36.5
Cross sections [mm^2]	
Total	1332
Nb3Sn + Bronze	109
Copper	200
Stainless Steel	659
Insulation	123
Solder	191
Helium	50

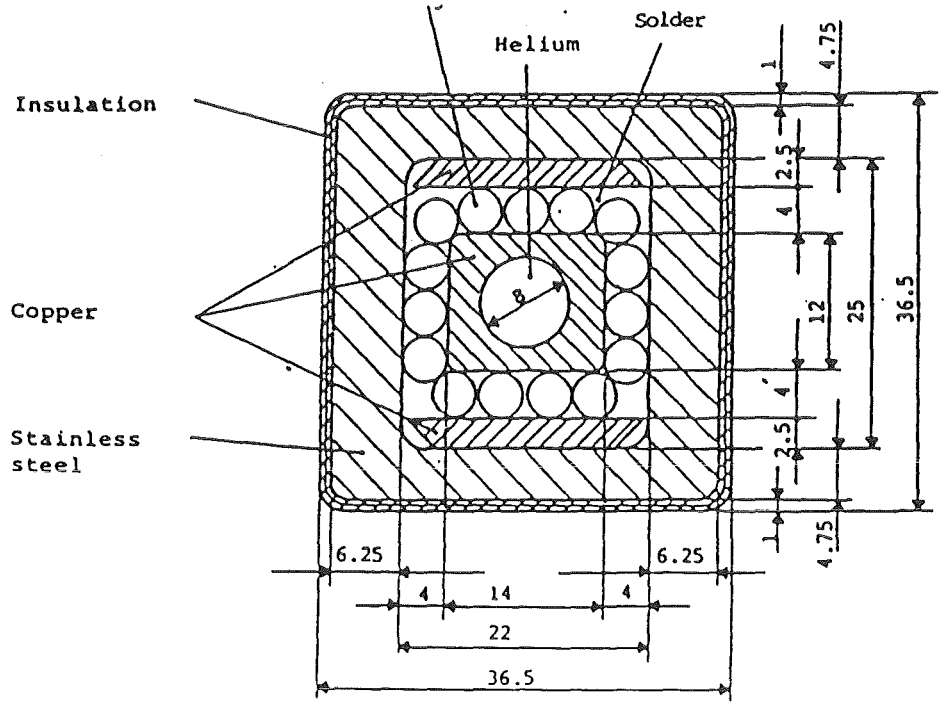

Figure 1.2.-2: SIN-Conductor

The fabrication process includes six operations: (1) manufacturing of the basic strand, (2) production of the three-stage subcable, (3) cabling and compacting the subcable around the central tube, (4) reaction heat treatment, (5) soldering of the copper strips and (6) insertion of the conductor into the steel jacket and welding.

1.2.3.1.1 conductor stresses

The stresses in the conductor components were estimated assuming pure tension (no bending) and taking into account only the out-of-plane forces due to the poloidal field. Some results are presented below with the tolerable static and dynamic (for 10^6 load cycles) stress limits at 4 K shown in parenthesis. All values are in [N/mm^2].

Steel Jacket	
Hoop Stress	420 (900/400-500)
Compression due to in-plane forces	212 (900/400-500)
Compression due to out-of-plane forces	140 (900/400-500)
Epoxy	
Contact Pressure due to in-plane forces	73 (400/180 a)
Contact Pressure due to out-of-plane forces	37 (400/180 a)
Shear Stress	32 (100/ b)

(a) dynamic value at 77 K
(b) static value measured/dynamic value not available

1.2.3.1.2 conductor cooling

All 24 pies are cooled in parallel by forced flow of supercritical Helium. Each pie has the inlet at the inner ring and the outlet at the outer ring. The cooling characteristics which provide adequate temperature margins for steady-state operation are the following (for one pie):

Length of Cooling Channel (average) [m]	632
Pressure Drop [atm]	7.5
Mass Flow Rate [g/s]	22.4
Reynolds Number x 1000 [-]	650
Flow velocity [m/s]	2.8
Steady State Heat Transfer Coeff. [$W/m^2/K$]	3075

1.2.3.1.3 quench characteristics

The quench characteristics of the SIN conductor presented in /1/ were updated to take into account the larger conductor steel cross section and the new length of the cooling channel. The latter effect is responsible for the only signifi-

cant difference in the results, namely the increase of the max. pressure. All quench characteristics, which are summarized below, are not critical.

Discharge Time Constant [s]	20
Discharge Voltage [kV]	11
Max. Pressure [atm]	145
Max. Temperature [K]	70
Max. Mass Flux [Kg/s	6

1.2.3.1.4 AC losses

Calculated losses for non-irradiated conductor and coil are listed in the table below. A twist pitch length of 180 mm was assumed for the last cabling stage. If the conductor is exposed to nuclear radiation, the AC-losses drop, since the copper resistivity increases. Total magnet losses are ~0.7 kW or 8.7 kW for the complete torus. The values [W/m] are given in the high field region, in the low field region and averaged over the magnet, respectively:

(dP/dl)max	4.0	10.0	8.0
(dP/dl) a	0.31	0.77	0.62
(dP/dl) b	0.024	0.06	0.136

(a) averaged over one winding length
(b) averaged over one winding length and total cycle time (246 s).

1.2.3.1.5 temperature margin

The increase of temperature in the conductor (metal and Helium) due to frictional and AC losses and to the thermal resistance of the copper tube were calculated assuming quasi-stationary conditions and neglecting the transversal effects in the superconductor. The results have shown that the minimum temperature margin - difference between saturation and conductor temperature, occurs in the first winding and is in the range 0.65-0.85 K. Because of high flow velocity no more than one poloidal field cycle is 'active' at one time along one pie length. The maximum temperature margin is approx. 10 times higher (~8.5 K) and occurs near the Helium outlet, where the magnetic field changes sign. For lower Helium flow rates the minimum temperature margin is further reduced, while still occurring in the first turn (ie. for P=2.5 atm, 0.35-0.65 K)

1.2.3.1.6 stability

Previous LCT-CH stability studies have shown that in forced flow conductors the Helium contribution to the conductor stability is usually very small for disturbance durations up to approx. 10 ms. In this case it reasonable to approximate the critical energy of the conductor with the total heat capacity of the composite materials. For the INTOR conductor these values are given in the following table:

Field [T]	Critical Energy [J/m]	
11.5	28.4 (a)	17.5 (b)
8.0	107.1 (a)	65.6 (b)

(a) not including the effects of AC losses
(b) including the effects of AC losses

These results are in good agreement with a more detailed stability analysis performed for a disturbance length of 50 cm, for disturbance durations up to 100 ms. These results were updated with respect to the ones presented in /1/. As a comparison it can be pointed out that the amount of energy that can be absorbed by the conductor without a quench is approx. 15 times higher for the INTOR conductor at 11.5 T than for the Swiss LCT conductor at 8 T.

1.2.3.1.7 current density

All values are given in [A/mm^2].

Overall	18.0
Conductor (metal)	20.7
Copper	120.0

1.2.3.1.8 potential fabrication problems

The manufacturing route assumed for the Nb3Sn conductor is the 'external diffusion' technique. The development of the multifilamentary conductor strand was completed at BBC in 1981 and only the wire fabrication in long unit lengths with reproducible properties has to be proved.

No unusual manufacturing problems are expected in the production of the three-stage subcable and the cabling process around copper cooling tube. This operation is partly based on the experience gained from the fabrication of the Swiss LCT conductor. Subsequent to this step, the actual design considers the reaction heat treatment of the conductor.

In order to check the critical current behaviour of the reacted conductor during the subsequent operations a series of handling tests (bending, tensile and compressive stresses) has to be performed. A special soldering machine has to be developed in order to join the conductor components together. The penetration of the solder into the already diffusion-soldered cable has still to be investigated.

A critical fabrication step could be the insertion of the reacted conductor in the steel jacket followed by welding. This operation has to be preceded by extensive research work to develop a special tooling for continuous operation and optimal welding technique. Several metallurgical problems, including diffusion soldering between conductor components or the mechanical stability of the solder bond during bend straining as well as the hydraulic and electrical connection techniques between pancakes have to be investigated. An open question is the effect of the location of the copper within the subcable on stability. Finally, the effect of stress cycling on the hysteresis loop of the multicomponent conductor (heat generation) has to be investigated.

1.2.3.2 ENEA-conductor

In the figure below a schematic drawing of the proposed conductor is shown. It consists of a superconducting flat cable cooled by means of forced flow of supercritical He.

Its structure is as follows:

a) Sub-strands 0.54 mm in diameter containing 361 20 microns Nb3Al filaments.

b) Strands obtained by cabling 19 sub-strands. The diameter of a strand is 2.8 mm while its twist pitch is 15 mm.

c) Final flat cable made of 32 strands + 8 dummy copper wires in a coaxial Rutherford cable structure - its twist pitch is 14 cm.

The cable is then soldered between six copper tubes as shown in the figure. Insertion of resistive barriers, in order to keep AC-losses at a minimum level, is foreseen among the strands and among the copper tubes.

Overall dimensions [mm^2]		31 x 32
Cross section	[mm^2]	
	- Nb3Al	69
	- copper	521
	- stainless steel	62
	- helium	231

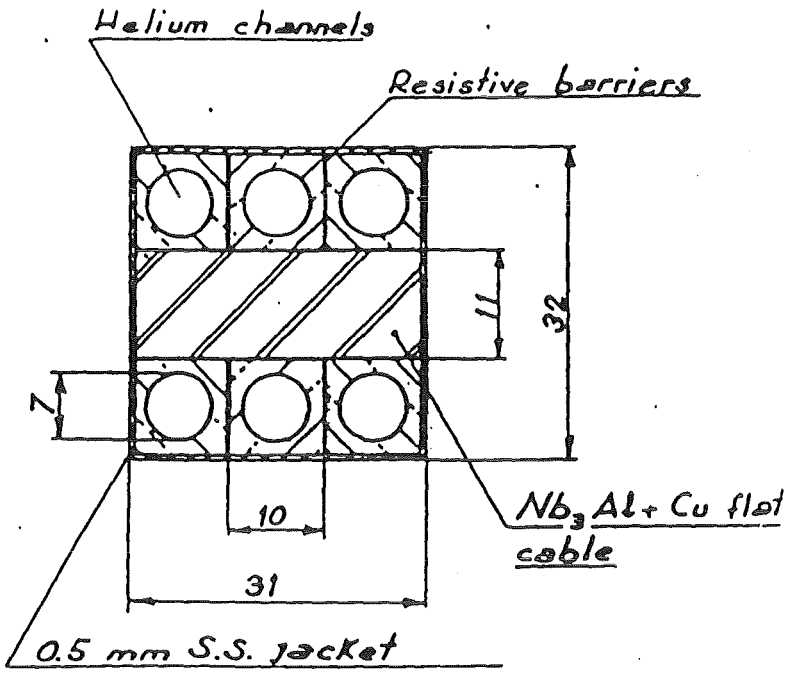

Figure 1.2.-3: ENEA-Conductor

1.2.3.2.1 losses

The losses have been calculated taking into account the different losses mechanisms as well as the poloidal field distribution.
The total losses per cycle averaged over the whole A-15-coil are then 74 W. Therefore, the total losses per cycle for all three coil sections result to be about 0.44 kW, that means 5.3 kW for the 12 INTOR coils.

1.2.3.2.2 stability

a) Adiabatic

The adiabatic stability is assured when the filament diameter is less than 110 ÷ 120 μ. The sub-strand twist pitch of 3 mm enable us to have a very weak coupling among filaments as the critical length is such that $2\ell_c$ = 7.2 mm.

b) Cryogenic

In the case of a quench when all the current is carried by the copper the resulting heat transfer to helium is q = 0.39 W/cm^2. This figure, even if it is not loo low, can be handled in principle by a suitable choice of the cooling parameters.

- current density

Overall 21.4 A/mm^2

1.2.3.2.3 fabrication problems

a) sub-strand fabrication
The technology is well established in principal and long lengths can be produced with reasonable reliability - their tests can be considered as a normal laboratory routine provided a 10 to 12 T magnet of small dimensions is available.

b) strand fabrication
This successive step is somewhat more complicated but it should exhibit problems similar to those which have already been solved for manufacturing Nb-Ti strands - their test, however, will require high field facilities of rather large size as experiments on significant length have to be performed with limitation in the maximum bending.

c) soldering
Soldering of the strand is necessary both for preventing sub-strand movemt. and for relatively good thermal contact. This is a rather delicate aspect as soldering must be made on the already reacted strand with all the well known problems related to the brittleness of Nb3Al.

d) the hollow conductor
The final hollow conductor is realized by soldering six parallel square copper tubes to the flat rectangular cable and by encasing the conductor with a thin stainless steel sheet for the sake of compacteness.
A possible alternative to this method, particularly useful if monolithic cable is used, is to encase the conductor with the stainless steel sheet without heat treatment and soldering, then to pass the whole through a die to give it the appropriate dimensions and a certain degree of mechanical compaction. The subsequent heat treatment could assure sufficient thermal contact among different parts a consequence of self diffusion of copper. The obvious big advantage of this method is that heat treatment necessary for the formation of brittle Nb3Al is performed on the finished hollow conductor.

d) resistive barriers
Our design foresees the insertion of suitable resistive barriers inside the conductor. A question arises concerning how to realize these barriers. Cu-Ni alloys are commonly used for these purposes, however, as a consequence of the high temperature heat treatment, there is the possibility that nickel contaminates the copper matrix by diffusion. At the present stage this problem needs further clarification and the possibility of using some different material is also to be considered. For our calculations we have assumed that we are able to make suitable resistive barriers with properties similar to those of Cu-Ni.

1.2.3.3 ECN-conductor

The ECN-conductor which is matched for use with the KfK-housing is a cryostable conductor based on the ECN powder metallurgy Niobium-Tin technique only 4.3 % of the conductor area is reserved for Niobium-Tin and powder. The critical current of the conductor is 42.9 kA at 12 T and 5 K, whereas the operational current is 24.3 kA at 11.5 T. The conductor is wide (50 mm) and flat (20 mm) in order to keep the bending strain on the Niobium-Tin material low and to have a large surface available for heat transfer to the coolant (s. Fig. 1.2.-4). Since most of the stabilizing copper will be added to the conductor after reaction heat treatment cold worked copper may be used contributing a great deal to the mechanical stresses.
The superconducting material is wrapped around a CrNi-core: the 38 elements of this cable are 2.15 mm in diameter. Each element coprises 6 Nb3Sn strands and 1 copper strand: each Nb3Sn strand comprises 36 filaments with an outer diameter of 81.10^{-3} mm. The material cross sections for the ECN-conductor are:

	[mm^2]
Overall cross section	20 x 50
Nb3Sn + powder	43
copper	498
stainless steel + CrNi	165
helium	240
solder	40

The fabrication process includes:

- manufacturing of the basic strand
- production of the basic strand
- compaction of this subcable
- wrapping the subcable around the CrNi-core
- heat treatment
- soldering conductor core to stabilizing copper
- welding of stainless steel jacket

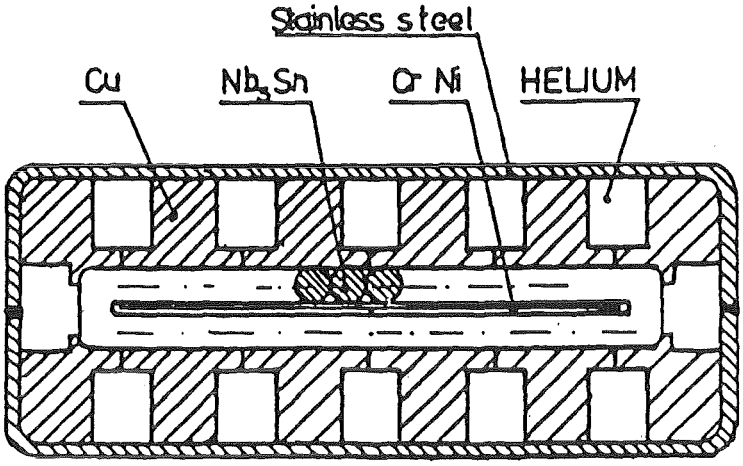

Figure 1.2.-4: ECN-Conductor

1.2.3.3.1 stresses and strains

Since in the chosen conductor concept main part of the Lorentz-forces is taken by the coil casing, the definite geometry of this casing defines the exact stress level within the conductor. There is some confidence that the axial conductor strain can be limited to about 2.10^{-3}. Bending strain in the conductor during coil winding can be limited to 1.3×10^{-3} (minimum bending radius of 1.99 m).

1.2.3.3.2 conductor cooling

The Nb3Sn coil is forced-flow cooled by supercritical helium entering the coil at 4.5 k. There are 5 sets of 4 pancakes which are connected hydraulically are:

length of 1 coolant channel	4 x 285	m
pressure drop	0.21	MPa
total massflow rate	5 x 28.8	g/sec
Reynolds number	112000	
coolant velocity	0.8	m/sec
steady state heat transfer coefficient	742	w/m^2k
equivalent diameter	4.44	mm

1.2.3.3.3 quench characteristics

Due to a relatively large fraction of copper and coolant within the conductor the quench characteristics are uncritical and a large discharge time constant may be used.

discharge time constant	55	sec
discharge voltage	4	kV
maximum temperature	34	k

1.2.3.3.4 AC-losses

The estimated AC-losses averaged over one cycle for one Nb3Sn TF-coil are:

hysteresis losses	47	watt
coupling losses	70	watt
eddy current losses	85	watt
TOTAL	202	watt

1.2.3.3.5 conductor stability

By using a flat conductor with a large surface-volume ratio the conductor can be made cryogenically stable against thermal disturbances. The dissipation during local quenching amounts 880 W/m. Adiabatic and dynamic stability is attained easily even for filaments with a diameter of 81 um, since the Niobium-Tin filaments are surrounded by pure high-conductivity copper.

1.2.3.3.6 current densities

	[A/mm^2]
Overall current density (winding region)	17.6
Conductor current density (metal)	23.7
Nb3Sn + powder current density	544
Copper current density	47

1.2.3.3.7 potential fabrication problems

Key element in the fabrication of the Nb3Sn-conductor is the brittle nature of the Nb3Sn-material. A second element in the fabrication is the reacting process needed to form the Nb3Sn.
For INTOR-size coils the only feasible fabrication sequence will be the react and wind procedure. As the INTOR TF-conductor is a highly stressed conductor it will be an advantage to have the stabilizing copper and the stainless steel in a state in which it can contribute its utmost to take the electromagnetic forces; this demands for a solution in which the superconductor itself is reacted before assembly with stabilizing material and stainless steel. Furthermore, it offers the opportunity to have a solder-bond between the materials used. As far as can be seen now, there is not a principal restriction with regard to fabrication and operation of the Nb3Sn INTOR TF-conductor.

1.2.4 Comparison of Alternate Conductor Approaches

High T_c values and upper critical fields at 4.2 K, but also economical aspects make the materials Nb_3Sn and Nb_3Al promising candidates for INTOR-coils with magnetic field $\geq$11 Tesla. Both materials being very brittle, particular fabrication procedures are required for obtaining multifilamentary composite wires. The commonly used technique at present is the so-called bronze process, but other fabrication processes, e.g. external diffusion, ECN powder technique and the ENEA jelly roll technique have also been developed to an industrial level. A common feature of all these techniques is the reaction heat treatment at temperatures between 700 and 800° C at the end of the wire drawing process. Due to the large dimensions of INTOR, the reaction heat treatment will preceed in each case the coil winding (react and wind process), provided that the location of the strands allows low bending strains. In order to keep the mechanical stresses during operation below 0.2 %, an appropriate steel reinforcement has to be added to the conductor, either before or after the reaction heat treatment. Additional aspects are a) the influence of mechanical prestress on the current carrying capacity (this influence is enhanced by the presence of reinforcing steel), b) AC-losses, which determine the He consumption and depend on the conductor configuration as well as on the relative fractions of superconductor, stabilizing Cu, structural material and insulating layers, c) thermal stability (prevention of quenches) and d) transmission of forces between structural materials (in conductor and case) and superconductor. Based on the present knowledge, the construction of an INTOR coil appears to be feasible, but several points of the above mentioned aspects and manufacturing processes need further investigation. Different proposals have so far been studied in the European Community (see Fig. 1.2.-5 and Table 1.2.-1).

ENEA-Conductor

The proposed conductor consists of a flat Nb_3Al based cable cooled by means of forced flow of supercritical helium through six parallel channels symmetrically located with respect to the superconductor. The realisation of the flat cable is made in three subsequent stages:

a) fabrication of sub-strands by mechanical processing, with the so-called "jelly-roll" method, the Nb-Al filaments embedded in a copper matrix down to the required diameter;

b) fabrication of strands by cabling together 19 sub-strands;

c) final cabling of 32 strands and subsequent shaping to the flat rectangular geometry.

The flat cable and six copper tubes are then sheated with a thin stainless steel jacked and a final passing through a die is made in order to give good mechanical compaction. Moreover, resistive barriers are inserted around the strands and among the copper tubes. The hollow conductor is then reacted at about 800° C to form the Nb_3Al compound. Heating at high temperature should result also in a good thermal contact among different parts. The most relevant aspects of the proposed solution can be summarized as follows: i) relatively easy construction; ii) helium tightness problems devolved to copper tubes, avoiding any soldered conduit; iii) heat treatment performed on the final hollow conductor.

ECN-Conductor

ECN has given preference to a wide (50 mm) and flat (20 mm) conductor in order to keep the bending strains on the Nb_3Sn-material low and to have a large surface available for heat transfer. The conductor is matched for use with the KfK-housing.

The cryostable conductor is based on the ECN powder metallurgy Niobium-tin technique. Due to a superior performance of material made by this technique only 4.3 % of the conductor area is reserved for Niobium-Tin and powder.

Operating the conductor at 24.3 kA at 11.5 t and 5 k the current density for the Niobium-Tin and powder area is 544 A/mm^2 , leaving ample margin for possible strain degradation.

Adiabatic and dynamic stability are easily attained since the superconducting filaments are surrounded by pure high conductivity copper.

The superconducting material is wrapped around a Cr-Ni-core: the 38 element of this cable are 2.15 mm in diameter. These subcables are first stage cables each containing 6 basic strands and 1 copper strand. The basic strands contain 36 filaments of 81 µm. After reaction heat treatment the cable will be solder filled and the cold worked stabilizing copper will be soldered to it. After soldering the stainless steel will be added to the assembly and the conductor will be leak-tight closed by two welds in the neutral zone.

The conductor will not be strained beyond $4 \cdot 10^{-3}$ bending and magnetic forces. The AC-losses averaged over one cycle may be limited to 0.2 kW for 1 TF-coil. A total helium massflow rate of 144 g/sec at pressure drop of 0.21 MPa is needed for cooling one TF-coil: the inlet temperature has to be 4.5 k. The quench characteristics are not critical.

SIN-Conductor

The SIN conductor proposed for INTOR is representing an attempt to distribute the structural material needed to withstand the inplane loads in order to eliminate the AC losses generated in a thick-wall coil case.

As discussed in detail in /1/, current density at nominal and quench conditions, coil geometry (bending radius), electro-thermal and mechanical stability, cryogenic loads, production considerations and costs are the requirements on which the selection was based. It is a three-stage cable of Nb_3Sn strands cabled around a central cooling tube and enclosed together with copper stabilizing strips in a stainless steel jacket (Fig. 1.2.-2). The purpose of this jacket is to withstand all the in-plane forces and part and the out-of-plane forces due to the poloidal field. Conductor geometry is given in the next table:

Overall dimensions [mm^2]	36.5 x 36.5
Cross sections [mm^2]	
Total	1332
Nb_3Sn+Bronze	109
Copper	200
Stainless Steel	659
Insulation	123
Solder	191
Helium	50

The fabrication process includes six operations: (1) manufacturing of the basic strand, (2) production of the three-stage subcable, (3) cabling and compacting the subcable around the central tube, (4) reaction heat treatment, (5) soldering of the copper strips and (6) insertion of the conductor into the steel jacket and welding.

KfK-Conductor

Based on experimental investigations on the behaviour of J_c in Nb_3Sn as a function of steel reinforcement (added either before or after the reaction heat treatment), the following criteria for the KfK-INTOR conductor have been used:

a) Simultaneous annealing of conductor and reinforcing steel (no soldering), b) Additions to Nb_3Sn (Ta,Ti,Ni + Zn,..) for counterbalancing the degrading effects of reinforcing steel on J_c, c) thermal stability similar to Stekly conditions, d) minimum bending stresses (rectangular conductor), e) minimum AC losses, and f), the coil forces are transmitted to the case.

Several conductor configurations have been studied. The design is also based on the LCT-Euratom technology and fits with the NbTi conductor proposed for the low field part of the INTOR-coil. The cross section of the conductor consists of:

Superconductor + Bronze	:	123.6 mm^2	= 11.9 %
Helium conduits	:	214.8 mm^2	= 20.7 %
Copper	:	327.7 mm^2	= 31.6 %
Stainless steel	:	372.0 mm^2	= 35.8 %
(3,62 x 5,42) mm^2	=	1038.1 mm^2	= 100 %

A certain number of problems, including manufacturing aspects (presently investigated) will lead to a modified version, but the conductor parameters are still representative and can thus be used for coil design.

Ref. /1/: INTOR Phase IIA-TF coil Intermediate Reports on studies of the SULTAN group - June 1982

Not available in public; for further information contact the authors.

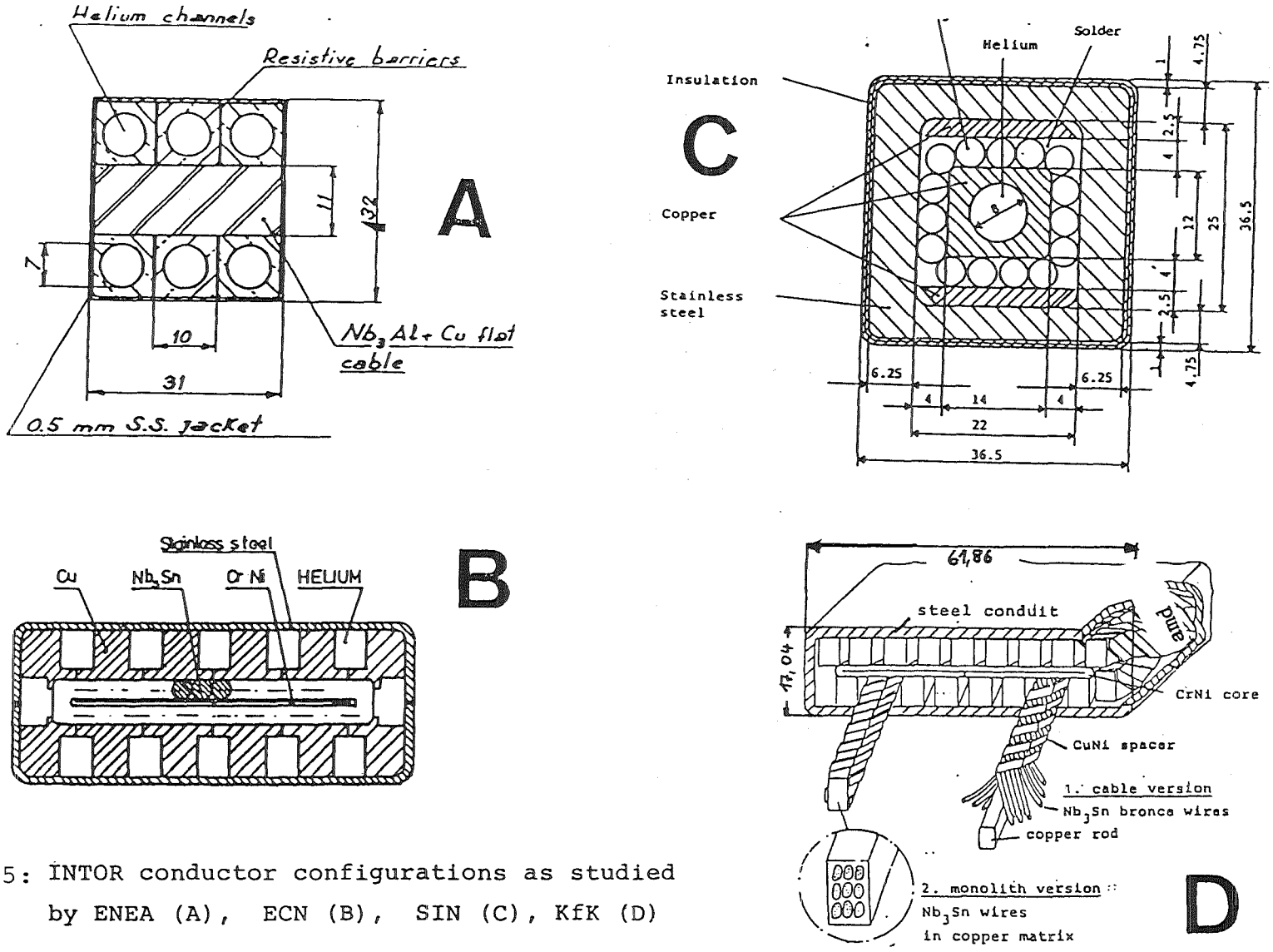

Fig. 1.2.-5: INTOR conductor configurations as studied by ENEA (A), ECN (B), SIN (C), KfK (D)

	ENEA	ECN	SIN	KfK
A-15-part of the coil				
Conductor dimensions (mm^2)	31 x 32	50 x 20	36.5 x 36.5	61.86 x 17.04
SC material	Nb_3Al	Nb_3Sn	Nb_3Sn	Nb_3Sn
Superconductor fabrication technique	ENEA Jelly Roll	ECN Powder	External Diffusion	Bronze Process
Max. field at conductor (T)	11.0	11.0	11.5	11.0
Critical current (kA), 12 T	30.2 (5 K)	36 (5 K)	37 (5 K)	60 (3.8 K)
Operating current (kA)	21.2	25	24	20.0
Conductor current density in the material without steel (A/mm^2)	27.9	30	43.6	33.3
Overall conductor current density (with steel) (A/mm^2)	22.8	25	20.0	18.7
Complete coil including NbTi parts				
Coil current density (A/mm^2) (insulation, coil structure)	10	10	18	10
AC-losses (per coil):				
- Winding (kW)	0.44	0.2	0.7	0.4
- Casing (kW)	2.3	2.3	0.0	2.3
- He mass flow rate (g/s)		420	540	430

Parameters for forced flow INTOR conductors as studied by ENEA, ECN, SIN and KfK

Table 1.2.-1

1.3 Other Studies

1.3.1 Design Criteria for Austenitic Steels at 4 K

1.3.1.1 Fatigue Endurance Limit

For high cycle numbers the fatigue endurance limit gained from S-N data can be interrelated to the threshold of the stress intensity factor ΔK_{th}, at which principally no crack propagation exists. In general σ_{Fat} is determined under a reversal of axial stress at R = -1, where R is the stress ratio $\sigma_{min}/\sigma_{max}$. For a zero-to-tension axial loading (R = 0) the fatigue stress is about 20% lower than the case R = -1. The fatigue endurance ratio σ_{Fat}/tensile strength for austenitic steels varies between 0,35 - 0,40 at ambient. Tests with austenitic 20 Cr-16Ni-6Mn steels carried out at 11 T confirm this endurance ratio.

Cryogenic austenitic materials have tensile strengths of ∿ 1500 MPa at 4 K (e. g. 304 LN, 316 LN). The fatigue strength σ_{Fat} at 4 K and R = 0 will be ∿ 440 MPa, taking into account a reduction of 20% for R = 0 and the endurance ratio of 0,35.

1.3.1.2 Fracture Mechanics Considerations

However, weldments can reduce this range drastically because of the entrapped defects during the welding process. By using the fracture mechanics an indication can be gained for the magnitudes of the stress to which a flawed member can be subjected under cyclic stress without the flaw propagating to failure. With the penny shaped crack morphology the equation $\Delta K_{th} = 2.\Delta\sigma\sqrt{\Pi.a}/\Pi$ calculates the radius a of a crack at given $\Delta\sigma$ and known ΔK_{th}. ΔK_{th} of 18/8 austenitic steels is 6.1 MPa$\sqrt{m}$ (R = 0 and at 293 K). This value will increase at 4 K to 18 MPa$\sqrt{m}$ because the tensile strength ratio between 18/8 austenitics at ambient and cryogenic 316 LN materials at 4 K is about three.

At 200 MPa almost 5 mm flaw size (a) can exist without growing to failure. The flaw size reduces to about 1.5 mm at 400 MPa. The diagnostic practice (NDT) is at present capable of detecting flaw sizes of ∿ 2 mm (2a) in weldments. Therefore with a flaw size of ∿ 2 mm one has enough margin of safety at 200 MPa cyclic load which is the INTOR maximum cyclic stress design value.

1.3.1.3 Cycle Numbers before Brittle Failure

The K_{IC} weld metal data at 4 K given in fig. 17 gives the critical boundary value above which the structure collapses under brittle failure. The calculated number of cycles to failure according to the integral equation $da/dN = C_o \cdot \Delta K^n$ at different stress ranges 1, 2 and 3 has been given for different materials in table XII. At 200 MPa stress range the number of cycles to failure are between 44,000 and 115,000 for various materials.

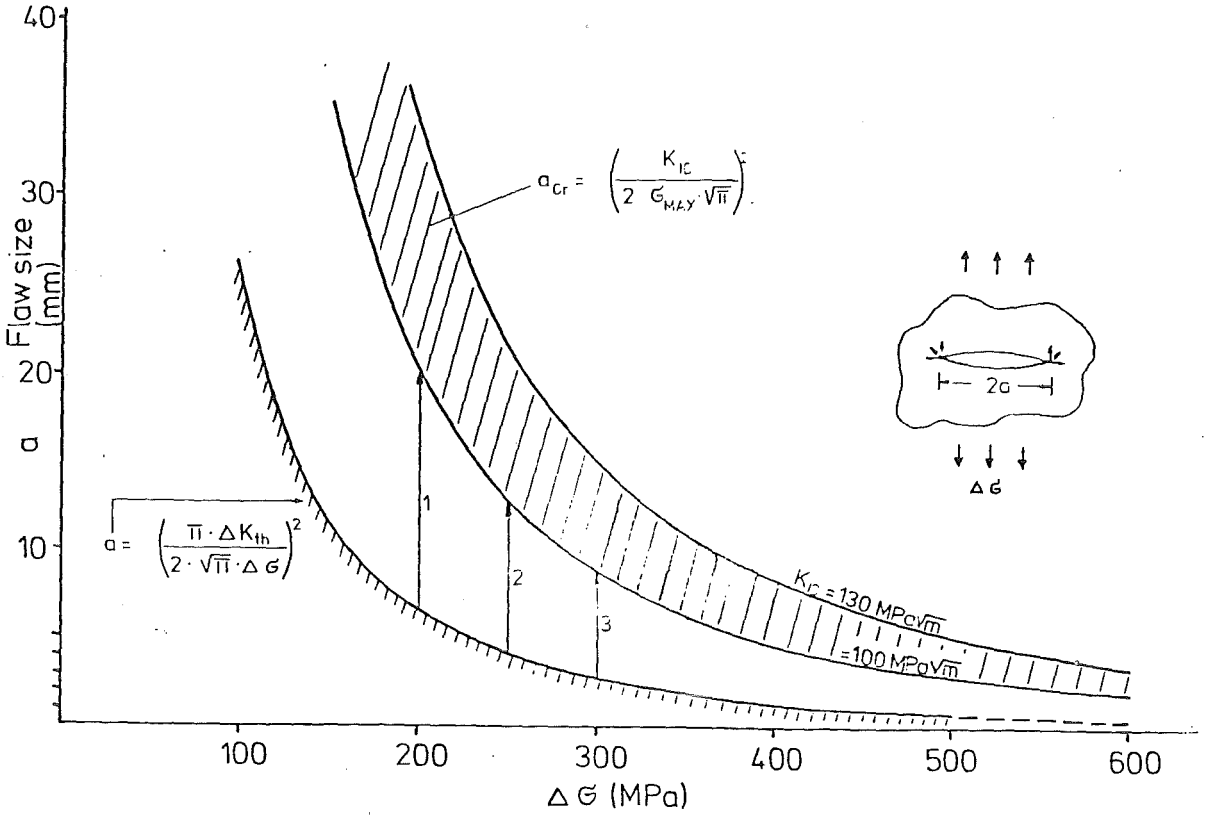

Fig. 17 Fatigue response of austenitic materials

Table XII. Calculated Fatigue Crack Growth of Different Materials at 4 K

Code	Material	$\leq \Delta K \leq$ Mpa$\sqrt{m}$	n	C_o Metric units	Number of cycles of stress range		
					200 MPa	250 MPa	300 MPa
1	316 L weld	30 - 100	3.45	5.85 - 13	44,000	29,286	19,852
2	ASTM A 637	29 - 34	7.43	1.06 - 19	88,100	60,441	40,900
3	316 LN weld	-	3.36	1.43 - 12	25,300	16,820	11,400
4	316 LN weld	40 - 100	3.86	4.77 - 14	115,170	76,783	52,090

The following investigations about austenitic steels have been performed at KfK since October 1981:

- fracture toughness measurements by J-test at 77 K and 4 K of commercially available austenitic CrNi-steels of the following series (German material numbers): 1.4301, 1.4541, 1.6903, 1.4435, 1.4404, 1.4429.
- Material 1.4429 equivalent to 316 LN has been thoroughly investigated with respect of its microstructure. Electro slag remelted TESR) forging showed a two-fold increase in fracture toughness in comparison to normal plate 316 LN at 4 K.
- Strong dependency of fracture toughness data on material fabrication (e.g. hot rolling, cold working) has been observed.
- Investigations of shielded metal arc (SMA) weldment have been performed with respect to fracture toughness and fatigue at 4 K.
- The tests reveal a strong anisotropy in case of fracture toughness. The weakest point presumably is the boundary between bulk and weld.
- Fatigue measurements of the weldments at 4 K revealed an even better performance in comparison to the bulk. Residual stresses, small slag inclusions delay the crack propagation.
- Cyclicly loaded 304 N material at 4 K (with a cycle number of 2 000 and a stress range of 60% of the yield) showed no degradation of the microstructure.
- Magnetic measurements revealed no stress induced martensitic phase transformation, whereas under plastic deformations at 4 K large martensitic transformations occur.

- Non destructive testing (NDT) of the austenitic welds with ultrasonic technique could be successfully used during the weld fabrication of the LCT case.
- Location, orientation and size of the weld defects could be well detected down to a minimum size of two millimeters in diameter.
- By standardization of the flaw shapes in weldments the application of the fracture mechanics to weldments could be successfully done.
- Evaluation of cyclic and fracture data in order to get a safe operation of the manget structure at 4 K under static and cyclic stresses resulting in principles for the use of the material at 4 K.
- The cyclic stress range of 200 MPa at 4 K for an "infinite" number of cycles had been confirmed for 316 LN material.

1.3.2 Ripple Control by the TF Coil Currents

1.3.2.1 Computation of INTOR Toroidal Field Ripple

The profile of the magnitude of the magnetic field produced by the 12 TF coils has been investigated, based upon the geometry of the actual INTOR design II A. The quantity of interest is the field ripple, defined as

$$\Gamma = 2 \cdot \frac{B_{max} - B_{min}}{B_{max} + B_{min}} \qquad (1)$$

Here B_{max} (resp. B_{min}) denotes the maximum (resp. minimum) value of the magnitude of the magnetic field on a circle around the z-axis of the machine in a plane z=const (the horizontal midplane has coordinate z=0).

The investigation consisted of two steps:
The first was to determine the relative change of currents in the TF coils necessary to create a certain edge ripple (of 6% at z=0, r = 6.5 m, r = R + a, R = main radius, a = minor radius of plasma) under the assumption that the TF coils are formed into two groups, the coils in either group having the same current deviating from the nominal current I

$$I_j = I + \Delta I_j, \qquad j = 1,2$$

according to the condition

$$\Delta I_2 = - \frac{n_1}{n_2} \cdot \Delta I_1 \qquad (2a)$$

$$n_1 + n_2 = 12 \qquad (2b)$$

Three different cases have been considered, each one having different numbers N_1, N_2 of coils in both groups: case 1: $N_1 = 6$, case 2: $N_1 = 4$, case 3: $N_1 = 3$.

The second step was to calculate lines of constant ripple for these 3 cases in the domain : 4 m <= r <= 7 m, 0 m <= z <= 3 m.

In order to get a ripple value connected with a coordinate pair (r,z), the field - and its variation due to current changes - along the circumference of a circle (r=const, z=const, azimuthal coordinate varying from 0 to 90 degrees) had to be known.

A number of small computer programs have been written; the first one, which uses the HEDO program /1/ as a subprogram, calculates the field of each single TF coil being powered by a "unit current" while all other coils have no current. In this way one gets 12 field vectors for each point in the area of interest.

The other programs perform linear combinations of these field vectors according to condition (2) giving fields B_1 and B_2 produced by the two groups of coils. From these the final field B is composed in the following way:

$$\begin{aligned} B &= B_1(1+\delta_1) + B_2(1+\delta_2), \qquad \delta_j \equiv \frac{\Delta I_j}{I} \\ &= (B_1+B_2) + (B_1+\eta B_2)\delta_1, \qquad \eta \equiv -\frac{n_1}{n_2} \end{aligned} \tag{3}$$

Thus, the field B is composed of two terms; the first one is the regular field, the second one is the correction due to current changes, depending on the particular case.

Looking only at points on the circle with r = 6.5 m, z = 0 m, one can determine the value of δ_j, which satisfies eqns. (3) and (1), putting Γ = 6%. Using the results of this calculation one can evaluate (3), determine B_{max} and B_{min} for the quarter circle belonging to any coordinate pair (r,z) and compute the ripple as a function of r and z.

Table XIII shows, for the cases considered, the value of $\Delta I_1/I$, $\Delta I_2/I$, which bring Γ to the desired value of 6% (at r = 6.5 m, z = 0 m). Obviously, the necessary current change is smallest in case 3, but not significantly smaller than in case 2. The table contains also the smallest ripple values and their positions.

Figures 18 to 20 show lines of constant ripple for cases 1 to 3. The difference in ripple from line to line is 1% in all three cases. Moreover, the line belonging to 6% ripple starts at r = 6.5 m. The point of smallest ripple is marked A.

From the figures and the table one can see that the ripple profile is less pronounced in case 3 than in case 2, and again in this case less pronounced than in case 1.

References

/1/ P. Martin, H. Preis, HEDO-2 Magnetic Field Computer Program, IPP II/34, April 1977

Table XIII

Number of coils if groups 1 and 2, relative current changes to create 6% edge ripple, minimum ripple value and its position in cases 1, 2, 3.

Case	N_1	N_2	$\Delta I_1/I$	$\Delta I_2/I$	Min. Ripple	at position
1	6	6	23.5 %	-23.5 %	1.67 %	r = 4.5 m
2	4	8	13.1 %	- 6.56%	2.15 %	r = 4.4 m
3	3	9	12.3 %	- 4.09%	2.76 %	r = 4.5 m

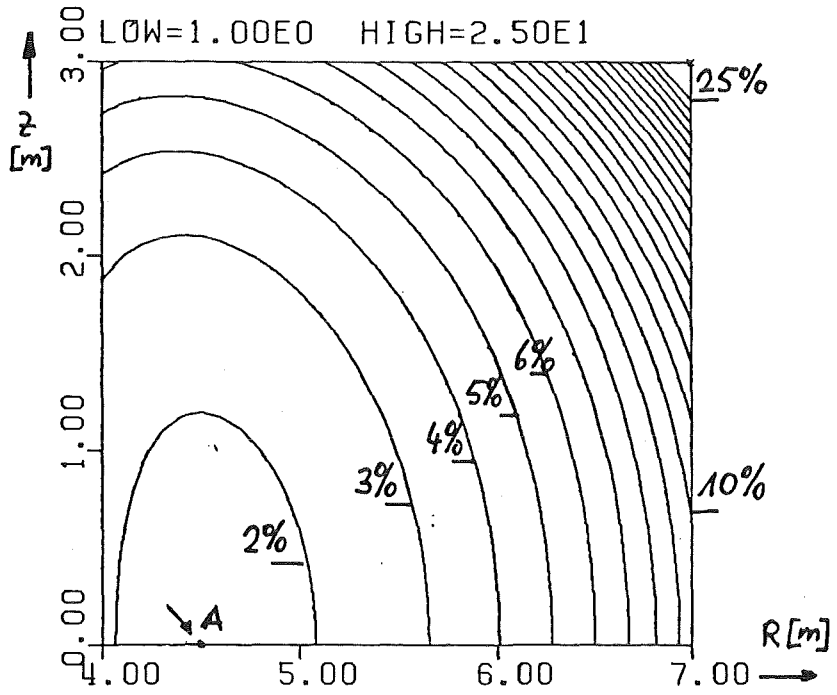

Fig.18 Lines of constant ripple (6 % ripple line at r = 6.5 m); Case 1: $n_1 = 6$.

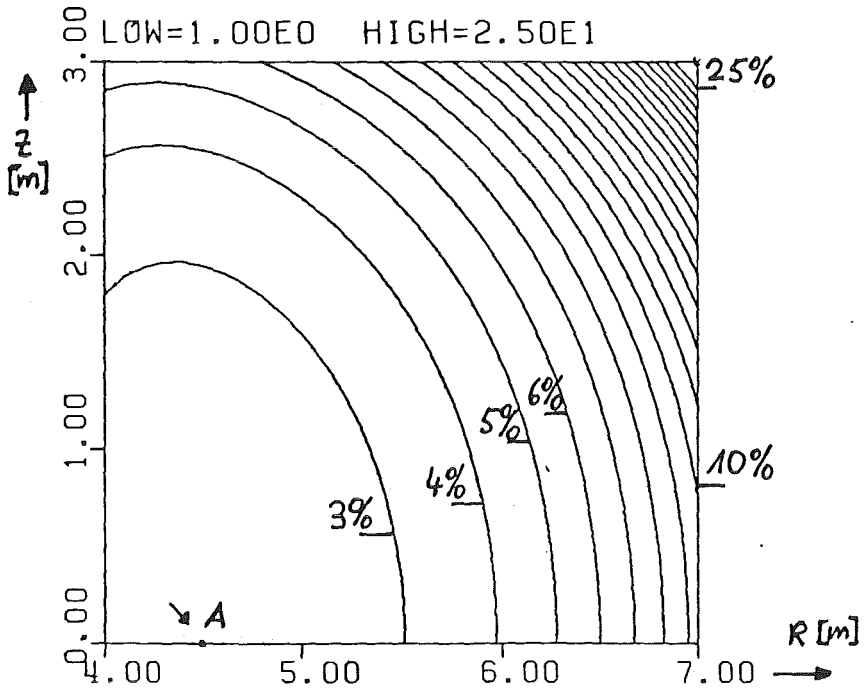

Fig.19 Lines of constant ripple (6 % ripple line at r = 6.5 m); Case 2: $n_1 = 4$.

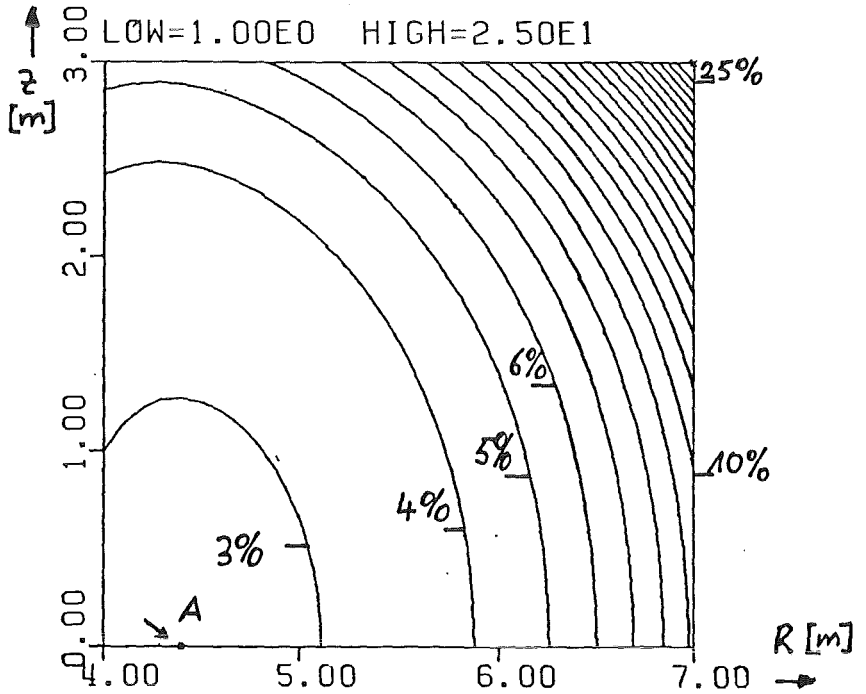

Fig. 20 Lines of constant ripple (6 % ripple line at r = 6.5 m); Case 3: $n_1 = 3$.

1.3.2.2 Induced voltages in the TF coils due to the ripple control currents

The voltage U_1 of each coil in the first group of coils (see Fig.21) is given by:

$$U_1 = \frac{\Delta I_1 L_1^* + \Delta I_2 M_1^*}{\Delta t} ,$$

and the voltage U_2 of each coil in the second group of coils is given by:

$$U_2 = \frac{\Delta I_2 L_2^* + \Delta I_1 M_2^*}{\Delta t} .$$

It is assumed, that all coils of each group are powered in series. Then the inductance L_1^* is the sum of self- and mutual inductances for the considered coil of group one. M_1^* is the sum of mutual inductances between the considered coil of group one and the coils of group two. The inductance L_2^* is the sum of self- and mutual inductances for the considered coil of group two. M_2^* is the sum of mutual inductances between the considered coil of group two and the coils of group one.

The TF coil inductances were calculated. With the values of Table XIII for the current changes and Δt = 3s the voltages were calculated. The results are given in Table XIV. The indices of the coils can be taken from Fig. 21 for the different cases.

Table XIV Induced voltages due to the current changes in the three different cases.

Case	Coil	Voltage [kV]
1	U_1	6.35
	U_2	- 6.35
2	U_1	3.06
	U_2	- 1.53
3	U_1	3.2
	U_{21}	- 0.82
	U_{22}	- 1.52

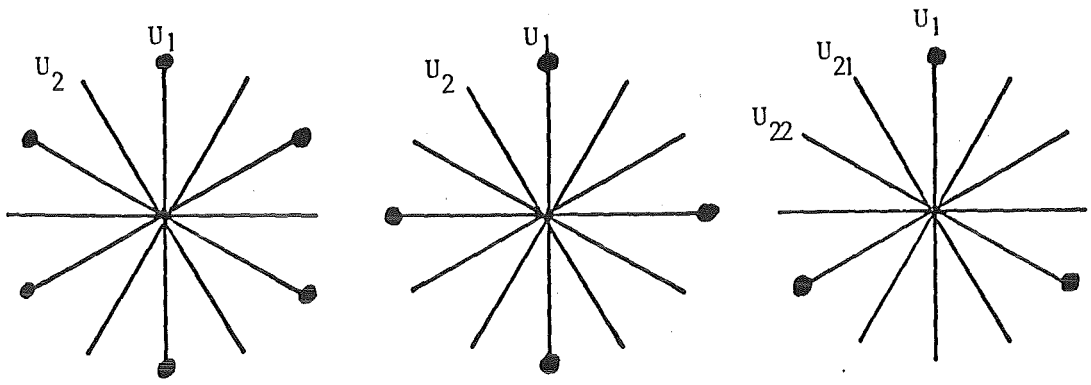

Case 1: $n_1 = 6$, $n_2 = 6$ Case 2: $n_1 = 4$, $n_2 = 8$ Case 3: $n_1 = 3$, $n_2 = 9$

Fig. 21 Indication of the three different cases for the current change in the TF coils in order to control the TF ripple. (Group 1 in each case with dots)

In the cases two and three the induced voltage of about 3 kV in the group one coils is near the discharge voltage, which is assumed to be in the range 2 kV to 3 kV.

It now has to be checked, wether the insulation of the coil and especially the current leads can operate safely under high voltage pulses.

1.5 Safety Aspects and Fault Conditions

1.5.1 Out-of-plane Loads on the TF Coil

The worst case of the TF coil faults is one coil without current. This gives the maximum out-of-plane forces on the TF coil. The results are given in Table XV for the coil elements (see fig. 1).

It has to be discussed wether this worst case should be a design case, or not. This fault is not likely to occur in reality.

The pressure values according to this fault case are given in Table XVI.

TABLE XV. IN-PLANE-LOADS AND OUT-OF-PLANE LOADS ON THE INTOR TF COIL DUE TO THE FAULT CONDITION : NEIGHBOURED COIL W I T H O U T CURRENT FORCES IN MN

ELEMENT	NB3SN SUBCOIL			NBTI SUBCOIL			SUM OF FORCES		
	FX	FZ	FY	FX	FZ	FY	SFX	SFZ	SFY
1	21.34	1.43	2.21	0.15	0.01	3.37	21.49	1.44	5.58
2	8.68	1.66	0.90	0.31	0.06	1.43	8.99	1.72	2.33
3	9.36	2.95	1.00	0.49	0.16	1.59	9.85	3.11	2.59
4	5.84	2.51	0.65	0.37	0.16	1.03	6.21	2.67	1.68
5	4.79	2.48	0.55	0.33	0.17	0.88	5.12	2.65	1.43
6	5.11	3.12	0.62	0.39	0.24	0.99	5.50	3.36	1.61
7	4.10	2.90	0.52	0.35	0.24	0.83	4.45	3.14	1.35
8	6.10	5.08	0.84	0.56	0.47	1.34	6.66	5.55	2.18
9	7.09	7.35	1.10	0.76	0.79	1.76	7.85	8.14	2.86
10	4.97	6.42	0.90	0.61	0.79	1.44	5.58	7.21	2.34
11	9.07	16.54	2.18	1.37	2.53	3.51	10.44	19.07	5.69
12	5.04	16.51	2.12	1.00	3.31	3.45	6.04	19.82	5.57
13	1.89	18.88	2.50	0.47	4.92	4.12	2.36	23.80	6.62
14	-2.24	21.13	3.03	-0.79	7.22	5.06	-3.03	28.35	8.09
15	-3.93	11.89	1.88	-1.80	5.41	3.46	-5.73	17.30	5.34
16	-8.13	13.10	2.41	-4.27	6.85	4.61	-12.40	19.95	7.02
17	-19.54	16.31	4.19	-11.95	9.90	8.62	-31.49	26.21	12.81
18	-30.43	8.94	5.44	-21.14	6.15	12.44	-51.57	15.09	17.88
19	-43.92	2.32	7.81	-27.58	1.45	16.44	-71.50	3.77	24.25
20	-51.07	0.93	9.47	-32.73	0.60	20.05	-83.80	1.53	29.52
SUM	-65.88	162.45	50.32	-93.10	51.43	96.42	-158.98	213.88	146.74
TOTAL COIL	-131.76	0.0	100.64	-186.20	0.0	192.84	-317.96	0.0	293.48

TABLE XVI IN-PLANE-PRESSURE AND OUT-OF-PLANE PRESSURE ON THE COIL ELEMENTS DUE TO THE FAULT CONDITION : NEIGHBOURED COIL W I T H O U T CURRENT PRESSURE VALUES IN MPA

ELEMENT	PY NB3SN	PY NBTI	PR NB3SN	PR NBTI
1	7.87	8.90	16.12	0.12
2	7.90	8.91	16.42	0.60
3	7.97	8.99	16.60	0.91
4	8.07	9.09	16.71	1.09
5	8.16	9.20	16.79	1.22
6	8.27	9.32	16.88	1.34
7	8.38	9.46	16.97	1.47
8	8.55	9.66	17.08	1.64
9	8.82	9.99	17.27	1.92
10	9.15	10.39	17.48	2.24
11	9.76	11.14	17.88	2.83
12	10.80	12.45	18.58	3.87
13	12.18	14.21	19.54	5.28
14	14.16	16.77	21.06	7.48
15	16.18	19.55	22.80	9.99
16	17.96	22.54	24.32	12.26
17	20.57	27.77	26.53	15.57
18	23.42	35.18	29.05	19.42
19	25.19	40.66	30.01	21.18
20	26.79	43.46	30.53	21.99

1.5.2. Magnet System Safety

The magnet system represents a major role in the overall safety analysis of INTOR. The energy stored in the toroidal field magnet system is 26,7 GJ, that in the poloidal field magnet system 11,6 GJ.

For the magnet safety analysis it is important to distinguish between "abnormal operating conditions", which cause a temporary shut down of the magnet system without a damage and "accident situations" with the possibility of subsequent destruction. A general analysis of both cases for fusion magnets has been published earlier |1|. Thus, here only the specific conclusions as related to INTOR will be given.

1.5.2.1 Abnormal operating conditions

As such a condition the so called "quench", a sudden transition of a part of the superconductor to normal conductivity, is defined. The INTOR-coils in all design options are built under the design criteria for cryogenic stability, which means that a certain amount of heat associated with a local disturbance can be transfered to the cooling medium, so that even a locally created normal conducting zone disappears again within a short time. Therefore a quench can only be triggered if the conditions for cryogenic stability are disturbed by abnormal events as they are shown in the fault tree Fig. 22. They mainly concern the

- lack of cooling (rupture or blockage of He-lines or channels, vacuum break down)
- sudden excessive local heating above the design limits (movements, magnetic field variations beyond the design field sweeping rate).

As indicated by the event tree several detection systems must be available to initiate a safety discharge in an external resistor circuit. This discharge is accompanied by

- coil heating,
- high discharge voltage
- helium pressure increase
- asymmetric mechanical loads.

The proper design of the coil system will keep the maximum values within acceptable limits, but to keep the unbalanced mechanical load on coils and structure within the static yield strength and have it appearing only for a short time, a simultaneous discharge of the whole coil system, including also all nonquenched coils, will be stringent.

In case of a failure within the external discharge circuit a pure internal discharge in the developing normal resistance of the winding will occure. If the normal zone grows fast enough, even then the coil will be save.

In summary, all events connected to a coil quench are non-destructive in a proper coil design. Therefore, a quench will remain as a abnormal operating condition that can be taken by the system without damage. This does not mean, however, that quenches could be accepted to occure frequently, as they are costly events in both, operating time and expenses for subsequent cooldown.

1.5.2.2 Accident situations

They are associated with the generation of high power arcs, which are driven by the energy stored in the magnet system. Accidents are most likely to occure in individual magnets. As shown in the fault tree, Fig. 23, the appearance of an arc is caused by short circuits or rupture of the leads or conductor turns. The predictable damage for a single magnet can be quite severe if the arc developes into a multiple arc system, which will depend on the place where the single arc occurs.

Independent of the uncertainties about the electric characteristic of the arc a rough prediction as carried out in |1| shows that an arc power of ~ 1 GW involving the whole winding in the arcing zone will develop within about 1 s, and lasting for few seconds, until the energy is dumped. Thereby about 500 kg of conductor material will be vaporized.

Simultaneously, the detection system must have initiated the safety discharge of the whole coil system, so that together with the fact, that the arcing discharge process runs so fast, it is most likely that the other coils and the intercoil structure remain undamaged.

Obviously the damaged coil must be replaced afterward. In addition it cannot be excluded that the arc burning through the cryostat can damage adjacent elements around the magnets. Thereby it can be assumed, that the arc is driven away from the torus center and the blanket area by the background field of the coil system.

In |1| also a very hypothetical accident situation is considered, namely the rupture (by multiple arcing) of the winding simultaneously on two positions within a certain, not too small distance. This would cause a missile generation of the ruptured part which will fly in the direction of the wall of the reactor building with a final velocity of about 70 - 80 m/s. While this event is very hypothetical it is recommended to design the building capable to withstand such an impact.

|1| F. Arendt, P. Komarek
Potential Failures and Hazards in Superconducting Magnet Systems for Fusion Reactors
Nuclear Technology/Fusion, Vol. 1, pp. 552-569, Oct. 1981

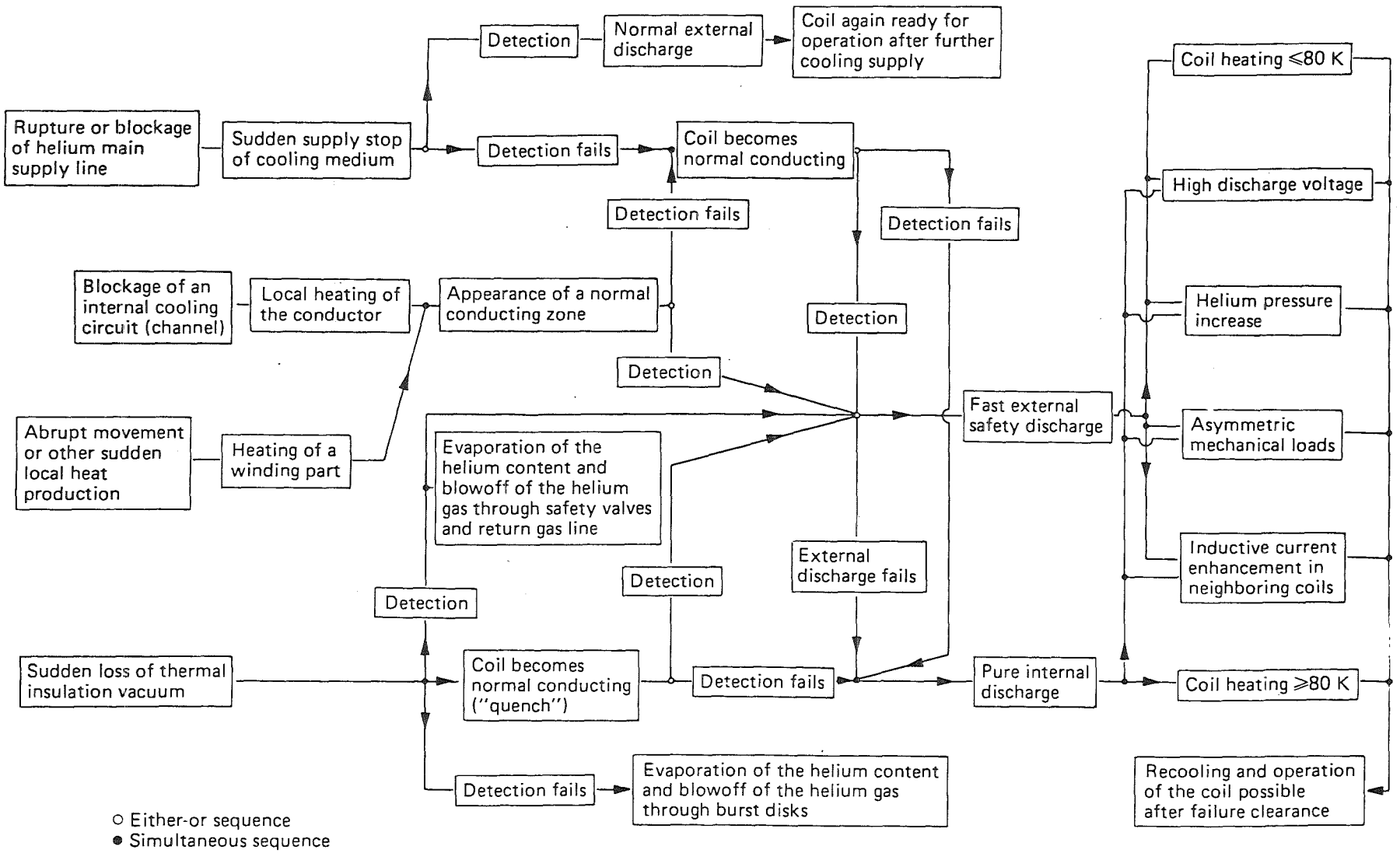

Fig. 22 Event tree for abnormal operating conditions in superconducting coil systems. /1/

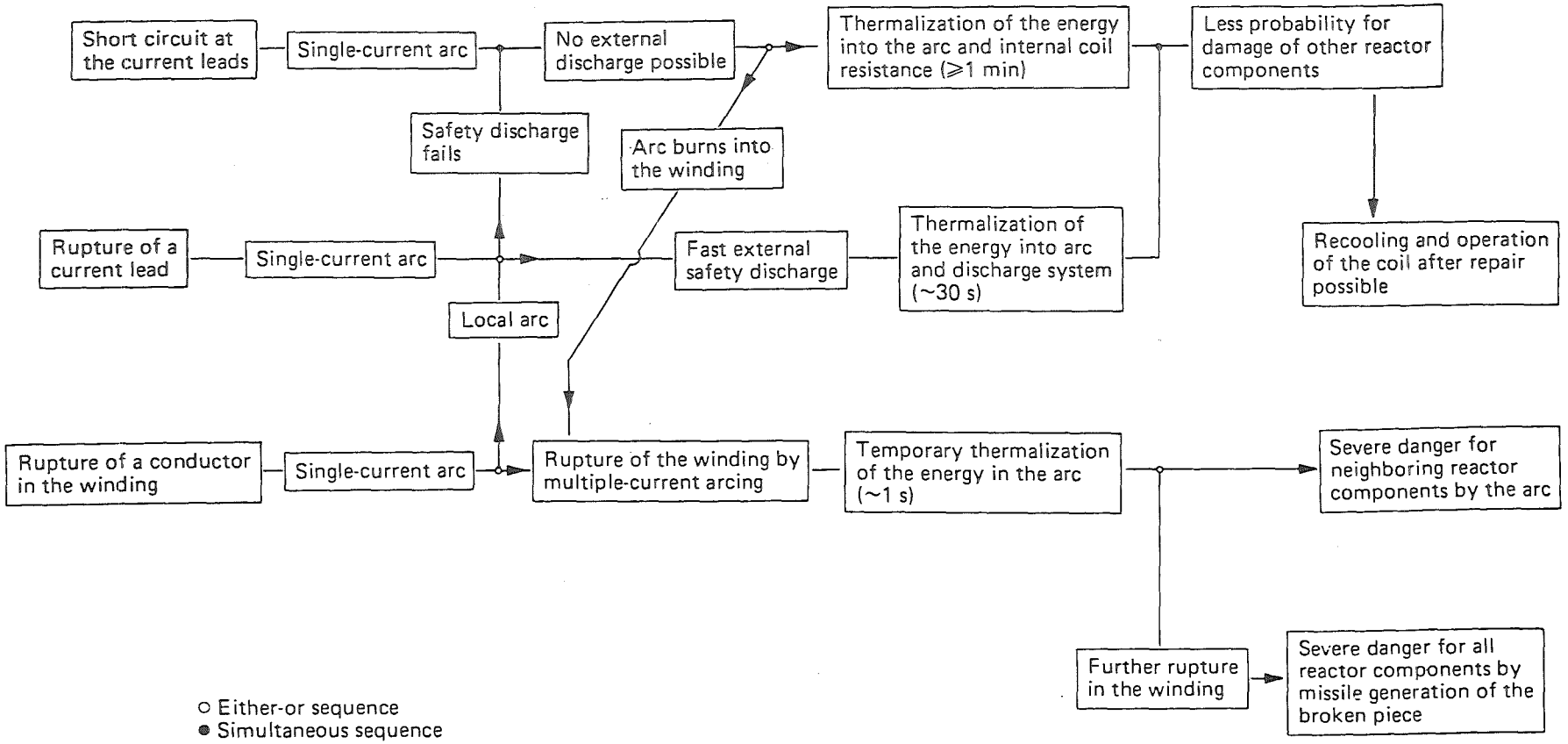

Fig. 23 Event tree for possible accidents in superconducting fusion magnets. /1/

1.6 Research and Development required to establish INTOR Phase II A TF magnet technology

1.6.1 Introduction

The following is based on the situation in Europe and the present status of program discussions within EURATOM.
A significant present step is the international Large Coil Task Project (LCT), initiated in 1977 as a joint experiment by the USA and its partners EURATOM, Japan and Switzerland. The final phase of the construction and the experimental phase of LCT will fall into the program period 1982-86. The Community contribution to this experiment is coming mainly from KfK Karlsruhe, the Swiss contribution from SIN-Villigen.

Another important step will be the operation by 1986 of the French TORE SUPRA at Cadarache, the first Tokamak in Europe equipped with superconducting TF coils.
Neither the Large Coil Task, nor TORE SUPRA will give the final answer to all problems of the toroidal field system for the Next Step.

To obtain fields in excess of 8 Tesla, several possibilities can be envisaged: the use of A15-type conductors, like Nb_3Sn, cooled by normal helium at about 4 K; or, alternatively, of ternary alloys like NbTiTa, (or A15) cooled at superfluid helium temperature ($\leq$ 2 K). In most cases different cooling modes can also be applied in principle, pool boiling or forced flow.

These approaches should be explored in the program, up to the point where a clear choice can be made for the NET prototype coil.
A single full size coil of NET/INTOR represents an investment of the order of 40 Mio $. A fully relevant operational test is only possible with at last three such coils forming a torus segment and will require structural and cryogenic installations comparable to the corresponding final components of NET/INTOR itself.

The associated cost suggests that full size coil fabrication and tests will only be possibel as a first phase of the final commissioning of NET/INTOR, with the sequence of coil fabrication being influenced by successive performance tests of the first set of coils.

In order to close the gap LCP-NET, a comprehensive development program is proposed which through the successive steps of laboratory conductor development and testing, industrial conductor development, testing of the "full size" conductor in an actual pancake winding, will finally allow to design and construct the prototype coil for NET.

1.6.2 Required Program Steps between LCT and NET/INTOR

A. High Field Conductor Development

The aim is the development of high field conductors of techically relevant size with integrated stabilizer and reinforcement, and their testing under relevant operating conditions.
The corresponding program consists of
a) the development of composites,
b) testing of basic conductors and,
c) industrial development of the full size conductors.

a) Development of composites

This subprogram includes the investigation and comparative evaluation of different conductor materials, differnet conductor configurations and different cooling techniques.

The following options are in consideration:
- Use of Nb-Ti-Ta conductors at superfluid temperature, capable of generating at its limits typically about 11 Tesla.

- Use of A15 material at 4.2 K with capabilities of generating 12 Tesla or more.
- Application of A15 conductors in combination with potential advantages of superfluid cooling with regard to local stability.

Correspondingly different materials and production techniques are still in investigation:

Nb_3Al - sandwich-technique by ENEA,
Nb_3Sn - powder metallurgy by ECN,
Nb_3Sn - external diffusion by SIN,
Nb_3Sn - quaternary alloying by KfK.

b) Test of Basic Conductors

These tests must cover not only short sample characteristics, but also the behaviour of ready wound and impregnated loops in the form of inserts to larger test magnet systems.

Thus, in addition to the usual short sample measurements for which test magnet systems are available in most laboratories, specific larger scale facilities have been brought into operation or are under construction (SULTAN, HOMER, qT-facilities in CEA, 14T-sample test facility with tensile frame).

With this effort the conductor development could proceed such that beginning in 1984 an industrial step can follow and sufficiently reliable results should be reached until 1986.

c) Industrial Development of Full-Size Conductor

Such an industrial step is necessary and will consist of the development of a "full size"-NET-type conductor, based on proven basic or subsize conductors as well as on the accompanying desigh studies. "Full size" means that all components (conductor strands, reinforcement element, solder, etc.) are

of appropriate size or amount so that all fabrication steps and the stresses thereby are representative, albeit the final NET-conductors may be slightly larger. Major goals of the development should be to optimize the fabrication process concerning

- required principles,
- possible unit length of fabricated conductors,
- number of fabrication steps,
- influence of several fabrication steps on the conductor performance,
- costs.

The development in industry must be accompanied by component tests in the laboratories, e.g. electric and mechanical tests of the elements and conductor samples.
The conductor development program could achieve its objectives by 1986/87.

B) Coil Technology Verification Tests

A real performance test of the "full size" conductor should be carried out in windings, where the conductor is placed in the true geometry and cryogenic environment (including the cooling mode) and has had the full load of winding fabrication.

In spite of most real test conditions, the test system should be still reasonable in costs and flexible enough to compare several conductor and cooling principles for the winding. For conductors with good scalability from subsize, subsize test windings in the SULTAN-facility can be foreseen.

For "full size" conductors, a cluster test arrangement in the KfK-TOSKA-facility with the two European LCT-coils providing the background-field and testing pancakes in between has been proposed as a useful system. Typically 2 - 3 km of a 20 kA conductor would be required for such a pancake, which thus can

be defined as a representive test piece for investigation of the conductor performance in TF-windings.

Completion of these tests should give enough information that the design of NET-coils can be started with confidence.

1.6.3 Construction and Test of a NET-Prototype Coil

This is an expensive undertaking and can probably be justified only after final decision to go into detailed design phase of the NET-project and carried out as part of a design verification phase. The aim should be the final proof of the design and the fabrication methods before the series production is initiated.

One problem is the best test arrangement for the coil. If simultaneously three coils could be built an optimum test system would be a cluster arrangement of these coils, already on NET-site. But probably this will be too time consuming because it means that the fabrication facilities and the cryogenic installations on site are already available.

To reach the above mentioned goal, it could be more appropriate to restrict the work just to a single coil test of the prototype coil, which can be carried out e.g. in the TOSKA-facility. The experiences with the LCT-single coil tests already carried out at JAERI and envisaged at KfK with the TOSKA-facility show that several key items of coil performance can still be investigated with such a test. They concern mainly the cryogenic performance, conductor stability (not at the rated magnetic field), sensors and measuring probes and mechanical inplane loads. Together with the information gained during the earlier program steps (e.g. pancakes tests, Tore Supra operation) and the fabrication experience in manufacturing the prototype coil, this should be sufficient to justify the release of series production of coils.

1.6.4 Time Frame

Based on the required program steps as introduced overleaf and summerized in a diagram, Fig. 24, the earliest starting data for serial manufacturing of NET-TF-coils would be 1992, if a decision about detailed design for NET including construction and test of a NET-TF-prototype coil could be taken in 1987.

1.6.5 Base Technology

For the successful operation of a complete Tokamak magnet system, components other than the superconducting magnet windings are equally important and may require an additional R & D effort. The main areas of R & D identified so far are:

- low temperature fatigue data on structural materials and components,
- combination of matallic and nonmetallic structure and cryostat parts for reduced a.c. losses,
- fault detection and protection circuits for a integral magnet system,
- radiation resistivity of insulations,
- radiation resistive windings for plasma stabilization.

Some of this are, at least partially, covered by existing or planned activities in other low temperature technology programs (e.g. fatigue data for steel, or fault detection and protection).
Others lead to the following R & D proposals:

- Radiation damage experiments on all nonmetallic used at present in superconducting magnet construction.
- Development of metallic-nonmetallic connections and interlays as well as of fibre reinforced structural components with stress-strain data similar to steel in at least two dimensions.

Fig. 24

NET TF - Development Programme

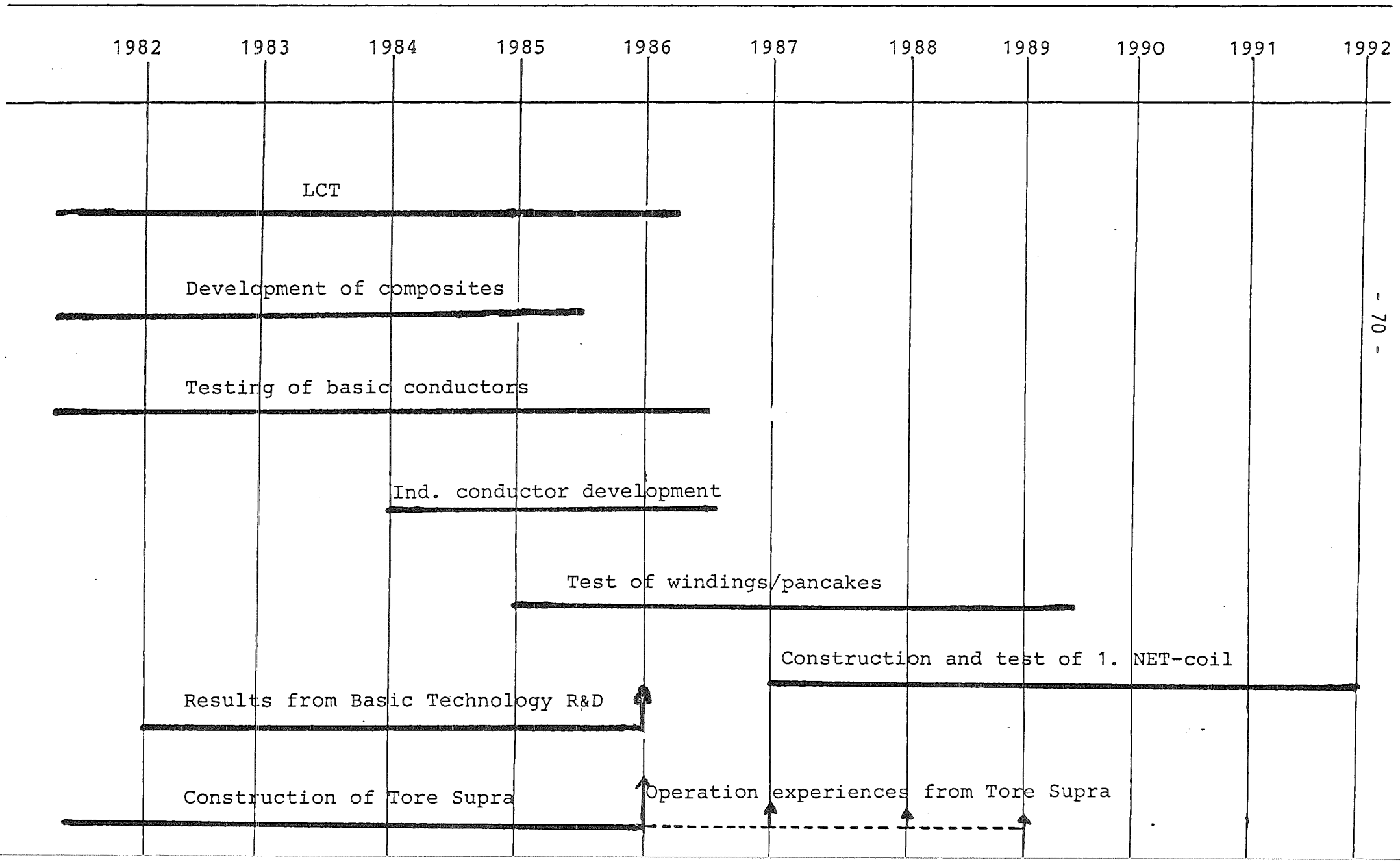

- Test on radiation resistive windings with sufficiently high strength and current density.

The key results of these R & D tasks should be available by about 1987, in time to be incorporated into the final stages of development of the large TF-coils (i.e. the pancakes tests and the design of the NET-prototype coil).

Description of the TF coil contour for the INTOR Phase II A coil

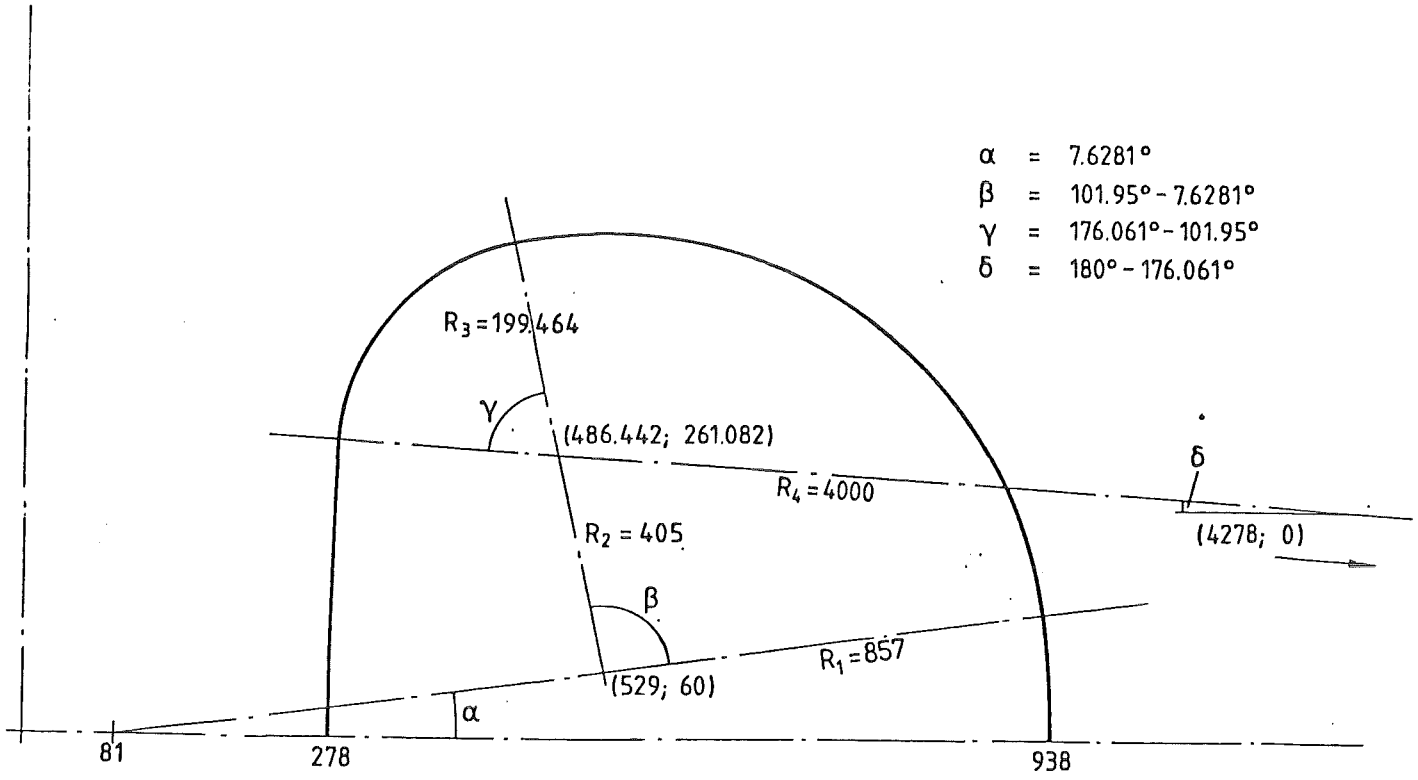

Fig. A1 Basic contour of the inner perimeter of the TF coil following the INTOR design specifications.

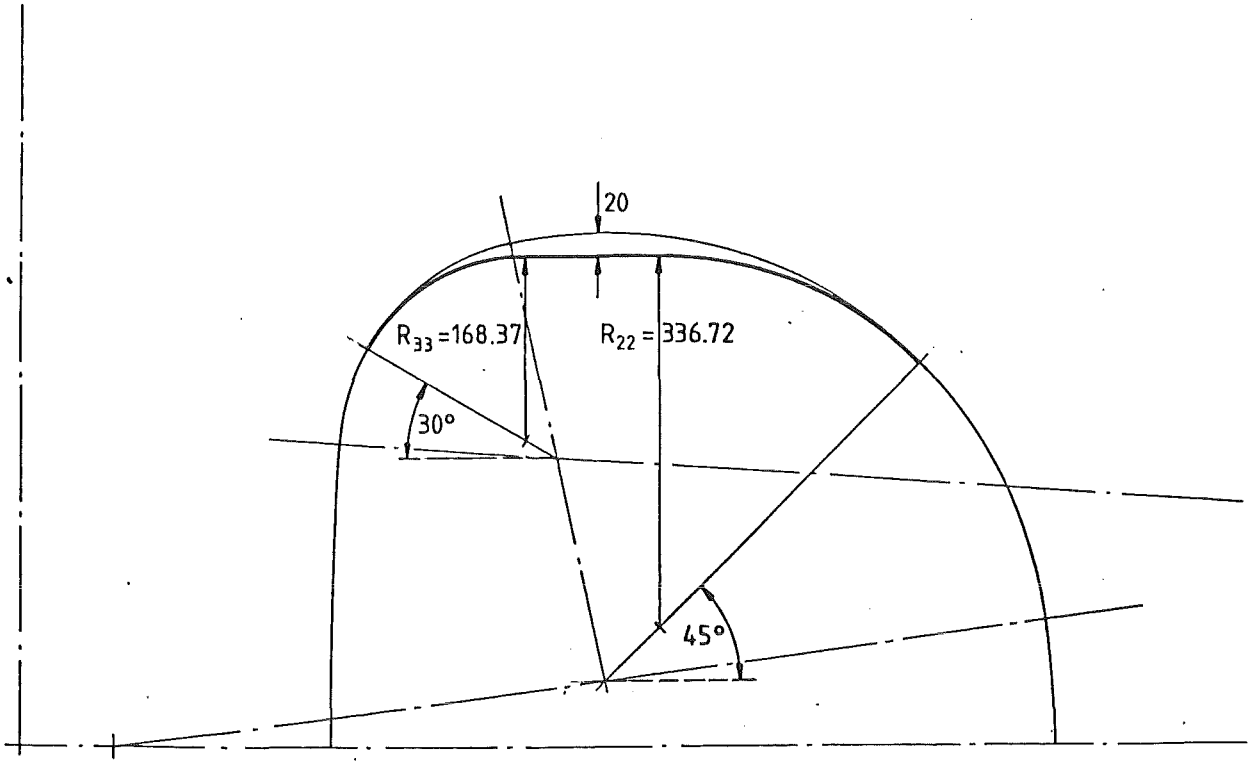

Fig. A2 Inner TF coil contour, region for the LHe inlet to the Nb_3Sn coil and the conductor connection of the Nb_3Sn subcoil parts.

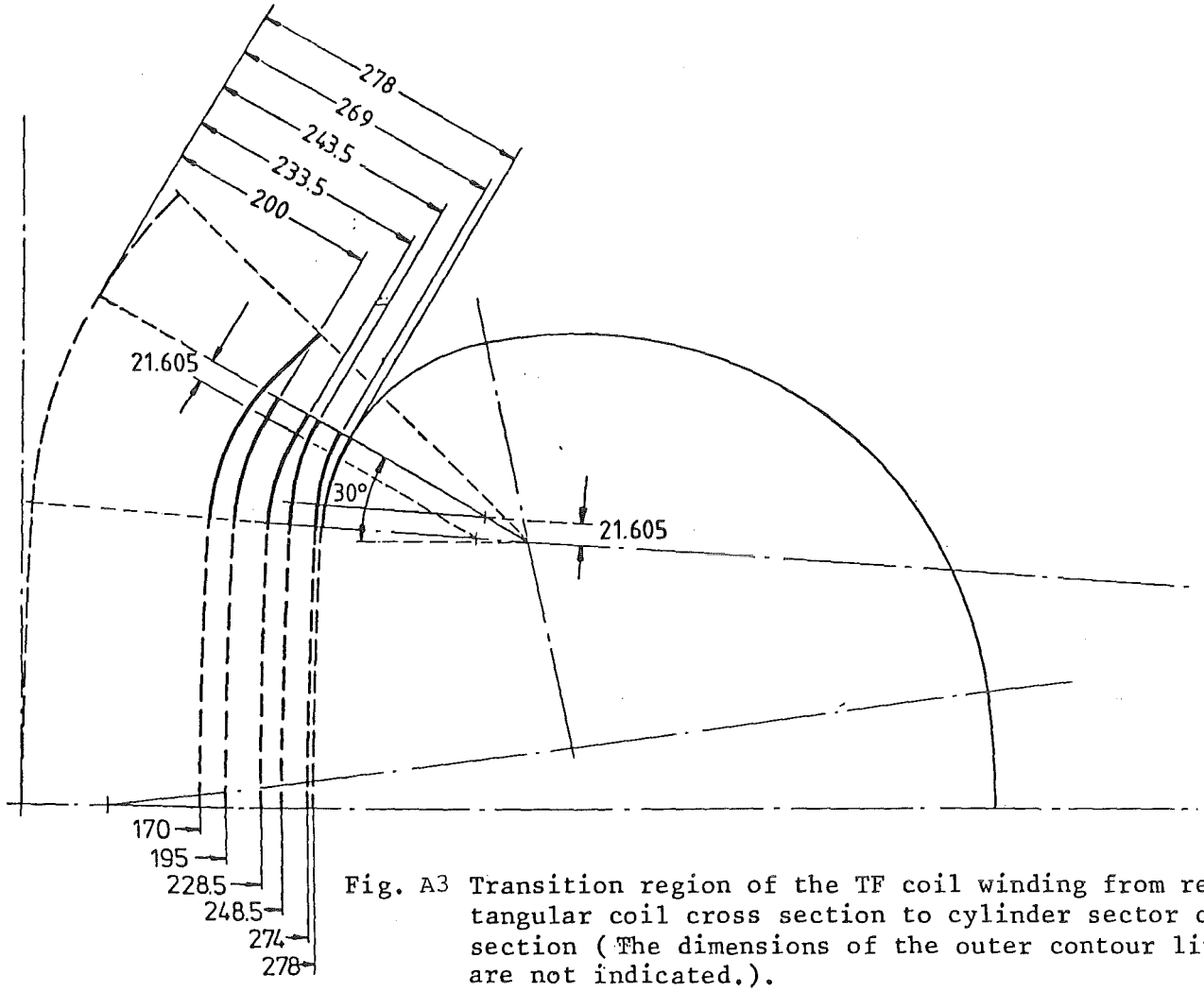

Fig. A3 Transition region of the TF coil winding from rectangular coil cross section to cylinder sector cross section (The dimensions of the outer contour line are not indicated.).

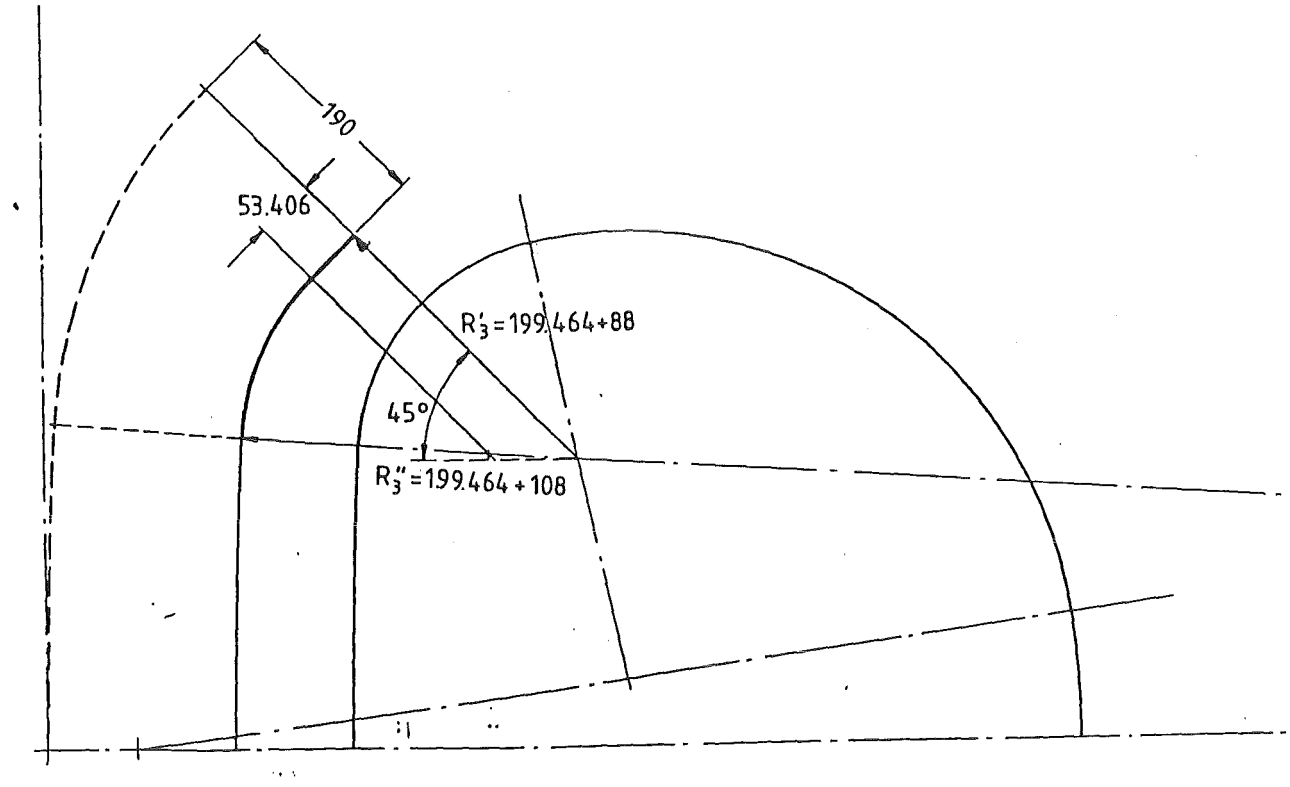

Fig. A4 Outer contour of the transition region.

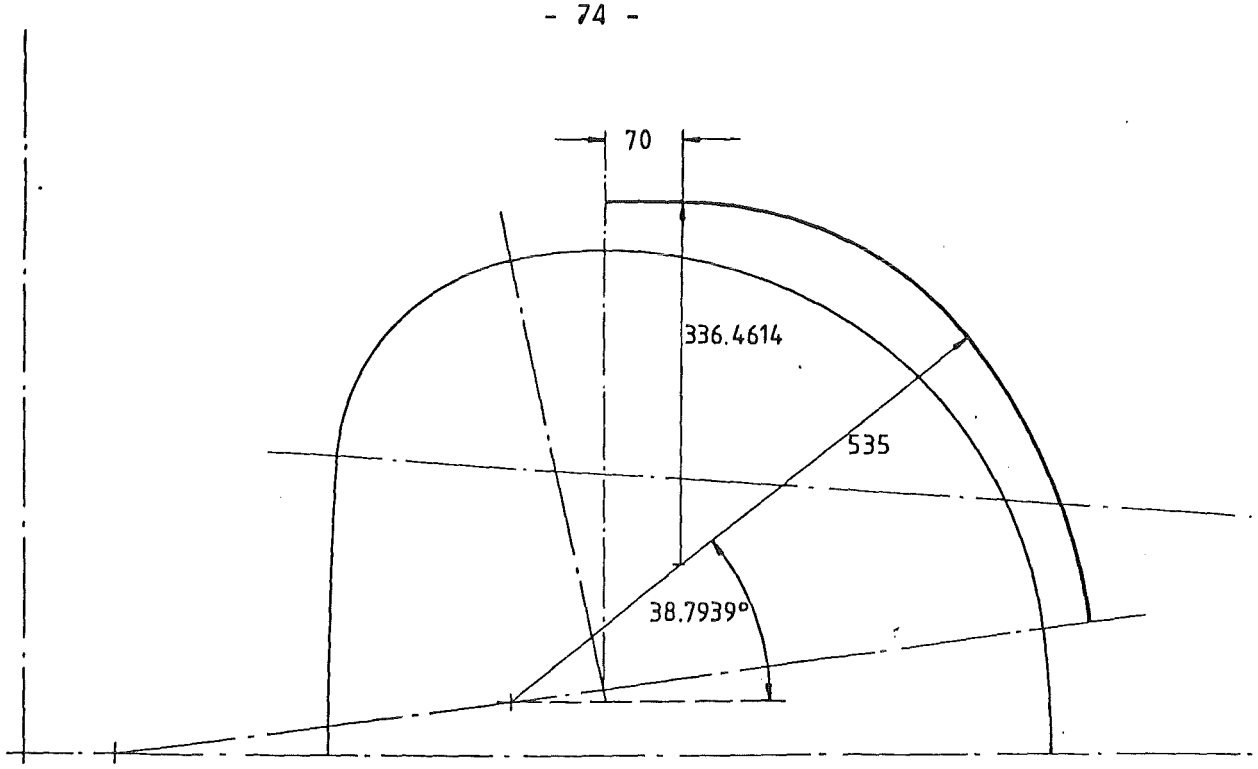

Fig. A5 Inner contour of the NbTi subcoil providing the necessary space for the pancake conductor connections (outer contour of the Nb_3Sn subcoil hoop stress support ring).

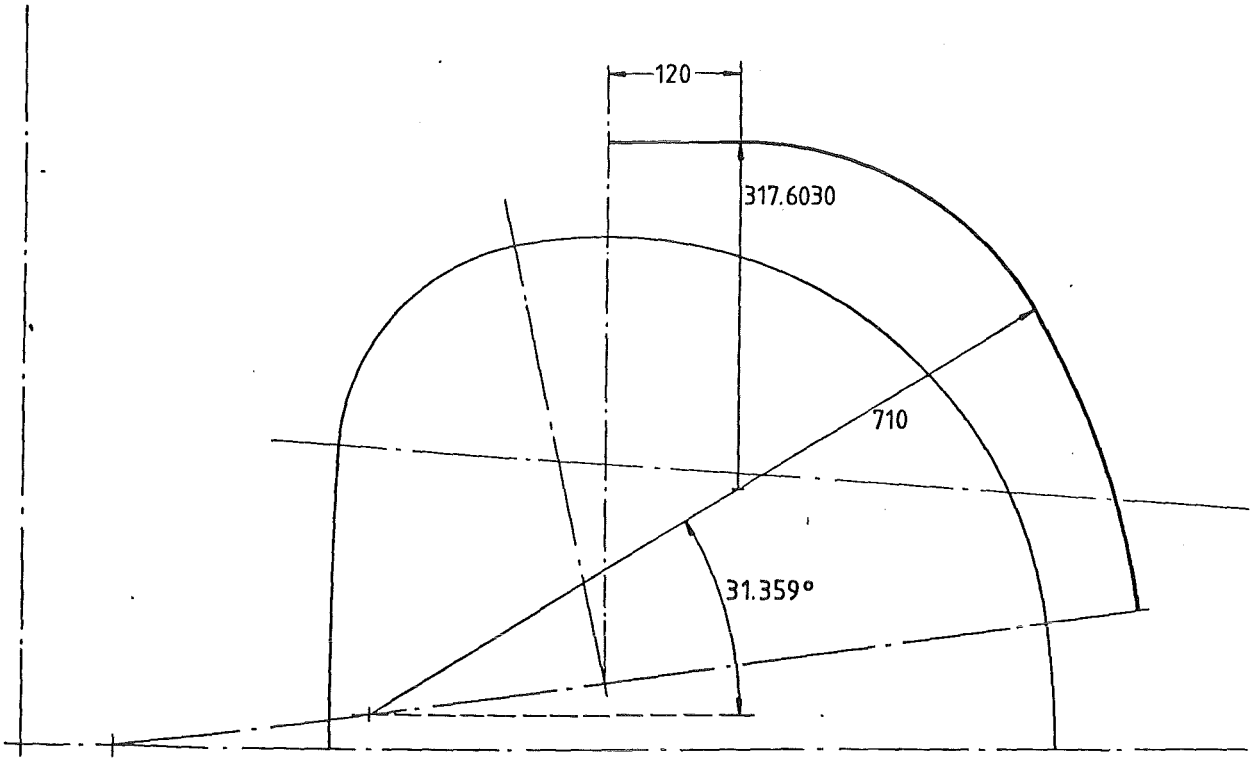

Fig. A6 Outer contour of the TF coil, providing the necessary space for the NbTi conductor connections and the current leads.

2.3 Poloidal Field Coil System for the Divertor Case

2.3.1 General design

The poloidal field (PF) system consists of 21 solenoids, see Fig. 25. They are all located outside the toroidal field coils with the consequence, that all of them have to be superconducting.

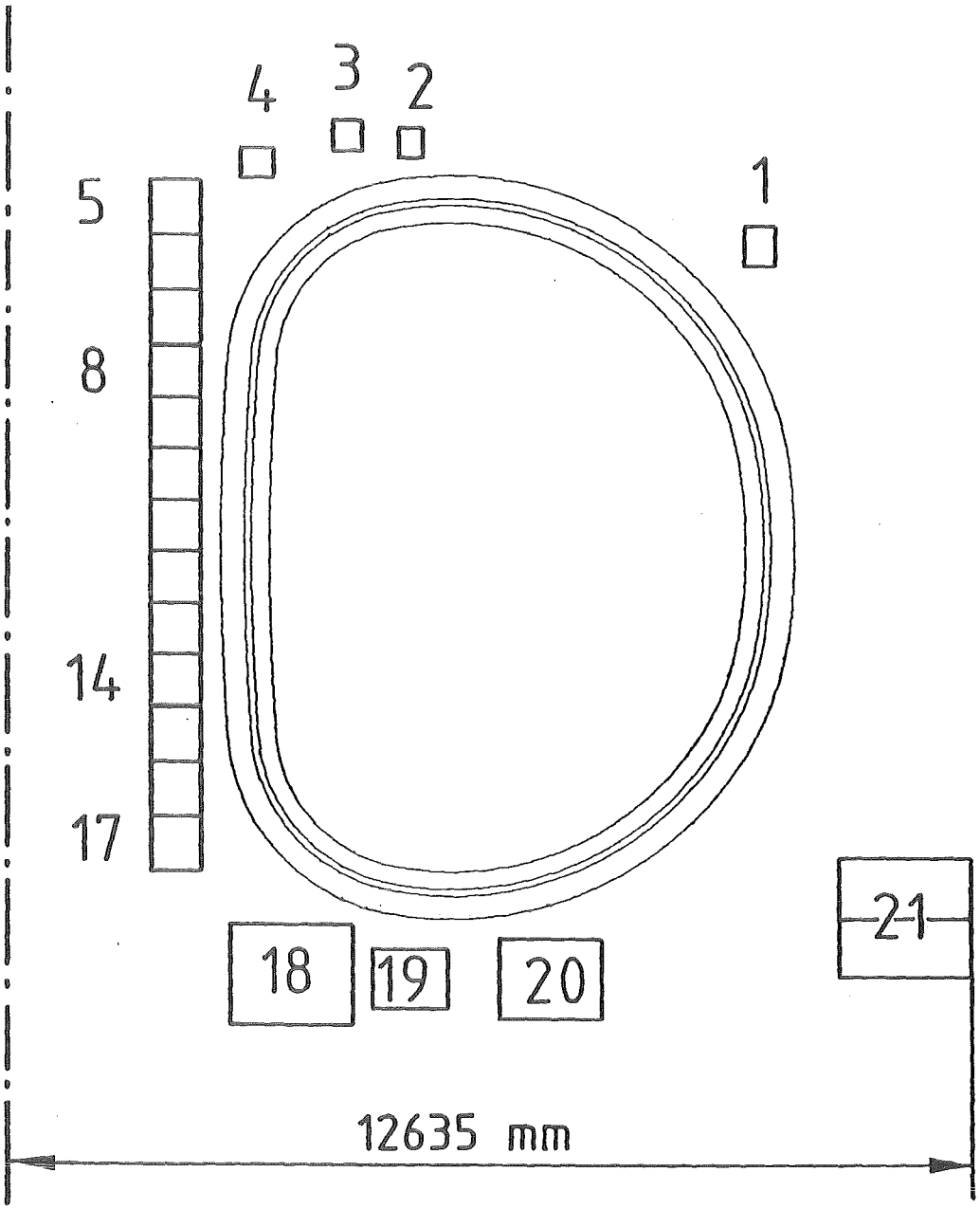

Fig. 25 Poloidal field coils arrangement of the INTOR phase IIA. Coil No. 21 is divided into 2 subcoils in order to reduce the induced voltages.

The coil configuration of Fig. 25 provides a single null poloidal divertor configuration. This is causing a highly unsymmetric PF coil distribution and big divertor coils at the bottom of the reactor. The medium position and the current-time scenario of the PF coils are given in Table XVII.

For the first design approach, a poloidal conductor is taken, which follows the Japanese Concept (see Japanese Contributions to the 3rd Workshop-Meeting, Dec. 1981). The conductor has a design current of I = 50 kA with overall dimensions of 14.5 x 2.28 cm^2 for all coils exept for coils 5, 6, 7, and 15, 16, 17 which have a conductor with a cross section of 13.33 x 2.28 cm^2.

A principle view of the winding concept is given in Fig. 26. The conductor is considered of carrying no load in circumferential direction. Hoop stresses are taken over by additional co-wound steel strips of 13.0 x 0.1 cm^2 cross section. Using such thin steel strips enables a more simple fabrication process avoiding weldments of the supporting steel. The conductors are electrically insulated from each other by 2mm thick epoxy strips. Between each two pancakes there is an insulating epoxy layer of 15 mm thickness (for coils No. 5 - 7 and 15 - 17 it is 3.3 mm). The layer is provided with a large number of bores which allow a good permeation of Helium through the pool-boiling cooled winding.

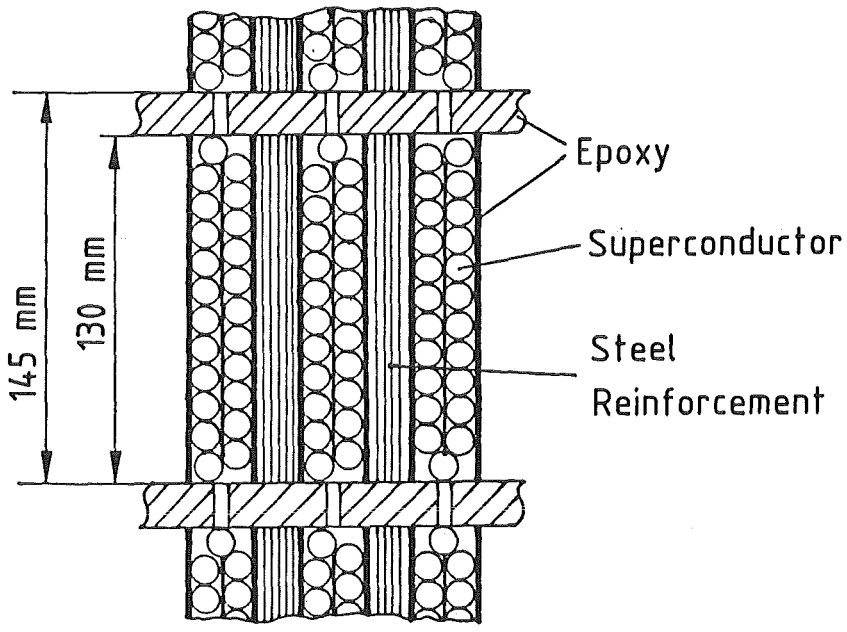

Fig. 26 Principle view of the winding concept

Table XVII Medium position of the PF coils and the plasma and Ampère winding numbers at different times after discharge initiation

Coil	Medium pos./cm		I/MAt				
	vertical	radial	0 s	0.3 s	5 s	11 s	211 s
1	440	965	0.38	0.19	-1.57	-2.38	-2.59
2	590	470	0.41	0.55	1.69	1.60	1.71
3	600	380	2.36	2.21	1.37	1.55	1.03
4	560	250	2.31	1.96	-0.51	-0.10	-0.85
5	495	135	5.73	5.32	2.30	1.20	-0.09
6	415	"	"	"	"	"	"
7	335	"	"	"	"	"	"
8	255	"	4.56	3.42	-4.38	-3.97	-4.99
9	180	"	"	"	"	"	"
10	105	"	"	"	"	"	"
11	30	"	"	"	"	"	"
12	-45	"	"	"	"	"	"
13	-120	"	"	"	"	"	"
14	-195	"	"	"	"	"	"
15	-275	"	5.73	5.32	2.30	1.20	-0.09
16	-355	"	"	"	"	"	"
17	-435	"	"	"	"	"	"
18	-625	300	6.45	8.00	21.37	1.36	-0.21
19	-630	470	0.49	0.96	4.82	8.68	8.67
20	-630	670	0	0.01	0.10	12.84	12.85
21	-540	1170	0.40	-0.92	-12.83	-23.40	-23.40
Plasma	76	525	0	0.60	5.40	6.4o	6.40

2.3.2 PF coil cross sections due to conductor needs and hoop stress support

As the conductor current is limited at 50 kA the necessary number of turns can be calculated from the maximum Ampère turn number of table XVII for each coil. Axial and radial numbers of turns are then chosen, in order to obtain an almost square coil cross-section. The total conductor cross section of the winding is then obtained by multiplying the cross section of one conductor with the total number of turns.

To this value the cross section of the steel reinforcement has to be added in order to obtain the total coil cross section. For a first-step-calculation an overall coil current density of 1.5 kA/cm^2 maximum current density is assumed for all coils exept for the central solenoids (5 - 17) which have 1 kA/cm^2 maximum current density. These current densities give the first-step-coil cross sections. For these cross sections the maximum local hoop stresses are calculated for each coil with the SOLKRAFT code, which uses the model of a total force transmission system (see chap. 2.3.4).

It is recommended that the stress in the steel reinforcement is limited at 200 MPa. As the whole hoop stresses are taken over by the steel strips, the necessary steel cross section is obtained by multiplying the assumed first-step-coil cross section by the ratio:

maximum local hoop stress divided by 200 MPa.

From the chosen axial number of turns and the supporting steel cross section, the radial supporting steel thickness is calculated. Finally the supporting steel thickness of each conductor can be calculated in terms of 0.1 cm thick steel strip numbers from the radial number of turns and the total radial steel thickness.

With these new coil dimensions the hoop stress calculation is repeated in order to obtain the final cross sections. The results of these calculations are given in table XVIII.

Table XVIII Composition of the poloidal field coil windings due to hoop stresses

Coil	NZ	NR	ACo / cm^2	NSt	ASt / cm^2	ΔRSt / cm	ΔRtot / cm	ΔZtot / cm
1	4	14	1851	8	582	11.2	44	58
2	3	12	1190	4	187	4.8	33	44
3	3	16	1587	3	187	4.8	42	44
4	3	16	1587	6	374	9.6	47	44
5 - 7	6	19	3379	12	2028	26	70	80
8 - 14	5	20	3306	12	1560	24	70	75
15 - 17	6	19	3379	12	2028	26	70	80
18	10	43	14216	18	10062	77.4	176	145
19	6	29	5752	14	3167	40.6	107	87
20	8	33	8728	21	7207	69.3	145	116
21	12	39	15472	25	15210	97.5	187	174

total cross section of one conductor is 145 x 22.8 mm^2 for the coils No. 1 - 4, 8 - 14, and 18 - 21. It is 133.3 x 22.8 mm^2 for the coils No. 5 - 7 and 15 - 17.

NZ axial number of turns
NR radial number of turns
ACo total cross section of the conductor
NSt number of co-wound steel strips 130 x 1 mm^2 for each conductor
ASt cross section of steel reinforcement
ΔRSt total radial steel thickness
ΔRtot total radial thickness of the winding
ΔZtot total axial thickness of the winding

2.3.3 Intercoil forces of the poloidal field coil system and supporting coil case thickness

As all poloidal field coils are solenoids with a common axis, the z-axis, the body forced are axisymmetric to the Z-axis and the resulting intercoil forces lie on the Z-axis. Only these resulting vertical forces have to be supported by a special support system. All other forces must be supported by the coil casings or by the conductors themselves.

2.3.3.1 Forces under normal working conditions

Table XIX shows the vertical forces on the poloidal field coils which have been calculated with the SOLKRAFT code for the five steps of the current-time scenario. In order to simulate the influence of the plasma current another coil with constant current density and fixed dimensions was added. The Z-position of this coil had been established by an interaction process so that the force on it was zero.

As can be seen in Table XIX the maximum forces act on the coils No. 20 and 21 beginning from 11 seconds after discharge initiation. Here they reach amounts of about 100 MPa.

2.3.3.2 Forces under fault situations

If single coils are not energized the resulting vertical forces on the other coils will change. They can be higher or lower than under normal working conditions. For each coil there exist two special combinations of not energized coils which result maximum vertical forces; one combination for the upward (positive) direction and one for the downward (negative) direction. All other combinations of not energized coils result forces which are lower. For these maximum forces the coil cases and the support structure have to be layed out in order to control any possible fault situation.

For each coil these maximum possible forces have been calculated. They are presented in Table XX. The absolute value of nearly all these forces are well below 100 MN. Only the coils 20 and 21 are loaded with 126 MN and 180 MPa respectively at the end of the burn cycle. These forces have to be controlled by the supporting system.

Table XIX Vertical forces F_Z on poloidal field coils in MN at different times after discharge initiation under normal working conditions

Coil	Time				
	0 s	0.3 s	5 s	11 s	211 s
1	- 0.7	- 0.5	- 8.1	- 21.8	- 24.6
2	- 1.8	- 2.3	0.1	0.9	2.7
3	- 19.5	- 17.3	- 2.2	- 2.0	0.7
4	- 22.2	- 17	0.5	0.0	- 2.3
5	- 75.0	- 63.8	- 8.2	- 1.2	- 0.2
6	- 15.6	- 10.1	9.3	4.7	- 0.4
7	9.3	19.1	38.7	16.1	- 1.1
8	6.3	12.1	- 78.5	- 56.1	- 69.0
9	2.5	4.3	- 26.8	- 19.2	- 23.5
10	1.1	1.5	- 8.5	- 6.3	- 7.7
11	0.3	0.0	1.7	0.7	0.9
12	- 0.5	- 1.7	12.5	8.0	9.9
13	- 1.8	- 4.6	32.6	21.8	26.9
14	- 5.3	- 12.4	87.6	59.9	74.1
15	- 7.5	- 20.0	- 46.6	- 17.7	1.2
15	17.5	8.1	- 21.9	- 6.7	0.5
17	72.7	56.9	- 10.5	- 1.2	0.3
18	38.0	42.6	15.5	- 1.0	0.4
19	2.5	4.6	8.4	- 9.0	- 19.2
20	0.0	0.0	- 0.2	- 70.5	- 81.3
21	0.1	1.4	4.8	100.7	111.8

Table XX Maximum possible vertical forces $F_{Z,max}$ in MN on poloidal field coils under fault situations at different times after discharge initiation (upward pos., downward neg.)

Coil	Time				
	0 s	0.3 s	5 s	11 s	211 s
1	0.3/ -0.9	0.1/ -0.6	10.4/-18.5	25.7/ -47.4	27.5/ -52.1
2	0.6/ -2.4	0.7/ -3.0	9.8/ -9.7	12.4/ -11.4	14.0/ -11.3
3	0.0/-19.9	0.0/-17.3	5.9/ -8.1	7.9/ -9.9	6.5/ -5.8
4	4.1/-26.3	3.3/-20.3	2.7/ -2.2	0.4/ -0.5	2.1/ -4.4
5	11.3/-86.2	9.2/-73.0	6.0/-14.2	3.2/ -4.4	0.1/ -0.3
6	67.5/-83.1	57.9/-68.0	21.0/-11.6	8.5/ -3.8	0.1/ -0.5
7	81.9/-72.6	70.5/-51.5	41.3/ -2.6	17.6/ -1.5	0.1/ -1.3
8	68.0/-61.7	47.5/-35.4	5.0/-83.5	5.0/ -61.2	7.8/ -76.8
9	64.3/-61.8	39.8/-35.5	40.1/-66.9	33.7/ -52.9	52.2/ -75.7
10	63.0/-61.9	37.2/-35.7	51.9/-60.3	43.0/ -49.3	66.2/ -73.9
11	62.4/-62.1	36.2/-36.3	57.9/-56.3	47.6/ -47.0	72.6/ -71.7
12	62.1/-62.6	35.7/-37.4	63.8/-51.3	51.4/ -43.4	76.6/ -66.7
13	61.9/-63.7	35.5/-40.1	72.3/-39.7	55.9/ -34.1	79.3/ -52.4
14	61.8/-67.1	35.3/-47.8	92.1/ -4.5	65.1/ -5.1	81.5/ -7.4
15	72.7/-80.2	51.3/-71.3	2.1/-48.6	1.4/ -19.1	1.4/ -0.1
16	83.2/-65.7	67.9/-59.8	10.8/-32.7	3.6/ -10.3	0.6/ -0.1
17	86.3/-13.6	72.9/-16.0	13.3/ -2.4	4.1/ -5.3	0.4/ -0.1
18	38.2/ -0.2	43.1/ -0.6	62.9/-47.4	3.1/ -4.1	0.7/ -0.3
19	2.5/ -0.0	4.6/ -0.6	23.7/-15.3	27.9/ -36.9	21.8/ -41.0
20	0.0/ -0.0	0.0/ -0.0	0.4/ -0.6	49.6/-120.1	44.7/-126.0
21	0.8/ -0.1	1.7/ -0.3	40.3/-35.6	172.1/ -71.4	180.0/ -68.0

2.3.3.3 Necessary thickness of casing for coil No. 21

The control of the maximum force of 180 MN was investigated with a simple geometry of the coil casing and a simple supporting arrangement. It was assumed that coil No. 21 is supported at 12 points along its circumference every 30 degrees. For this arrangement the bending load M, the torsional moment T and the shearing force Q had been calculated. They are plotted in Figure 27 over the arc of the coil between two supporting points. As one can see the torsional moment is only of secondary importance. Both the bending load and the shearing force have a maximum at the supporting points. There are the critical points of the coil casing.

For a simple rectangular casing with a constant wall thickness of 13 mm a maximum reduced stress S had been calculated for the cross section of the casing with the shearing stress τ and the tensile stress σ:

$$S = (\sigma^2 + 4 \cdot \tau^2)^{1/2}.$$

In Figure 27 S is also plotted over the arc of the coil between two supporting points. As it could be expected the maximum of the reduced stress appears at the supporting points where it amounts about 200 MPa.

This calculation of S is based on the assumption that the intercoil force is acting equally over the cross section of the coil casing. In reality, however, the force acts only on one bottom of the casing, where it causes in addition stresses which superpose on the already existing stresses. As preliminary calculations have shown a wall thickness of about 110 mm for this loaded bottom is sufficient to keep the resulting stresses lower than 200 MPa.

The simple calculations have shown that a supporting arrangement for this maximum loaded coil No. 21 seems feasible. It must be emphasized however, that these calculations do not include the influence of the toroidal field coil system. This system does not increase the resulting vertical forces indeed but it causes in addition bending loads which could be of large influence on the resulting stresses.

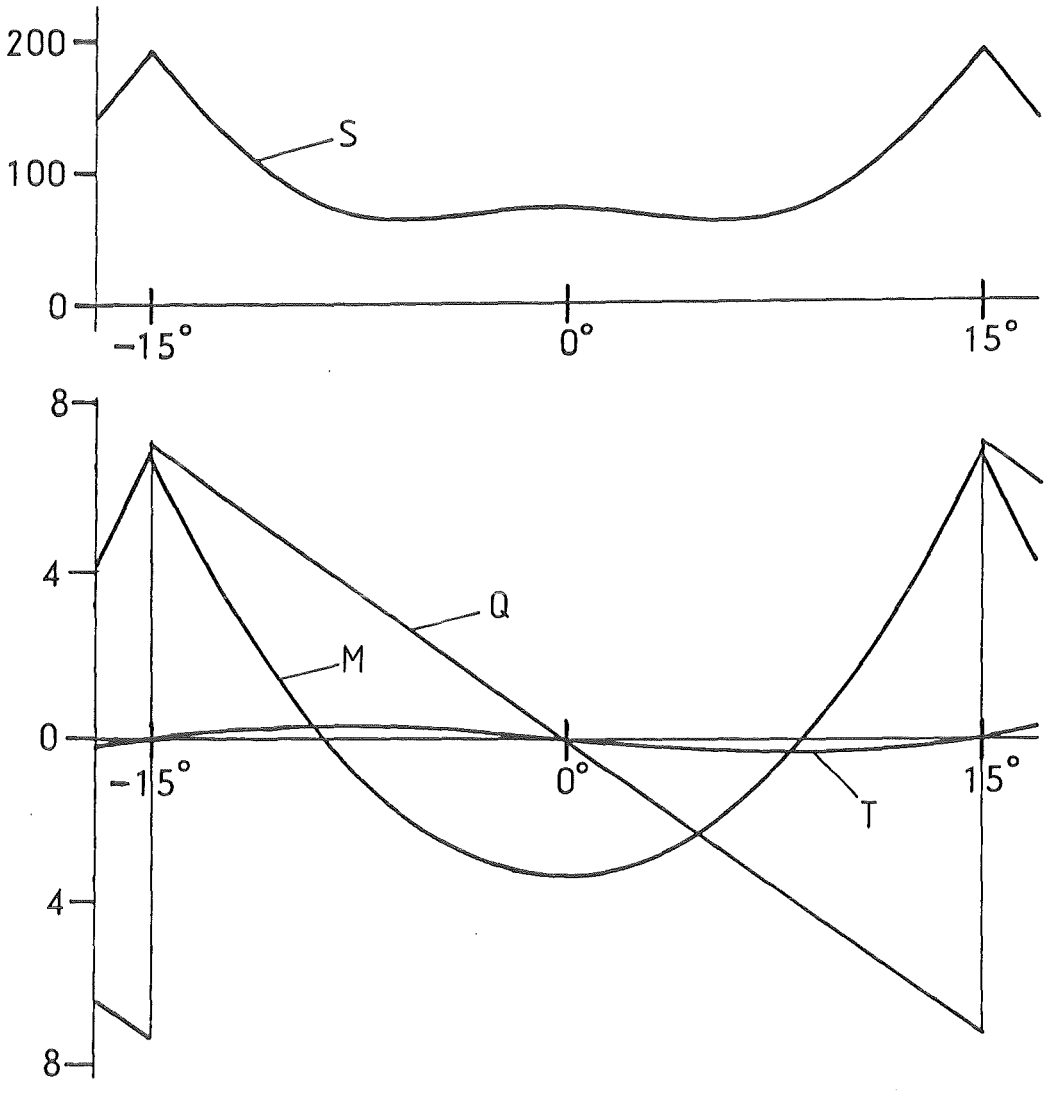

Fig. 27 Bending load Q in MNm, torsional moment T in MNm, shearing force Q in MN and reduced stress S in MPa over the arc of coil 21 between two supporting points.

It must also be mentioned that this simple design with a closed steel casing can only be used as base for a preliminary investigation of the feasibility. In the final design a closed steel case cannot be used because of the induced eddy current. Therefore further and more detailed investigations are necessary.

2.3.4 Hoop stress calculations

The results of the hoop stress calculations depend very much on the model on which the calculations have been based. The SOLKRAFT code which has been developed especially for these calculations uses in parallel two models: the system with self-supporting loops and the force transmission system. In both cases each coil is divided into 30 x 30 single loops. For each of these loops the hoop stress is calculated.

In the first model it is assumed that each single loop is self-supporting; that means no force transmission in radial direction from loop to loop. The results of these calculations are given in Table XXI. In most cases the maximum local hoop stress is well below 100 MPa. It is essentially higher than 100 MPa in the coils 1, 18, 19, 20, and 21. In coil 21 it is even 431 MPa. This value is too high because it would lead to too large crossections of steel reinforcement. That means for the layout of coils with such high loads this simple calculation model is no more sufficient.

The calculations have shown that nearly all coils are tensile loaded at the inner radius and compressive loaded at the outer radius. In this case the application of the force transmission system leads to averaged stress values. The force transmission system is based on the following assumptions:

- all loops are supported radially by each other,
- no compressible medium between the loops,
- radial thickness of each loop kepps constant.

This model was used for the layout of the coil crossections of chapter 2.3.2. The results of the hoop stress calculation with this model are presented in Table XXII. Here the values are efficiently lower than for the calculation model with self-supporting loops. The maximum local hoop stress which appears at all is 92 MPa at coil No. 21.

Table XXI Maximum local hoop stresses in MPa on self-supporting loops of the PF coil windings at different times after discharge initiation (tensile stress pos., compressive stress neg.)

Coil	Time				
	0 s	0.3 s	5 s	11 s	211 s
1	- 4	- 1	75	175	203
2	- 8	- 12	- 91	- 91	- 99
3	105	95	44	49	24
4	72	54	- 5	- 1	- 8
5	82	70	10	3	0
6	86	73	10	2	0
7	86	73	7	- 4	0
8	69	44	39	34	59
9	68	41	46	39	65
10	67	40	48	40	67
11	67	40	48	40	67
12	67	40	48	40	67
13	67	41	45	38	65
14	68	44	37	33	58
15	85	73	12	- 3	0
16	85	74	17	4	0
17	81	72	20	4	0
18	14	21	131	6	- 1
19	- 1	- 2	- 74	161	166
20	0	0	- 1	- 271	- 270
21	0	- 1	126	431	430

Table XXII Maximum local hoop stresses in MPa on loops supporting each other (force transmission system) of the poloidal field coil windings at different times after discharge initiation (tensile stress pos., compressive stress neg.)

Coil	0 s	0.3 s	5 s	11 s	211 s
1	0	0	17	41	45
2	- 4	- 5	- 13	- 22	- 18
3	18	19	16	13	9
4	35	28	- 2	0	- 1
5	66	57	6	2	0
6	68	58	6	1	0
7	68	58	3	- 2	0
8	57	37	20	19	37
9	55	35	26	23	43
10	55	34	29	25	45
11	54	34	29	25	45
12	54	34	28	25	44
13	55	35	24	22	42
14	56	37	16	17	35
15	67	58	10	2	0
16	66	59	18	4	0
17	63	58	25	5	0
18	9	14	77	5	- 1
19	- 1	- 1	- 42	64	68
20	0	0	- 1	- 85	- 84
21	0	0	25	92	91

It must be remarked however, that in this case the assumptions mentioned above lead to optimistic values of the hoop stresses. In reality little radial motions caused by elastic layers between the loops lead to higher local hoop stresses than the values which are presented in table XXII.

2.3.5 Compressive stress on the conductor in axial direction

The axial stresses on the conductor are very much lower than the hoop stresses. The values are given in table XXIII. As one can see the maximum local axial stress which appears at all is 15 MPa at coil No. 14, 5 seconds after discharge initiation. All other values are lower.

2.3.6 Maximum induction at the conductor

The induction at the conductor has also been calculated with the SOLKRAFT code. In table XXIII the maximum absolute value (B) of the induction is given which has been calculated by the relation: $B = SORT(B_r^2 + B_z^2)$. The maximum induction which appears at all is 8.4 T at coil 7, at discharge initiation. This value seems low enough to allow the use NbTi as superconductor.

2.3.7 Induced voltages in the PF coils

The maximum induced voltages are given in table XXIV. For the coils No. 1 - 17 the maximum induced voltage is lower than 2.7 kV for the whole coil and lower than 32 V between two loops. For the divertor coils at the bottom of the reactor these values are higher. The highest values appear at coil No. 21. Here the maximum induced voltage is 26.5 kV for the whole coil and 113.3 V between two loops. In these values it is already taken into account that this coil has been devided into two subcoils which are electrically switched into parallel. The induced voltage can of course still be decreased by choosing a higher number of subcoils.

2.3.8 Stored energy of the whole PF coil system

The stored energy of the whole PF coil system is at the different time steps:

time/sec	0	0.3	5	11	211
energy/GJ	1.62	1.41	5.11	11.40	11.54

Table XXIII Maximum induction at conductor B_{max} and maximum compressive stress in vertical direction ($Sigz_{max}$) on the conductor of the poloidal field coils

Coil	B_{max}/T	Time/s	$Sigz_{max}$/MPa	Time/s
1	2.1	211	3	211
2	1.7	211	2	211
3	2.4	0	4	0
4	3.1	0	4	0
5	7.9	0	14	0
6	8.3	0	3	0
7	8.3	0	7	5
8	7.9	0	14	5
9	7.7	0	5	5
10	7.6	0	1	5
11	7.6	0	0	-
12	7.6	0	2	5
13	7.6	0	6	5
14	7.7	0	15	5
15	8.2	0	8	5
16	8.2	0	4	5
17	7.8	0	13	0
18	7.3	5	13	5
19	4.2	211	7	211
20	4.7	11	8	211
21	5.6	11	14	211

Table XXIV Maximum induced voltage for a single loop U_{sing} and for the whole winding U_{tot} of the poloidal field coils

Coil	U_{sing}/V	U_{tot}/KV	time/s
1	31.2	1.7	0.3
2	4.8	0.2	0.3
3	11.9	0.6	0
4	15.8	0.8	0
5	9.3	1.1	0
6	11.5	1.4	0
7	14.9	1.8	0
8	21.5	2.1	0
9	24.6	2.5	0
10	25.6	2.6	0
11	25.7	2.6	0
12	25.2	2.5	0
13	23.6	2.4	0
14	19.7	2.0	0
15	12.0	1.4	0
16	7.1	0.9	0
17	2.7	0.3	0
18	36.8	15.8	0
19	50.1	8.7	0
20	39.7	10.5	0
21	113.3	26.5	0.3

2.4 Poloidal Field Coil System for the limiter case

2.4.1 General design

The poloidal field (PF) system for the limiter case consists of 19 solenoids, see Figure 28. Like in the divertor case they are all located outside the toroidal field coils and all of them are superconducting.

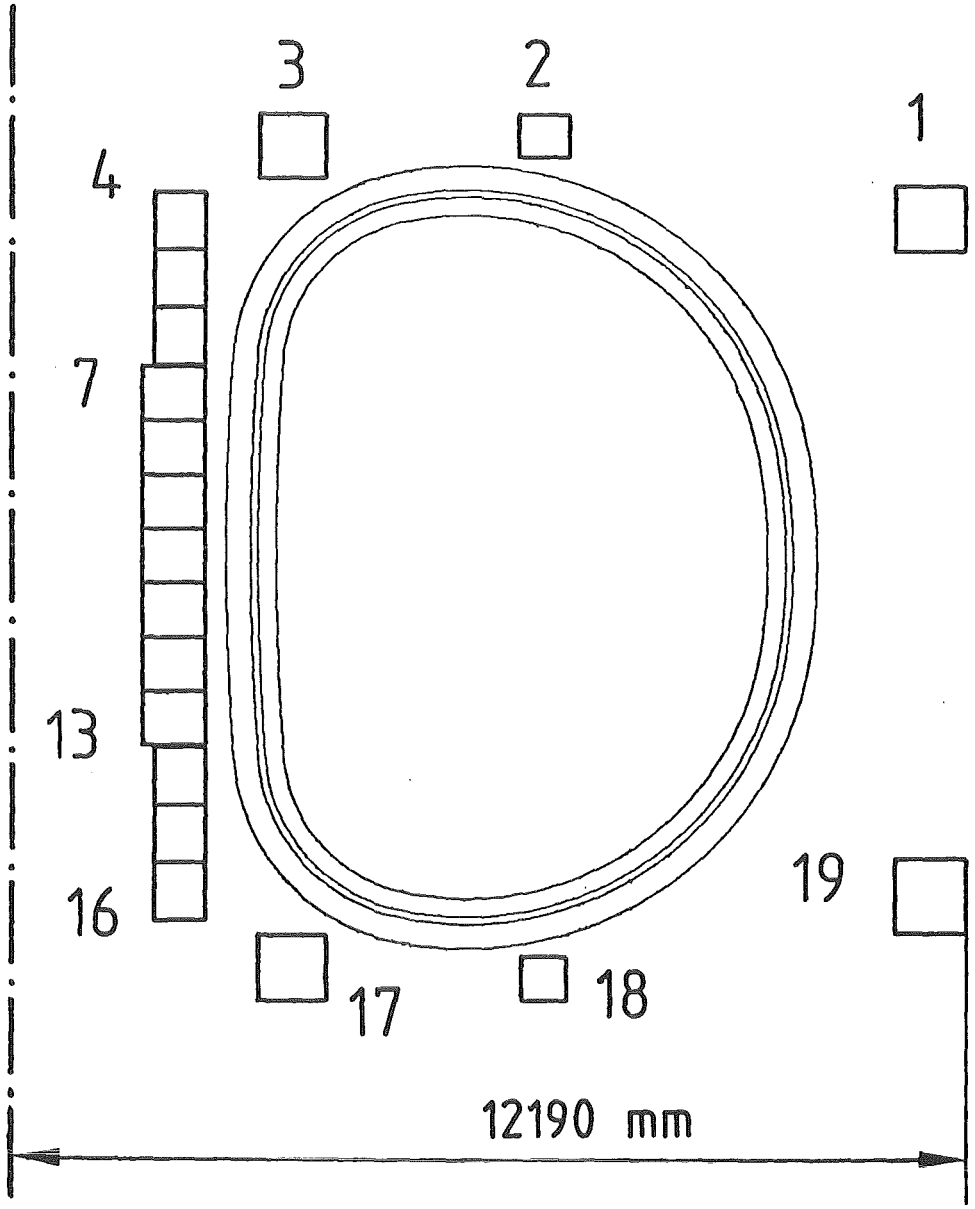

Fig. 28 Poloidal field coils arrangement of the INTOR phase IIa limiter case

Table XXV Medium position of the PF coils and the plasma and Ampère turn numbers at different times after discharge initiation

Coil	Medium pos./cm		I/MAt				
	vertical	radial	0 s	0.3 s	5 s	11 s	211 s
1	470	1170	0.8	0.31	3.56	-8.73	-8.92
2	585	635	0	-0.78	-0.78	3.74	3.74
3	570	290	5.56	5.79	8.10	3.66	2.38
4	305	135	5.73	5.22	1.55	0.69	-0.63
5	385	"	"	"	"	"	"
6	465	"	"	"	"	"	"
7	225	127	4.56	3.48	-4.81	-4.47	-5.52
8	150	"	"	"	"	"	"
9	75	"	"	"	"	"	"
10	0	"	"	"	"	"	"
11	-75	"	"	"	"	"	"
12	-150	"	"	"	"	"	"
13	-225	"	"	"	"	"	"
14	-305	135	5.73	5.22	1.55	0.69	-0.63
15	-385	"	"	"	"	"	"
16	-465	"	"	"	"	"	"
17	-570	290	5.56	6.90	18.02	12.63	11.35
18	-585	635	0	-0.24	-2.20	2.69	2.69
19	-470	1170	0.8	0.07	-5.67	-9.95	-10.14
Plasma	0	525	0	0.60	5.40	6.40	6.40

The PF coils are distributed symmetrically to the horizontal axis of the toroidal field coil. The medium position and the current-time scenario of the PF coils are given in Table XXV.

The winding concept is similar to this one of the divertor case (see chap. 2.3.1). Also a conductor is taken which follows the Japanese concept. The conductor has a design current of 50 kA, The overall dimensions of the conductor are 14.5 x 2.28 cm^2 for all coils exept for coils 4, 5, 6, and 14, 15, 16, which have a conductor with a cross section of 13.33 x 2.28 cm^2.

A principle view of the winding concept was already given in Fig. 26. The conductor is considered of carrying no load in circum ferential direction. Hoop stresses are taken over by additional co-wound steel strips of 13.0 x 0.1 cm^2 cross section. The conductors are electrically insulated to each other by 2 mm thick epoxy strips. Between each two pancakes there is an insulating epoxy layer of 15 mm thickness (for coils No. 4 - 6 and 14 - 16 it is 3.3 mm). The layer is provided with a large number of bores which allow a good permeation of Helium through the poolboiling cooled winding.

2.4.2 PF coil cross sections due to conductor needs and hoop stress support

The layout of the PF coil cross sections is similar to this of the divertor case. As the conductor current is limited at 50 kA the neccessary number of turns can be calculated from the maximum Ampère number of turns of Table XXV for each coil. Axial and radial numbers of turns are then chosen, in order to obtain an almost square coil cross section. The total conductor cross section of the winding is then obtained by multiplying the cross section of one conductor with the total number of turns.

To this value the cross section of the steel reinforcement has to be added in order to obtain the total coil cross section. For a first-step-calculation an overall coil current density of 1.5 kA/cm^2 maximum current density is assumed for all coils exept for the central solenoids (4 - 16) which have 1 kA/cm^2 maximum current density. These current densities give the first-

step-coil cross sections. For these cross sections the maximum local hoop stresses are calculated for each coil with the SOLKRAFT code, where the model of a total force transmission system (see chap. 2.3.4) was used.

As it is recommended that the stress in the steel reinforcement is limited at 200 MPa and the whole hoop stresses are taken over by the steel strips, the necessary steel cross section is obtained by multiplying the assumed first-step-coil cross section by the ratio:

maximum local hoop stress divided by 200 MPa.

From the chosen axial number of turns and the supporting steel cross section, the radial supporting steel thickness is calculated. Finally, the supporting steel thickness of each conductor can be calculated in terms of 0.1 cm thick steel strip numbers from the radial number of turns and the total radial steel thickness.

With these new coil dimensions the hoop stress calculation is repeated in order to obtain the final cross sections. The results of these calculations are given in Table XXVI. As can be seen also from Fig. 28 the OH-coils No. 7 - 13 have a larger cross section than the other coils in the inner vault. This results from a maximum current at the end of the burn cycle which is about 10 % higher than in the divertor case. The neccessary increase of the cross section could only be reached by decreasing the inner radius by 7 cm because the hight and the outer radius of these coils are already at their maximum. This reduction of the inner radius causes also a reduction of the medium radius by 3.5 cm compared with the original design. Plasmaphysisists have to check whether the influence of this decrease of 3.5 cm is tolerable.

Table XXVI Composition of the poloidal field coil windings due to hoop stresses

Coil	NZ	NR	$\frac{ACo}{cm^2}$	NSt	$\frac{ASt}{cm^2}$	$\frac{\Delta RSt}{cm}$	$\frac{\Delta Rtot}{cm}$	$\frac{\Delta Ztot}{cm}$
1	6	30	5951	9	2106	27	96	90
2	4	19	2513	14	1383	26.6	70	60
3	6	27	5356	10	2106	27	90	90
4 - 6	6	19	3466	13	1927	24.7	70	80
7 - 13	5	22	3637	12	1716	26.4	77	75
14 - 16	6	19	3466	13	1927	24.7	70	80
17	8	45	11902	11	5148	49.5	153	118
18	4	14	1851	21	1529	29.4	62	60
19	7	29	6711	11	2903	31.9	98	103

total cross section of one conductor is 145 x 22.8 mm^2 for the coils No. 1 - 3, 7 - 13, and 17 - 19. It is 133.3 x 22.8 mm^2 for the coils No. 4 - 6 and 14 - 16.

NZ axial number of turns

NR radial number of turns

ACo total cross section of the conductor

NSt number of co-wound steel strips 130 x 1 mm^2 for each conductor

ASt cross section of steel reinforcement

ΔRSt total radial steel thickness

ΔRTot total radial thickness of the winding

ΔZtot total axial thickness of the winding

2.4.3 Intercoil forces of the poloidal field coil system and supporting coil case thickness

As all poloidal field coils are solenoids with a common axis, the z-axis, the body forced are axisymmetric to the Z-axis and the resulting intercoil forces lie on the Z-axis. Only these resulting vertical forces have to be supported by a special support system. All other forces must be supported by the coil casings or by the conductors themselves.

2.4.3.1 Forces under normal working conditions

Table XXVII shows the vertical forces on the poloidal field coils which have been calculated with the SOLKRAFT code for the five steps of the current-time scenario. In order to simulate the influence of the plasma current another coil with constant current density and fixed dimensions was added. The Z-position of this coil had been established by an interaction process so that the force on it was zero.

As can be seen in Table XXVII the maximum forces act on the coils No. 1 and 19 beginning from 11 seconds after discharge initiation. Here they reach amounts of up to about 130 MN.

2.4.3.2 Forces under fault situations

The assumed fault situations are the same as described in chapter 2.3.3.2 for the divertor case. For each coil the maximum possible forces under these fault situations have been calculated. They are presented in Table XXVIII . The absolute value of nearly all these forces are well below 100 MN. Only coils 1 and 19 are loaded with 129 MN and 138 MN respectively at 11 seconds after discharge initiation. These forces have to be controlled by the supporting system.

2.4.3.3 Feasibility of a casing for coil No. 19

Coil No. 19 is the highest loaded coil of the PF system. For coil No. 21 of the divertor case (see chapter 2.3.3.3) it has been shown already that a casing seems to be feasible. This coil has the same medium radius as coil 19 of the limiter case and it is loaded much higher (180 MN). So one can say that a casing for coil 19 of the limiter case seems feasible as well.

Table XXVII Vertical forces F_Z on poloidal field coils in MN at different times after discharge initiation under normal working conditions

Coil	Time				
	0 s	0.3 s	5 s	11 s	211 s
1	-1.7	-0.5	13.1	-67.9	-73.8
2	0	3.3	2.0	6.6	10.3
3	-46.8	-44.2	-8.5	1.0	5.3
4	15.7	19.6	27.2	9.5	-8.3
5	-12.6	-7.2	11.0	3.6	-3.7
6	-71.2	-56.7	2.6	1.2	-2.9
7	9.8	11.8	-83.0	-61.3	-73.5
8	3.8	4.2	-29.4	-21.0	-25.1
9	1.4	1.4	-10.0	-6.5	-7.7
10	0	-0.2	0.8	1.4	1.8
11	-1.4	-1.9	12.0	9.6	11.6
12	-3.7	-4.8	32.7	25.1	30.2
13	-9.6	-12.6	88.6	67.4	81.0
14	-15.6	-21.3	-30.5	-11.0	9.8
15	12.7	4.7	-16.4	-6.0	5.8
16	71.2	53.5	-9.5	-4.0	5.5
17	46.8	52.4	25.6	-3.6	-25.6
18	0	-0.9	-6.6	-4.3	-6.9
19	1.7	0.1	-32.6	67.9	74.3

Table XXVIII Maximum possible vertical forces $F_{Z,max}$ in MN on poloidal field coils under fault situations at different times after discharge initiation (upward pos., downward neg.)

Coil	Time				
	0 s	0.3 s	5 s	11 s	211 s
1	0.2/ -1.8	0.1/ -0.6	27.1/-14.0	39.6/-107.4	39.1/-112.9
2	0 / -0	3.3/ 0	5.2/-3.2	29.1/-22.5	31.6/-21.3
3	0 /-46.8	0.1/-44.2	21.2/-29.7	11.5/-10.5	10.3/ -4.9
4	82.5/-66.8	69.3/-49.6	28.6/ -1.4	10.2/ -0.7	1.5/ -9.9
5	68.7/-81.3	58.4/-65.5	16.3/ -5.3	5.0/ -1.4	1.2/ -4.9
6	14.3/-85.5	13.6/-70.2	9.0/ -6.4	2.7/ -1.5	0.4/ -3.3
7	62.5/-52.7	46.1/-34.2	4.6/-87.5	4.8/-66.2	14.0/-87.5
8	56.6/-52.9	38.5/-34.4	44.3/-73.7	39.0/-60.0	60.7/-85.8
9	54.5/-53.1	35.9/-34.6	57.6/-67.6	50.2/-56.7	75.9/-83.6
10	53.6/-53.8	34.8/-35.0	63.7/-62.8	54.8/-53.4	81.8/-80.1
11	53.1/-54.5	34.4/-36.2	69.5/-57.5	58.9/-49.3	86.4/-74.8
12	52.9/-56.6	34.2/-38.9	77.3/-44.6	63.5/-38.4	90.2/-60.0
13	52.8/-62.8	34.0/-46.6	93.7/ -5.1	71.8/ -4.4	94.4/-13.5
14	66.8/-82.4	49.4/-70.7	1.6/-32.1	0.7/-11.6	11.3/ -1.5
15	81.3/-68.7	65.3/-60.6	5.5/-21.9	1.4/ -7.3	7.0/ -1.2
16	85.5/-14.3	70.1/-16.6	6.5/-16.0	1.5/ -5.5	5.9/ -0.4
17	46.8/ -0	52.7/ -0.3	67.1/-41.4	35.0/-38.6	22.5/-48.1
18	0 / -0	0 / -0.9	8.1/-14.7	16.5/-20.8	15.7/-22.6
19	1.8/ -0.2	0.1/ 0	8.9/-41.5	109.6/-41.8	115.3/-41.0

2.4.4 Hoop stress calculations

For the hoop stress calculations the SOLKRAFT code has been used which is described in chapter 2.3.4. Again the two models have been investigated: the system with self-supporting loops and the force transmission system which was the base for the layout of the supporting steel thickness.

The maximum local hoop stresses for the system consisting of self-supporting loops are given in Table XXX. In most cases the values are lower than 100 MPa. They are essentially higher than 100 MPa in the coils 1, 2, 17, and 19. In coil 19 it reaches even 444 MPa. That means that also for the layout of the coils for the limiter case the model with self-supporting loops is not sufficient.

The maximum local hoop stresses for the force transmission system are given in Table XXXI. Here all values are essentially lower than 100 MPa. The highest value which appears at all is 67 MPa at coils No. 4, 5, 14, 15, 16.

2.4.5 Compressive stress in axial direction

The axial stresses are very much lower than the hoop stresses. The values are given in Table XXXII. As one can see the maximum local axial stress which appears at all is 15 MPa at coil No. 13, 5 seconds after discharge initiation. All other values are lower.

2.4.6 Maximum induction at the conductor

The induction at the conductor has also been calculated with the SOLKRAFT code. In Table XXXII the maximum absolute value (B) of the induction is given which has been calculated by the relation: $B = SORT\ (B_r^2 + B_z^2)$. For all coils the maximum induction is not higher than 8.3 T. That means that NbTi can be used as superconductor.

Table XXX Maximum local hoop stresses in MPa on self-supporting loops of the PF coil windings at different times after discharge initiation (tensile stress pos., compressive stress neg.)

Coil	Time				
	0 s	0.3 s	5 s	11 s	211 s
1	3	0	63	418	436
2	0	7	-6	-144	-144
3	52	53	103	19	7
4	85	70	5	-3	4
5	85	70	7	1	2
6	82	68	9	1	1
7	60	39	38	38	63
8	58	35	45	43	69
9	57	34	48	44	70
10	57	34	48	44	71
11	57	34	47	44	70
12	58	35	45	42	68
13	60	39	37	36	61
14	85	71	6	-2	4
15	85	71	11	3	-2
16	82	70	18	5	-4
17	17	25	148	72	57
18	0	1	69	-106	33
19	3	0	132	429	444

Table XXXI Maximum local hoop stresses in MPa on loops supporting each other (force transmission system) of the poloidal field coil windings at different times after discharge initiation (tensile stress pos., compressive stress neg.)

Coil	0 s	0.3 s	5 s	11 s	211 s
1	0	0	3	49	42
2	0	1	0	-30	-30
3	18	16	62	5	1
4	67	52	4	-2	3
5	67	55	8	1	2
6	66	55	11	2	1
7	56	35	19	24	44
8	47	32	25	29	49
9	46	31	28	30	51
10	46	31	28	30	51
11	46	31	28	30	51
12	47	33	25	27	47
13	56	36	16	21	40
14	67	56	7	1	2
15	67	58	13	3	0
16	67	58	20	6	-4
17	9	11	57	25	19
18	0	0	26	-37	-37
19	0	0	13	57	58

Table XXXII Maximum induction at conductor B_{max} and maximum compressive stress in vertical direction ($sigz_{max}$) on the conductor of the poloidal field coils

Coil	B_{max}/T	Time/s	$Sigz_{max}$/MPa	Time/s
1	3.8	211	8	11
2	2.4	11	3	11
3	4.2	5	7	5
4	8.3	0	5	5
5	8.3	0	3	0
6	8.0	0	13	0
7	8.0	0	14	5
8	7.8	0	5	5
9	7.8	211	2	5
10	7.8	211	0	5
11	7.8	211	2	5
12	7.8	0	5	5
13	8.0	0	15	5
14	8.3	0	5	5
15	8.3	0	3	5
16	8.0	0	13	0
17	6.5	5	13	5
18	2.2	11	2	0.3
19	3.9	11	9	11

2.4.7 Induced voltages in the PF coils

The maximum induced voltages are given in Table XXXIII. For the coils No. 2 - 18 the maximum induced voltage is lower than 6.4 kV for the whole coil and lower than 84 V between two loops. For the largest coils No. 1 and 19 these values are higher. Here the maximum induced voltage for the whole coil is 21.4 kV for coil 1 and 28.2 kV for coil 19. Between two loops it is 119.1 V for coil 1 and 139.1 V vor coil 19. All together these values are low enough that it does not seem neccessary to divide single coils into sub-coils.

2.4.8 Stored energy in the whole PF coil system

The stored energy for the whole PF coil system is:

time/s	0	0.3	5	11	211
energy/GJ	1.58	1.27	2.72	5.25	5.49

Table XXXIII Maximum induced voltage for a single loop U_{sing} and for the whole winding U_{tot} of the poloidal field coils. All these values appear between discharge initiation and 0.3 s later.

Coil	U_{sing}/V	U_{tot}/KV
1	119.1	21.4
2	83.8	6.4
3	10.5	1.7
4	16.6	1.9
5	13.6	1.6
6	10.5	1.2
7	19.8	2.1
8	22.0	2.3
9	22.7	2.4
10	22.8	2.4
11	22.5	2.4
12	21.4	2.2
13	18.8	2.0
14	14.8	1.7
15	10.6	1.2
16	6.1	0.7
17	20.2	3.3
18	36.6	2.1
19	139.1	28.2

2.7 Safety Aspects and Fault Conditions

2.7.1 Safety Aspects

The safety aspects of the PF coil system have been described already in chapter 1.5 together with the TF coil system.

2.7.2 Special Fault Conditions

2.7.2.1 Single coils not energized

This case has been described in chapters 2.3.3.2 and 2.4.3.2.

2.7.2.2 Short circuit of one coil under normal working conditions

If one coil becomes shorted at the terminals during normal operation, the other PF coils will induce currents which cannot be controlled by the power supply of this coil. Then the following dangerous cases may appear:

- The current which is induced exeeds the critical current value. Then the coil becomes normal conducting what will lead to a quench.

- The induced current leads to vertical forces which do not appear under normal working condi This will happen especially when the direction of the current after a short is opposite to the normal direction.

- The induced current causes hoop stresses which exeed essentially the design value of the layout of the coil. For this case both the current and the induction at the conductor must be high.

For each coil and for each time step of the whole current scenario which contains also the time steps between the burn cycles the current after a possible short at the terminals has been calculated. The results are given in Table XXXIV.

Inorm means the current of the coil at the end of a time step under normal working conditions. Ishort means the current of the coil at the end of the time step in the event of a short at the terminals of the coil at the beginning of this time step.

Time steps

Coil No.	- 20 - 0 sec		0 - 0.3 sec		0.3 - 5 sec		5 - 11 sec		11 - 211 sec		211 - 226 sec	
	Ishort	Inorm	Ishort	Inorm	Ishort	Inorm	Ishort	Inorm	Ishort	Inorm	Ishort	Inorm
1	-4.27E+02	3.80E+02	1.03E+02	1.90E+02	-1.68E+02	-1.57E+03	-1.69E+03	-2.38E+03	-2.44E+03	-2.59E+03	-1.35E+03	0.0
2	-2.11E+03	4.10E+02	7.20E+02	5.50E+02	3.95E+03	1.69E+03	2.01E+03	1.60E+03	2.33E+03	1.71E+03	-9.37E+02	0.0
3	5.58E+01	2.36E+03	2.30E+03	2.21E+03	2.98E+03	1.37E+03	2.03E+03	1.55E+03	1.51E+03	1.03E+03	-3.56E+02	0.0
4	-1.74E+03	2.31E+03	2.19E+03	1.96E+03	1.83E+03	-5.10E+02	4.98E+02	-1.00E+02	-3.02E+00	-8.50E+02	2.96E+01	0.0
5	-1.93E+03	5.73E+03	6.00E+03	5.32E+03	7.90E+03	2.30E+03	1.92E+03	1.20E+03	1.71E+03	-8.67E+01	-1.14E+03	0.0
6	-4.03E+03	5.73E+03	6.26E+03	5.32E+03	9.86E+03	2.30E+03	2.26E+03	1.20E+03	2.15E+03	-8.67E+01	-2.03E+03	0.0
7	-4.19E+03	5.73E+03	6.65E+03	5.32E+03	1.25E+04	2.30E+03	1.76E+03	1.20E+03	2.16E+03	-8.67E+01	-4.44E+03	0.0
8	-5.60E+03	4.56E+03	4.74E+03	3.42E+03	5.87E+03	-4.38E+03	-3.30E+03	-3.97E+03	-2.70E+03	-4.99E+03	-4.38E+03	0.0
9	-5.34E+03	4.56E+03	5.10E+03	3.42E+03	8.35E+03	-4.38E+03	-3.96E+03	-3.97E+03	-2.76E+03	-4.99E+03	-6.74E+03	0.0
10	-5.24E+03	4.56E+03	5.22E+03	3.42E+03	9.20E+03	-4.38E+03	-4.19E+03	-3.97E+03	-2.79E+03	-4.99E+03	-7.56E+03	0.0
11	-5.20E+03	4.56E+03	5.23E+03	3.42E+03	9.35E+03	-4.38E+03	-4.22E+03	-3.97E+03	-2.80E+03	-4.99E+03	-7.72E+03	0.0
12	-5.21E+03	4.56E+03	5.16E+03	3.42E+03	8.99E+03	-4.38E+03	-4.09E+03	-3.97E+03	-2.80E+03	-4.99E+03	-7.42E+03	0.0
13	-5.28E+03	4.56E+03	4.98E+03	3.42E+03	7.86E+03	-4.38E+03	-3.72E+03	-3.97E+03	-2.79E+03	-4.99E+03	-6.42E+03	0.0
14	-5.48E+03	4.56E+03	4.54E+03	3.42E+03	4.95E+03	-4.38E+03	-2.83E+03	-3.97E+03	-2.74E+03	-4.99E+03	-3.80E+03	0.0
15	-4.00E+03	5.73E+03	6.32E+03	5.32E+03	1.08E+04	2.30E+03	2.73E+03	1.20E+03	2.10E+03	-8.67E+01	-3.47E+03	0.0
16	-3.74E+03	5.73E+03	5.75E+03	5.32E+03	6.86E+03	2.30E+03	4.11E+03	1.20E+03	2.04E+03	-8.67E+01	-5.50E+02	0.0
17	-1.61E+03	5.73E+03	5.23E+03	5.32E+03	3.02E+03	2.30E+03	5.31E+03	1.20E+03	1.57E+03	-8.67E+01	9.46E+02	0.0
18	3.70E+03	6.45E+03	7.67E+03	8.00E+03	2.33E+04	2.14E+04	-5.21E+03	1.36E+03	3.05E+02	-2.10E+02	7.23E+03	0.0
19	-2.85E+03	4.90E+02	4.02E+02	9.60E+02	4.76E+03	4.82E+03	1.08E+04	8.68E+03	9.44E+03	8.67E+03	1.05E+03	0.0
20	-2.11E+03	0.0	-5.38E+02	1.00E+01	2.73E+03	1.00E+02	1.84E+04	1.28E+04	1.33E+04	1.29E+04	-6.00E+03	0.0
21	-4.09E+02	4.00E+02	8.50E+02	9.20E+02	-1.35E+04	-1.28E+04	-2.57E+04	-2.34E+04	-2.32E+04	-2.34E+04	3.60E+03	0.0
22	-4.50E+03	0.0	9.15E+02	6.00E+02	1.28E+04	5.40E+03	8.11E+03	6.40E+03	7.41E+03	6.40E+03	-5.97E+03	0.0

Table XXXIV Comparison of the coil currents (kA-turns) at the end of a time step under normal conditions and under short circuit, which happened at the beginning of the time step

The following 3 framed cases which seem to cause the most severe effects have been investigated in more detail:

- coil No. 5 at discharge initiation (0 s),
- coil No. 7, 5 s after discharge initiation,
- coil No. 11, 5 s after discharge initiation.

The results are presented in Table XXXV. In all cases the hoop stresses are lower than under normal working conditions. Also the vertical forces are not higher than without a short circuit. Only the direction of the vertical force on coil No. 5 has changed from normally downwards to upwards. For this coil supporting elements have to be provided which avoid that the coil moves upwards. The same of cause must be said for coil No. 17 for a motion downwards.

The current at the end of the time step is in coils No. 7 and 11 about twice as high than without a short circuit. The induction at the conductor however is lower than 4 T in these coils. In this case the critical current is more than a factor of 2 higher than in the range of 7 - 8 T. That means that these high currents are not dangerous and the coil will stay superconducting.

As conclusion one can say that the upper regarded fault cases do not lead to dangerous situations neither in the mechanical point of view nor in the electrical.

Table XXXV Results for single coils under short circuit during one time step

	Coil No.		
	5	7	11
Time/s	0	5	5
Conductor current/kA	16.1	104.2	93.5
Max. induction at conductor/T	5.1	3.8	2.5
Vertical force/MN	25.3	-20.9	-9.2
Max. hoop stress self-supp./ MPa	-14.0	15.2	10.4
Max. hoop stress force transm./MPa	-14.9	11.6	6.9

2.8 Research and Development to establish INTOR Phase II A PF-Magnet Technology

The development for PF will have to start from scratch. If the INTOR specifications would remain as a Phase II A, the requirements would call for the rapid implementation of an extensive development that would have to be consistent in schedule with the anticipated TF magnet program as described in chap. IX.1.6. The recent interest and achievements in noninductive current drive in Tokamaks has changed the view on the necessities in PF magnet development which lead to assuming a possible important reduction in requirements such as much slower field and current variations and much longer plasma burn leading to essentially steady state characteristics taking into account, however, infrequent events as caused by start-up and shut-down, control actions and in design base fault situations. Whereas the definitions of such a less demanding PF magnet development have yet to be established, the European technology program foresees to begin conductor and coil development to form the basis for being able to start PF coil manufacturing consistent with the schedule of NET.

The program as discussed so far will include at least two sequential steps:

- coil conceptual designs, and conductor design and development.
- design, construction and test of an EF coil, in order to check the chosen solution to the constructional problems and proof of the developed conductor (NbTi + Cu/CuNi, ~ 50 kA) and concerning all aspects of coil technology and operation (including high voltage components of current leads). Eventually, for EF-coil qualification of the winding methods to be applied on site may have to be assured in advance by running tests in some existing Tokamak in Europe.

These steps can be carried out until 1986/87. Depending on the final definition of NET until that time, further remaining development issues will be identified and need to be started immediately.